Electrochemical, Photoluminescence, and Surface Studies of the Passivation of Surface Recombination Processes on Chemically Treated Gallium Arsenide Surfaces

Thesis by

Sharon Ruth Lunt

In Partial Fulfillment of the Requirements for the Degree of

Doctor of Philosophy

California Institute of Technology

Pasadena, California

1992

(Submitted July 1, 1991)

Acknowledgments

Along the way towards completing this thesis, I received a great deal of help from a variety of people. For help in the EXAFS experiments I would like to thank Ian Abrahams (who started it all), Bruce Tufts, Patrick Santangelo, Catherine Caley, Gordon Miskelly, Michael Sailor, Malcolm Forbes, Gail Ryba, Gary Shreve and Teresa Longin for shared long nights on the beam line. Gordon Miskelly and Michael Sailor also deserve thanks for synthesizing many of the model compounds. I would also like to thank Britt Hedman of SSRL for many useful discussions and advice, as well as Joseph A. Gordon of IBM Almaden for the use of the surface EXAFS equipment. Lastly, I would like to thank the entire staff of SSRL for their patience and persistence in solving problems.

The XPS experiments described in this work could not have been accomplished without the use of equipment in several different laboratories. I would like to thank Michael Hecht and Richard Vasquez of Jet Propulsion Laboratories, and Eun-Hee Cirlin and John Vajo of Hughes Research Laboratories for providing time on their instruments. I would also like to thank John Vajo for running an occasional SIMS and Auger spectra. At Caltech, I would like to extend a great deal of thanks to Alan Rice for keeping the CUSP instrument working. Lastly, thanks go to Bruce Tufts and Michael Hochella (of Stanford University) for help and useful discussions.

Special thanks for obtaining time resolved photoluminescence spectra go to Gail Ryba. General thanks goes to members of the Lewis group, past and present - Rik Blumenthal, Lou Casagrande, Malcolm Forbes, Amit Kumar, Teresa Longin, Gordon Miskelly, Sonbihn Nguyen, Patrick Santangelo, Mary Rosenbluth, Gary Shreve, Michael Sailor, Andrew Sykes, Ming Tan and Bruce Tufts. They taught me quite a bit, and are generally a great bunch of people. Of course, I also need to thank Nathan Lewis, my advisor for all these years, who taught me a lot and kept me on my toes.

Another group of people who deserve a great deal of credit for the completion of my degree are Melinda Lamont-Schnoes, Aide Tejeda, Nancy Shreve, Gina Dimino,

Jefferey Shrager, and Dan Sherman for reminding me that there is a world outside graduate school. I also need particularly to thank Lee Tutt, a very very good friend, for his understanding and help through the rough spots. Finally, thanks go to my parents and family, who have given me plenty of support and encouragement since year one, and made it all possible.

Abstract

This thesis describes work that has been done to study the chemical properties of GaAs surfaces relating to recombination processes. A variety of electrochemical, photoluminescence, and surface techniques have been used to study the mechanism an chemistry of the reduction of surface recombination in GaAs exposed to transition metal ions and complexes, and GaAs exposed to sulfur-containing molecules.

Electrochemical studies done on polycrystalline n-GaAs/liquid junctions treated with a variety of transition metal ions to study the mechanism of the observed improvement in I-V properties of GaAs(M^{3+})/$Se^{-/2-}$-KOH photoelectrochemical cells showed that the primary route is electrocatalysis. X-ray photoelectron spectroscopy (XPS) and extended x-ray adsorption fine structure (EXAFS) studies were performed on single crystal GaAs with Co, Ru and Cr ammines in order to determine the surface binding chemistry of the transition metals.

Steady state and time resolved and photoluminescence studies were done on GaAs surfaces exposed to sodium sulfide and a variety of organic thiols, alcohols and ammines. Unlike the transition metal ions, these types of complexes are shown to affect the cross section of surface recombination sites as determined by photoluminescence experiments. XPS studies were also done to correlate the observed changes in photoluminescence yield and lifetime with changes in surface chemistry.

Finally, some work has been done on an entirely different semiconductor system in order to explore the surface reactivity of a semiconductor surface at a more fundamental level. Several different types of metal dichalcogenides were exposed to strong Lewis acid complexes, and the surface chemistry was followed by XPS. These studies showed that there is a marked difference in the reactivity of metal dichalcogenide surfaces, which can be predicted from the known electronic structure of the conduction bands.

Table of Contents

List of Figures

List of Figures (continued)

List of Figures (continued)

List of Tables

List of Tables (continued)

Chapter 1. General Introduction

Semiconductor surfaces are important both in terms of practical device fabrication and fundamental understanding of electron transfer processes across interfaces. One interesting aspect of many of these surfaces is the existence of electrical trap sites. The chemical properties of these sites are currently rather ill defined, but their existence is responsible for current loss at semiconductor/metal or semiconductor/liquid junctions and for a phenomenon known as Fermi level pinning, which limits the maximum voltage that can be obtained from a junction.

When a semiconductor comes into contact with another material, charge transfer occurs so that the Fermi levels equilibrate (Figure 1.1), causing the bands at the junction to bend.[1] For a semiconductor/liquid junction, the Fermi level of the semiconductor equilibrates with the redox potential of the solution. The diagram in Figure 1.1 is for

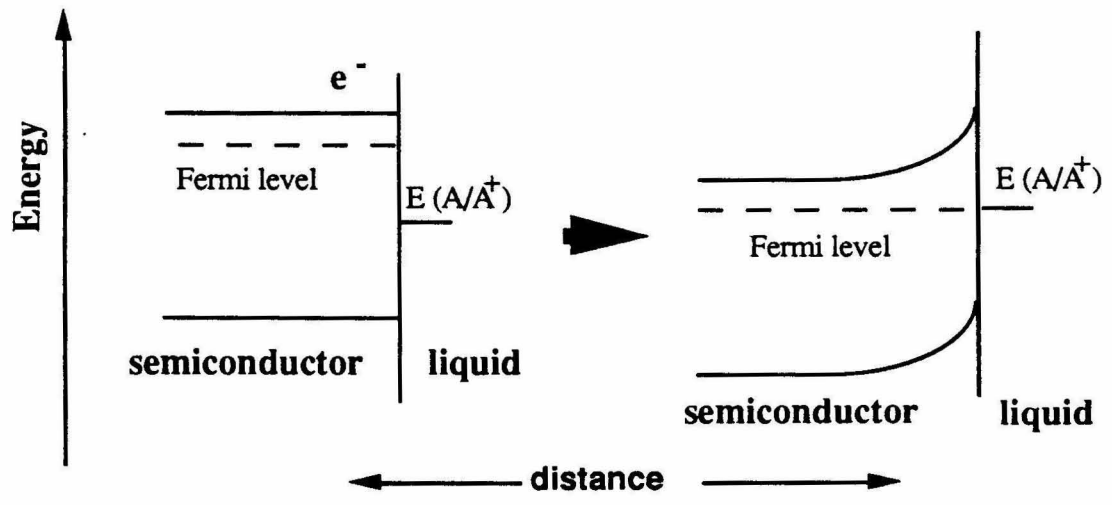

Figure 1.1 Schematic of charge equilibration between a semiconductor and a liquid containing the redox couple A/A^+.

n-type material, and all further discussion will be for n-type material unless specifically noted.

When light hits the interface, an electron-hole pair is created near the surface and charges are separated because of the band bending.[2] The holes go across the junction into the liquid to oxidize a species in solution, and electrons are collected as current. Loss of current occurs if the carriers recombine before they are collected. There are several different routes for recombination that are illustrated in Figure 1.2: recombination in the bulk (J_{br}), recombination in the space charge region (J_{dr}), trapping in surface states (J_{ss}), or majority carrier injection over the barrier (J_{th} and J_{tb}). Loss also occurs if there is a barrier for the injection of the hole into solution, since it will be more likely to combine

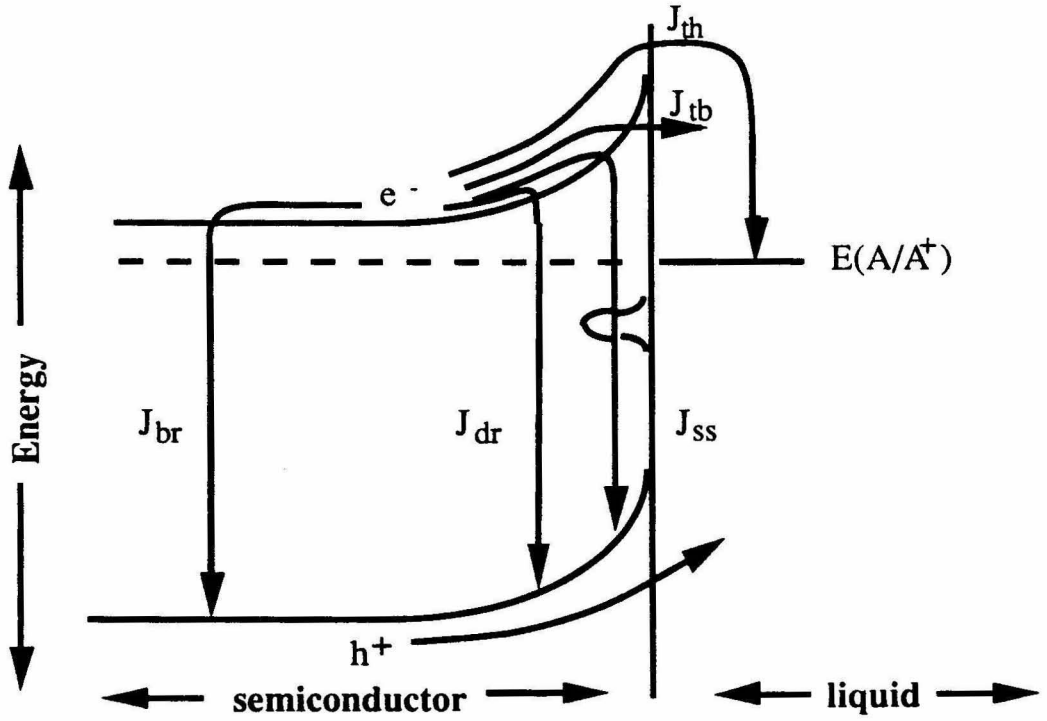

Figure 1.2. Illustration of possible recombination routes for electrons in n-type material.

through one of the aforementioned routes. For some redox couples (e.g., ferrocene/ferrocenium), the charge transfer is rapid and the barrier for holes is low. For other redox couples (e.g., selenium ions), the charge transfer is slow and the barrier for holes may be significant.

Polycrystalline material has additional losses that are due to the grain boundaries.[3] Boundaries are a result of a lattice mismatch between two adjoining crystallites and therefore have many dangling bonds that are electron deficient. One can think of the boundary as a p-type material sandwiched between two n-type pieces. The charges equilibrate, resulting in some band bending (Figure 1.3a). The grain boundaries contribute to current losses in two ways. First, the band bending results in barriers to an electron traveling across the surface (Figure 1.3b). Secondly, the boundary is a very effective trap for holes and therefore greatly increases the surface state density of a material.

For any given material, the current can be limited by either bulk or surface properties. If the rate limiting mechanism is surface kinetics, either because of surface trapping or a high barrier for hole diffusion into solution, then chemical modification of the surface is an ideal way to improve junction behavior. The chemical treatment could modify a surface trap (e.g. a dangling bond or a reactive surface site) by bonding to this site and raising its energy out of the band gap (Figure 1.4). A chemical species can also act as an electrocatalyst to hole injection into the electrolyte. Since the surface recombination velocity is the ratio of the surface trapping to the hole injection, either process will result in improved junction performance.

Semiconductor/liquid junctions are a convenient system to study processes occurirng at semiconductor interfaces. Such a junction is accessible to light or other probes and can be studied under operating conditions. The solution side can be easily modified to affect energetics of the semiconductor surface (e.g., through different redox couples) or the chemistry of the surface by introduction of reactive species. The semiconductor is easily removed for detailed analysis of changes at the surface. The above properties allow for the

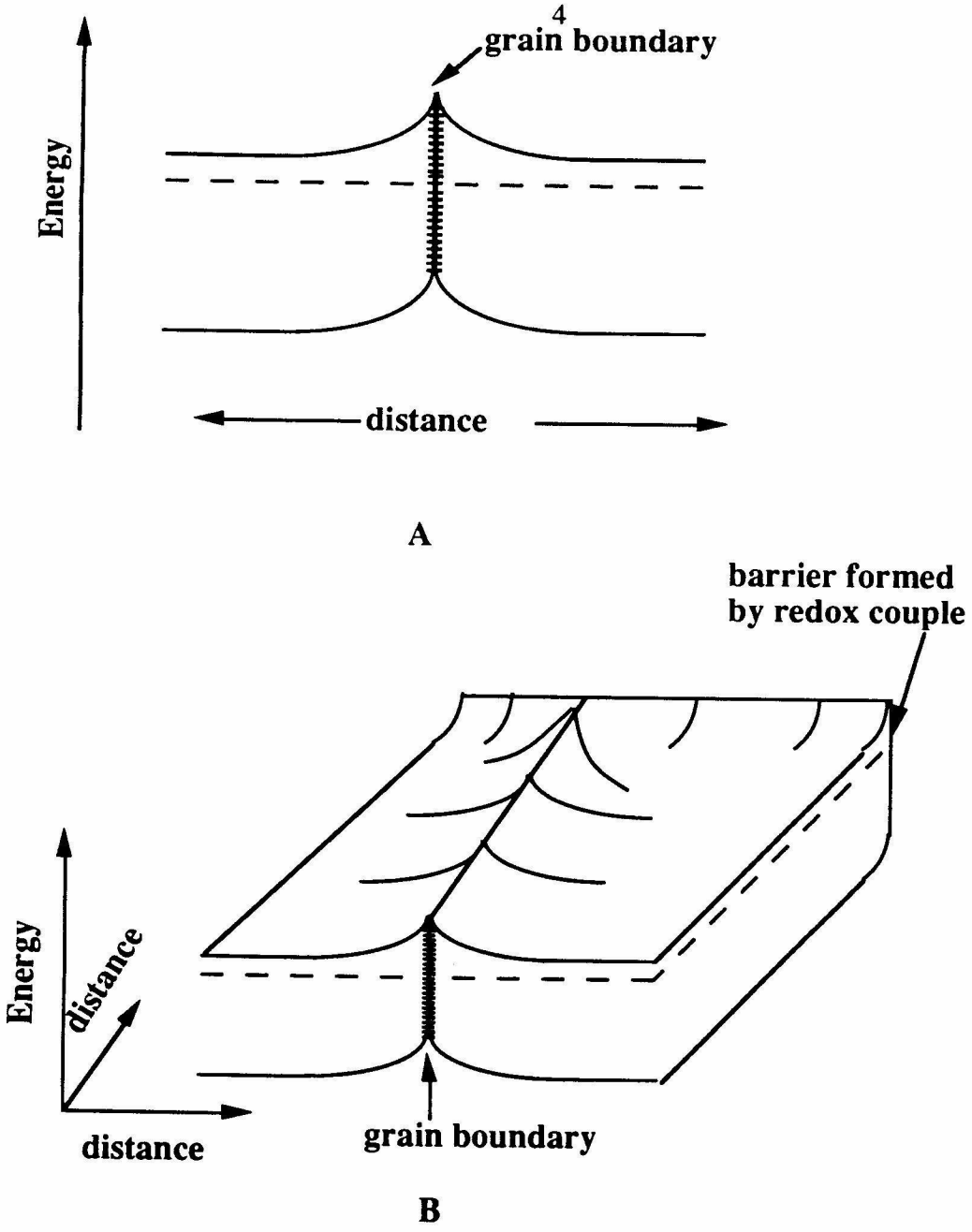

Figure 1.3. a) Equilibrium diagram for grain boundary energy levels. The boundary has many discrete, electron deficient states. b) Three dimensional diagram of band bending associated with a grain boundary on a semiconductor surface.

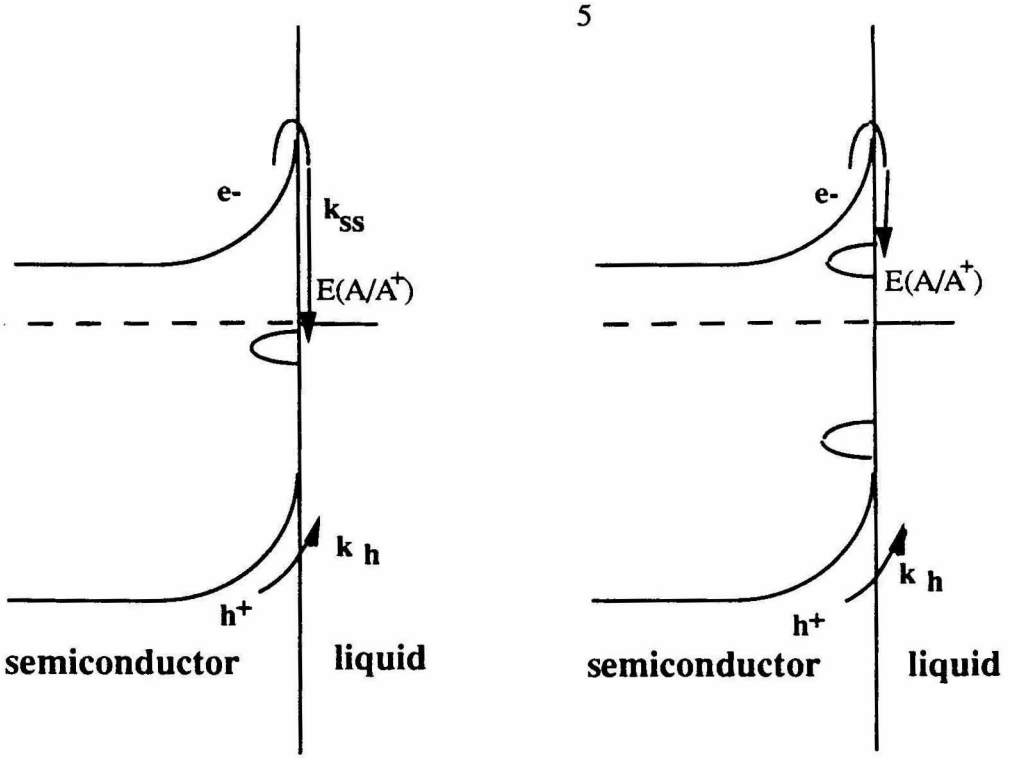

A B

Figure 1.4. Energy level diagram for proposed mechanism for alteration of surface states by chemical bonding.[15] a) Before chemisorption the surface states are at an energy level where electrons can easily recombine with a hole on the surface; b) After chemisorption, the surface states are split because of bond formation. The energy levels are now unfavorable for efficient surface recombination.

detailed study of charge transfer processes at the interface, and so correlations between observed chemical changes on the surface and changes in transfer processes can be made.

There are five main classes of semiconductors used in photoelectrochemical cells: metal oxide (e.g., TiO_2, $SrTiO_3$), elemental (e.g., silicon), transition-metal dichalcogenides (e.g., $MoSe_2$, WSe_2), II-VI semiconductors (e.g. CdS, CdTe), and III-V semiconductors (e.g., GaAs, InP). The band gaps of some of the compounds in the last four classes make

them ideal for applications involving conversion of solar energy to chemical energy (e.g., splitting H_2O). Unfortunately, most of these compounds are unstable in aqueous solutions and have poor current voltage characteristics because of recombination losses. Stability can be improved either by supplying a redox couple with faster electron transfer kinetics than the photocorrosion reaction[4] or by coating the semiconductor with a protective film.[5] The bulk of this manuscript is concerned with chemical modification of the surface to reduce recombination processes.

This thesis describes work that has been done to study the chemical properties of GaAs surfaces that relate to recombination processes. A variety of electrochemical, photoluminescence, and surface techniques have been used to study the mechanism and chemistry of the reduction of surface recombination in two systems. Chapter 2 describes electrochemical studies done on polycrystalline n-GaAs/liquid junctions treated with a variety of transition metal ions to study the mechanism of the observed improvement in I-V properties of GaAs(M^{3+})/$Se^{-/2-}$-KOH photoelectrochemical cells. Chapter 3 describes x-ray photoelectron spectroscopy (XPS) and extended x-ray adsorption fine structure (EXAFS) studies performed on single crystal GaAs with Co, Ru and Cr ammines in order to determine the surface binding chemistry of the transition metals.

Chapter 4 describes steady state and time resolved and photoluminescence studies done on GaAs surfaces exposed to sodium sulfide and a variety of organic thiols, alcohols and ammines. Unlike the transition metal ions, these types of complexes are shown to affect the cross section of surface recombination sites as determined by photoluminescence experiments. Chapter 5 describes XPS studies done to correlate the observed changes in photoluminescence yield and lifetime with changes in surface chemistry.

Finally, Chapter 6 describes work done on an entirely different semiconductor system in order to explore the surface reactivity of a semiconductor surface at a more fundamental level. Several different types of metal dichalcogenides were exposed to strong Lewis acid complexes, and the surface chemistry was followed by XPS. These studies

showed that there is a marked difference in the reactivity of metal dichalcogenide surfaces, which can be predicted from the known electronic structure of the conduction bands.

References

1 . G. W. *Neudeck, Modular Series on Solid State Devices, Vol. II The P-N Junction Diode* (Addison-Wesley, Reading, Mass., 1983).

2. A.L. Fahrenbruch and R. H.Bube, *Fundamentals of Solar Cells* (Academic Press, New York, 1983).

3. G. Hodes, S. J. Fonash, A. Heller, and B. Miller, *Adv. Electrochem. Electrochemical Eng.* **13**, H. Gerischer, Ed., 113 (1984).

4. a) P. Allongue, H. Cachet, P. Clechet, M. Froment, J. R. Martin, and E. Verney, *J. Electrochem. Soc.* **134**, 620 (1987). b) L. F. Schneemeyer and B. Miller, *J. Electrochem. Soc.* **129**, 1977 (1982). c) K. C. Chang and A. Heller, *Science* **196**, 1097 (1977). d) A. B. Ellis, J. M. Bolts, S. W. Kaiser, and M. S. Wrighton, *J. Am. Chem. Soc.* **99**, 2848 (1977).

5. a) R. Noufi, A. J. Nozik, J. White, and L. F. Warren, *J. Electrochem. Soc.* **129**, 2264 (1982). b) R. Noufi, D. Tench, and L. F. Warren, *J. Electrochem. Soc.* **128**, 2596 (1981). c) H. D. Abruna, and A. J. Bard, *J. Am. Chem. Soc.***103**, 6898 (1981).

Chapter 2. Studies of the Effects of Chemisorption of Transition Metal Ion Treated on the Photoelectrochemical Properties of Polycrystalline n-GaAs Photoanodes

I. Introduction

III-V semiconductors such as GaAs or InP have a band gap that is optimal for solar energy collection,[1] but they are prone to corrosion reactions in most semiconductor/liquid junction systems. Photoelectrochemical cells have been shown to be stable in only a very few electrolytes (e.g., 1.0 **M** $K_2Se^{-/2-}$ - 1.0 **M** KOH) where the kinetics of the electron transfer is apparently sufficiently rapid to predominate over the corrosion reaction.[2] These cells, though stable for extended periods of time, are not very efficient because of loss of current at the semiconductor/liquid interface via electrical trap sites (see Chapter 1). Chemical treatment of the surfaces of III-V semiconductors using transition metal ions has been shown by Heller, Miller and coworkers to improve the characteristics of several of these semiconductor/liquid junctions.[3,4,5,6]

Single crystal n-GaAs in the cell n-GaAs/$Se^{-/2-}$ showed improved I-V behavior after treatment with several different transition metal ions including Ru^{III}, Rh^{III},, and Pt^{II}.[5] Metal ions such as Cu^{II} and Cr^{III} showed no effect. Polycrystalline n-GaAs used in the same electrolyte improved after treatment with ruthenium ions.[6] Dare-Edwards, et. al showed that the photocurrent for p-GaP also improved after treatment with Ru^{III}, Rh^{III} and others.[7]

The mechanism for the improved properties of the III-V semiconductor/liquid junction was proposed by Heller to be the splitting of surface states out of the band gap by chemical bonding of the metal ion to the trap site. In the case of polycrystalline material, he proposed that the metal ions bond primarily to grain boundaries and so decrease recombination at these sites. However, as stated earlier in Chapter 1, an improvement in junction properties can be due to either a decrease in surface traps or an electrocatalytic effect.

In the case of single crystal n-GaAs, the primary mechanism for improvement appears to be electrocatalysis.[8] This was shown by experiments with Sn doped In_2O_3 (ITO) and n-, n^+-, and p-GaAs. The ITO experiments determined the electrocatalytic properties of the metal ions independent of the GaAs surface. Since ITO is a metal , there are occupied electronic states above the bottom of the conduction band, and surface traps are not electronically important. A chemical species that simply passivated surface states should have no effect on the junction properties of this material. However, when ITO is treated with metal ions, the overpotential of the reduction of Se^- and oxidation of Se^{2-} is reduced, indicating an electrocatalytic effect.[8a] In order to determine that the same electrocatalytic trends were dominant and n-GaAs surfaces, additional studies were done on p-type and n+-type GaAs.

In n^+-type material, there is such a high dopant density that the material behaves electronically, like a metal. If electrocatalysis is the dominant mechanism, then the overpotential should decrease on n+-type GaAs after metal-ion treatment, just as it did with ITO; this is indeed what is observed.[8b] In p-type material, the holes are the majority carriers, so in the dark, the collected current will be due to the sum of the recombination current and the injection of holes into solution. If surface states are removed, then the dark current decreases and the junction becomes more rectifying. If electrocatalysis occurs and more holes are injected into solution, the dark current increases. For the semiconductor/liquid junction p-GaAs/$Se^{-/2-}$, the dark current increased after metal-ion treatment.[8a]

As discussed in the previous paragraphs, the improvement of the n-GaAs/$Se^{-/2-}$ semiconductor/liquid junction seems to be dominated by electrocatalytic effects. In addition to the effect of electrocatalysis by metal ions, the passivation of surface recombination processes at n-GaAs/air interfaces[9] and the reduction in recombination losses for polycrystalline n-GaAs/metal Schottky barriers[6] and polycrystalline n-GaAs/KOH-$Se^{-/2-}$ liquid junctions[10] do seem to suggest an effect of grain boundary passivation at the n-

GaAs(Ru^{III}) surface. To investigate this possibility, we have studied the mechanism of I-V improvement of polycrystalline GaAs in contact with aqueous KOH-$Se^{-/2-}$ solutions and in contact with Au Schottky barriers. In this chapter, a set of experiments performed with a series of metal ions, all of which are efficient electrocatalysts for Se^{2-} oxidation and all of which yield improved I-V behavior in the single crystal n-GaAs/KOH-$Se^{-/2-}$ electrolyte, will be described.

Additionally, the I-V behavior of polycrystalline n-GaAs samples in contact with an outer sphere redox couple, ferrocene$^{+/0}$, in CH_3CN solvent was investigated. This interface is informative mechanistically because metal-ion induced grain boundary passivation effects should still be apparent, but the effects of electrocatalysis by chemisorbed metal ions should be greatly reduced in this weakly adsorbing, electrochemically reversible redox system.[11,12] Also described are the results of quantum yield vs. wavelength studies that were performed to identify any changes in the minority carrier collection length as a function of metal-ion chemisorption.

II. Experimental

All polycrystalline n-GaAs photoelectrodes were fabricated from material supplied by Professor S. Chu of Southern Methodist University. The material was an epilayer of the structure $p^+/n/n^+$-GaAs, which was grown on a W/graphite substrate with the n^+ layer contacting the W/substrate. The grain size, morphology, and solid-state solar cell characteristics of similar material have been published previously.[13] For this study, the p^+ layer was etched off with a 10 sec exposure to 1% Br_2-CH_3OH. Further etching yielded no difference in I-V characteristics until enough material was etched off to affect the value of the short-circuit photocurrent.

Photoelectrodes were fabricated by attaching the W/graphite substrates of the GaAs samples to a Cu wire with silver print, and the electrode assembly was then sealed into glass tubing with white epoxy resin. The electrochemical cell procedures, spectral response apparatus, and photoelectrochemical measurement techniques used in our

laboratory have been described in previous publications.[14,15] A schematic of the electrochemical cell is shown in Figure 2.1. All electrochemical measurements were performed under potentiostatic control with a Pt counter electrode and a Pt reference electrode. The potential of the Pt reference electrode was generally about -0.95 V. vs. SCE

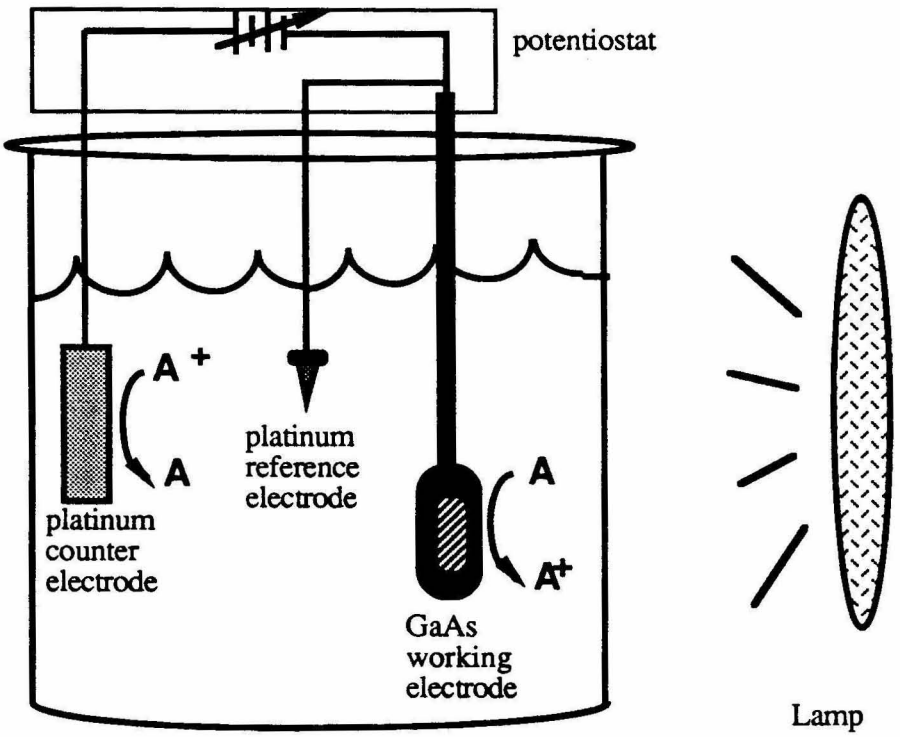

Figure 2.1. Schematic of the photoelectrochemical cells used in this study.

in the aqueous KOH-$Se^{-/2-}$ cell (of composition 1.0 **M** K_2Se and 0.01 **M** K_2Se_2 in 1.0 **M** KOH, unless otherwise specified) and was +0.17 V. vs. SCE in the CH_3CN-ferrocene$^{+/0}$-$LiClO_4$ cell (0.09 **M** ferrocene, 0.5 **mM** ferricenium, and 0.70 **M** $LiClO_4$ in dry, N_2 purged solvent). Illumination was provided by a 3200 K ELH type tungsten-halogen bulb with a dichroic rear reflector, and the open-circuit voltage was measured with a voltmeter after cycling.

The polycrystalline electrodes were etched (1% Br_2-CH_3OH for 10 s), rinsed with methanol, and dried with N_2 prior to introduction into the photoelectrochemical cell. Electrodes that received metal-ion treatments were etched as above, immersed in the metal-ion solution, rinsed with H_2O and dried in a stream of N_2 before use. The metal-ion solutions consisted of 0.010 **M** MCl_3/0.10 **M** HCl (M=Ru,Os,Ir,Rh) for 60 sec at room temperature (unless otherwise noted). Also tested were aqueous pH=1.0 solutions of 0.010 **M** $Co(bpy)_3Cl_3$, $Ni(NH_3)_6Br_2$, and $[Cr(NH_3)_5(OH_2)]NO_3 \cdot NH_4NO_3$, and a pH=9 solution of 0.01 **M** $Co(NH_3)_6Cl_3$, with electrode immersion times of 60 sec at room temperature. A convenient shorthand for these interfaces is GaAs(M^y), where M^y indicates the metal ion oxidation state initially present in the aqueous solution. Because of severe effects of cross-contamination that were observed in earlier studies of single crystal n-GaAs photoelectrodes,[8] all studies with a particular metal-ion were performed with a dedicated set of electrodes, redox-electrolyte solution, and glassware.

Schottky barriers were fabricated by depositing gold by filament evaporation in a base pressure of $< 8 \times 10^{-6}$ torr. The nominal thickness of Au was 125 Å, as indicated by a quartz crystal thickness monitor (R.D. Mathis, Inc.). The GaAs sample was polycrystalline material that had been either etched, etched and treated with metal ions, etched and immersed in KOH-$Se^{-/2-}$ solution, or etched, immersed in KOH-$Se^{-/2-}$ and then exposed to metal-ion solutions. In many cases, Au was deposited simultaneously onto the control and test samples, in order to insure that differences between runs were not simply due to variations in deposition conditions from sample to sample.

III. Results and Discussion

III.1. I-V Behavior of Polycrystalline n-GaAs Electrodes in KOH-$Se^{-/2-}$ Solutions

The I-V characteristics of polycrystalline n-GaAs photoanodes in the 1.0 **M** KOH-1.0 **M** Se^{2-}-0.01 **M** Se_2^{2-} electrolyte are shown in the dashed curves in Figure 2.2. Typical electrode samples displayed an I-V curve with a low open-circuit voltage and a

poor fill factor. Furthermore, no saturation in the collected photocurrent vs. applied voltage was observed for potentials as positive as +0.2 V vs. the equilibrium cell potential. These characteristics resemble those obtained for other small grain size GaAs and Si devices, which typically display grain boundary-induced recombination losses in open-circuit voltage, short-circuit photocurrent, and fill factor.[16,17,18]

In contrast, chemisorption of certain metal ions onto the GaAs electrode surface yielded much improved I-V behavior in the KOH-$Se^{-/2-}$ electrolyte. The effect was reversible in that etching of the surface after exposure to the metal ion was observed to eliminate the improvement in I-V properties. However, without deliberate etching of the surface, the improved junction properties were extremely persistent and stable under cell operation. Representative current-voltage curves for the various metal-ion treatments are depicted in Figures 2.2a-c, and Table 2.I summarizes the open circuit voltage (V_{OC}), short-circuit photocurrent density (J_{SC}), and fill factor. Fill factor is calculated through the relation $FF = (IV)_{max}/(V_{OC}J_{SC})$, where $(IV)_{max}$ is the maximum power point of the I-V curve.

Table 2.I. Electrochemical data for polycrystalline n-GaAs treated for 60 s with the given metal-ion complex before introduction into the KOH-$Se^{-/2-}$ electrolyte. The concentration for each metal-ion was 0.01 M in water at pH=1.

Metal-ion Complex	Open Circuit Voltage (mv ± 20)	Short Circuit Current (mA/cm^2)	Fill Factor
blank	-380	13	--
$RuCl_3$	-440	14.1	0.34
$RhCl_3$	-447	13.6	0.37
$IrCl_3$	-420	14.6	0.38
$Co(NH_3)_6Cl_3$ (pH=9)	-445	15.1	0.38
$OsCl_3$	-502	13.8	0.41

Every metal ion that we have observed previously[8] to yield improved performance at single crystal, n-GaAs photoanodes, n^+-GaAs dark anodes, In_2O_3 electrodes, and p-GaAs anodes was also observed to improve the performance of the polycrystalline, n-GaAs photoanodes used in this work. Furthermore, metal ions such as Ni and Cr, which were observed to have no effect on the I-V properties of n-GaAs photoanodes, yielded no change in the I-V properties of the polycrystalline samples. For single crystal, n-GaAs photoanodes, Os^{III} ions were found to yield the best junction properties,[8b] and the same behavior was observed in this study for the polycrystalline n-GaAs samples. The I-V curves for samples treated with Rh^{III} and Ir^{III} resemble that for Os^{III} (Figure 2.2c), but have slightly lower fill factors. The relative increase in efficiency of the n-GaAs(Os^{III}) sample vs. the n-GaAs(Ru^{III}) sample was 1.4, which compares with the 1.25 increase observed previously[8b] for single crystal n-GaAs surfaces.

The similarity in behavior of single crystal, n-GaAs and polycrystalline, n-GaAs photoelectrodes suggests that common mechanisms are producing the metal-ion induced efficiency improvements in the two systems. All of our observations to date can be explained by the electrocatalytic properties of chemisorbed metal ions in the KOH-$Se^{-/2-}$ solution. $Co(NH_3)_6^{3+}$ has been previously shown to chemisorb on (100) n-GaAs single crystals and on GaAs powders by reduction to the Co^{II} state,[19] and this GaAs(Co^{II}) system then yields an active electrocatalyst for Se^{2-} oxidation upon immersion into the aqueous KOH-$Se^{-/2-}$ solution.[19,20] Similar interfacial chemistry is implicated by the improved I-V characteristic, which was observed for the polycrystalline samples treated with $Co(NH_3)_6^{3+}$, (Figure 2.2b) and by the lack of improvement of polycrystalline GaAs electrodes that were exposed to the substitution-inert $Co(bipy)_3^{2+}$ ion. Furthermore, the best electrocatalyst for Se^{2-} oxidation has been identified previously to be the Os^{III} ion,[8b] and this metal ion yielded the best I-V behavior of the polycrystalline n-GaAs(M^{III})/KOH-$Se^{-/2-}$ systems surveyed in this study. Also, no change in the low level, steady state surface recombination velocity has been observed in our laboratory for single crystal, (100)

Figure 2.2. Current-voltage curves for polycrystalline n-GaAs/KOH-$Se^{-/2-}$ junctions. The illumination was 100 mW/cm^2 from an ELH type 3200 K tungsten-halogen lamp, and the data were obtained under potentiostat control with the photoanode as the working electrode. (---) I-V properties after a 10 second etch in 1% Br_2/CH_3OH and CH_3OH rinse. (____) I-V properties after chemisorption of metal ions. The metal ion in solution is as follows: a) $RuCl_3$; b) $Co(NH_3)Cl_3$; c) $OsCl_3$. The additional cathodic current in b) is from catalytic H_2 production by the metal-ion treatment.

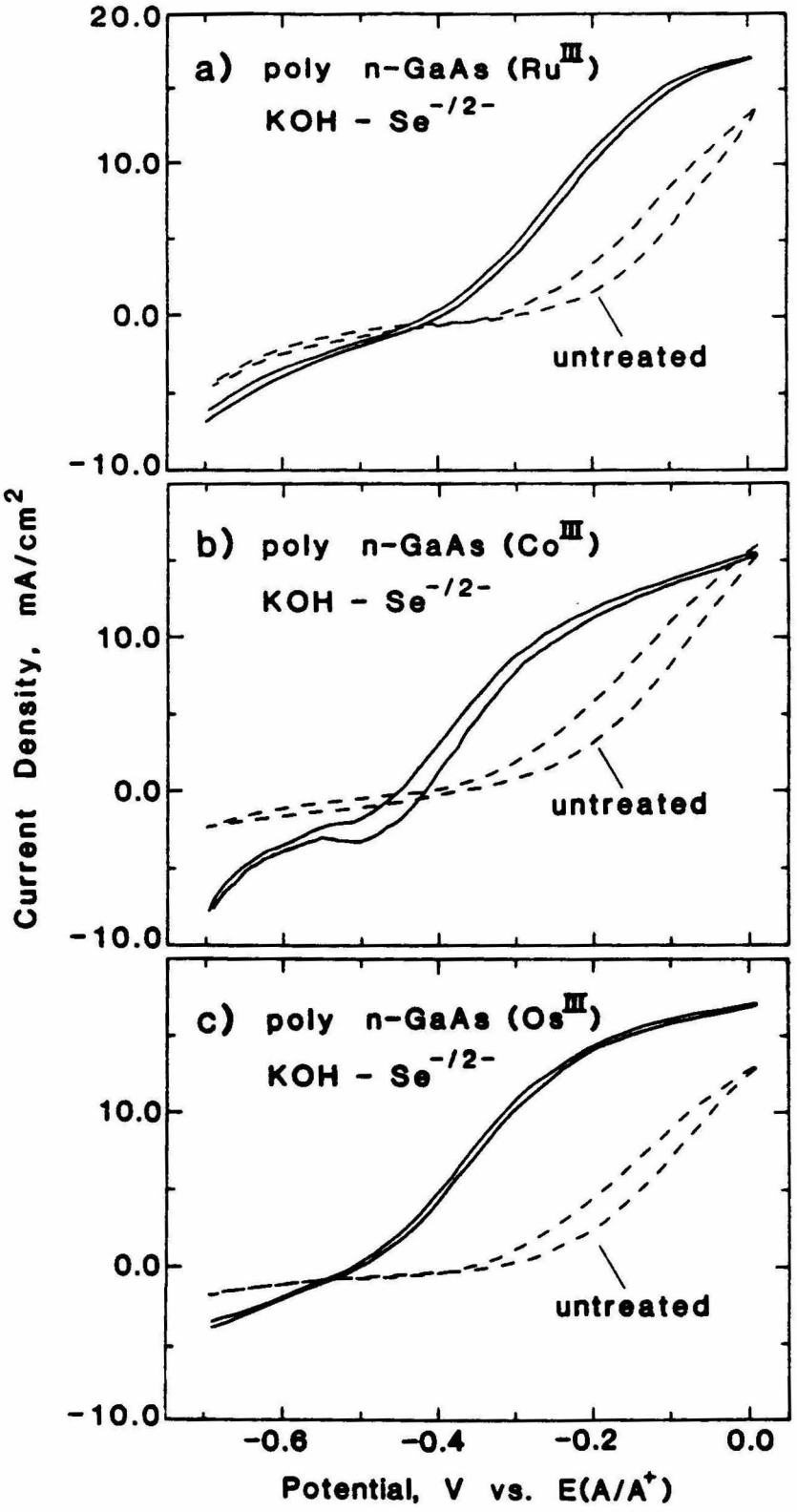
a) poly n-GaAs (Ru^{III})
KOH - $Se^{-/2-}$
untreated
b) poly n-GaAs (Co^{III})
KOH - $Se^{-/2-}$
untreated
c) poly n-GaAs (Os^{III})
KOH - $Se^{-/2-}$
untreated
20.0
10.0
0.0
-10.0
Current Density, mA/cm^2
-0.6
-0.4
-0.2
0.0
Potential, V vs. E(A/A$^+$)

oriented n-GaAs surfaces that have been treated with Ru^{III}, Os^{III},[8b] $Co(NH_3)_6^{3+}$,[20] or Ir^{III} ions, even though these surfaces did consistently display improved I-V properties in the KOH-$Se^{-/2-}$ electrolyte system. For all metal ions studied to date, the current-overpotential behavior at p-GaAs , n^+ -GaAs, and In_2O_3 electrodes has been a good indicator of the photoelectrochemical behavior of n-GaAs anodes in the KOH-$Se^{-/2-}$ system.

III.2. Behavior of Polycrystalline n-GaAs/Au and Polycrystalline n-GaAs/CH_3CN Interfaces

If the dominant feature of metal-ion chemisorption at the n-GaAs/KOH-$Se^{-/2-}$ junction were electrocatalysis of Se^{2-} oxidation, then the I-V behavior of junctions with rapid hole transfer kinetics, e.g., some nonaqueous systems and Schottky barriers, would not be expected to exhibit a strong dependence on surface treatment. Consistently, previous studies of single crystal, (100) n-GaAs photoanodes in CH_3CN-ferrocene$(Fc)^{+/0}$-$LiClO_4$ electrolytes indicated that no metal-ion treatment was necessary to obtain excellent I-V characteristics, and that pretreatment of the surface with Ru^{III} produced no change in the I-V properties of the junction.[21] Thus, the variation in I-V properties in the acetonitrile-ferrocene system is expected to be a very sensitive test of grain boundary passivation effects in polycrystalline GaAs electrodes.

The I-V properties of polycrystalline, n-GaAs photoanodes in CH_3CN-0.20 M Fc-0.5 mM Fc^+-0.7 M $LiClO_4$ electrolyte are depicted in Figure 2.3 and the electrochemical characteristics are given in Table 2.II. The nonaqueous cell I-V characteristics closely resembled that of the cell with the Ru^{III}-treated anode in KOH-$Se^{-/2-}$ media (Figure 2.2a vs. Figure 2.3). No improvement in the n-GaAs/CH_3CN-$Fc^{+/0}$ junction properties was obtained if the electrode was first treated with Ru^{III}, Ir^{III} or $Co(NH_3)_6^{3+}$ ions. Untreated electrodes that were evaluated in CH_3CN-$Fc^{+/0}$ and were subsequently cycled in the KOH-$Se^{-/2-}$ electrolyte exhibited I-V properties in the aqueous medium that were identical to the curves for untreated electrodes in Figure 2.2, indicating that the CH_3CN-$Fc^{+/0}$-$LiClO_4$

Figure 2.3. (___) I-V properties of polycrystalline n-GaAs/CH_3CN-$Fc^{+/0}$ junctions under 100 mW/cm^2 of tungsten-halogen illumination. For comparison purposes, (---) is the behavior in KOH-$Se^{-/2-}$ electrolyte.

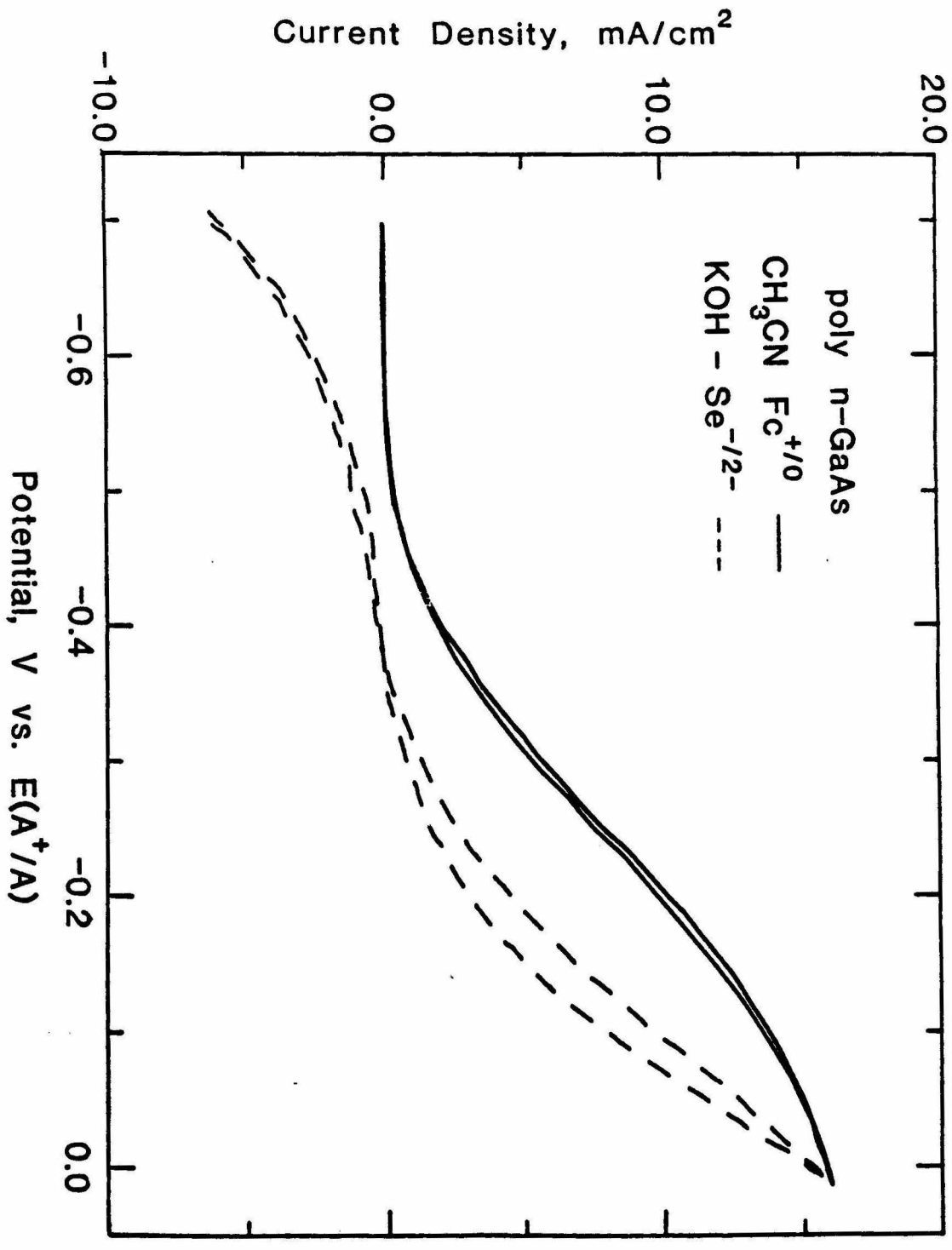
Current Density, mA/cm^2
20.0
10.0
0.0
-10.0
poly n-GaAs
CH_3CN $Fc^{+/0}$ ——
KOH - $Se^{-/2-}$ ---
0.0
-0.2
-0.4
-0.6
Potential, V vs. $E(A^+/A)$

Table 2.II. Electrochemical data for polycrystalline n-GaAs electrodes treated for 60 s with the given metal ion complex before introduction into CH_3CN-$Fc^{+/0}$-$LiClO_4$ electrolyte. The concentration for each metal ion was 0.01 **M** in water at pH=1.

Metal Ion Complex	Open Circuit Voltage (mv ± 20)	Short Circuit Current (mA/cm^2)	Fill Factor
blank	-511	14	0.26
$RuCl_3$	-514	14.1	0.27
$IrCl_3$	-502	13.6	0.28

solvent-electrolyte combination did not produce a persistent passivation of grain boundary recombination in the GaAs samples. Additionally, the beneficial effects on the KOH-$Se^{-/2-}$ I-V properties that were obtained by chemisorption of Ir or Ru were not altered by exposure of the treated electrode to the CH_3CN-$Fc^{+/0}$-$LiClO_4$ system.

The above results are consistent with the importance of the metal-ion catalyzed oxidation of Se^{2-} at n-GaAs electrode surfaces. In the aqueous KOH-$Se^{-/2-}$ cell, the beneficial I-V improvement was interpreted to arise from larger rates of electrocatalysis by the chemisorbed metal ions. This observation is consistent with the observation that the trend in fill factor improvement follows the trend of better to worse electrocatalyst. This is also consistent with the observation that the metal-ion chemisorption had no effect for the kinetically favorable n-GaAs/CH_3CN-$Fc^{+/0}$ interface. Also, given the persistence of the metal-induced I-V improvement in the KOH-$Se^{-/2-}$ electrolyte, it is highly unlikely that the grain boundaries are rapidly passivated by immersion of the polycrystalline n-GaAs into the nonaqueous electrolyte at room temperature, and then are reversibly and rapidly activated by subsequent exposure to the KOH-$Se^{-/2-}$ redox system.

A further test for possible effects of grain boundary passivation is the observation of improved performance of polycrystalline n-GaAs/metal Schottky barriers. Semiconductor/metal junctions should have high minority carrier collection velocities at the

Figure 2.4. I-V properties of polycrystalline n-GaAs/Au Schottky Barriers with (—) and without (---) chemisorption of Os^{III} prior to junction formation. For comparison purposes, the light intensity was adjusted to provide short-circuit photocurrent densities of 20 mA/cm^2 in each case.

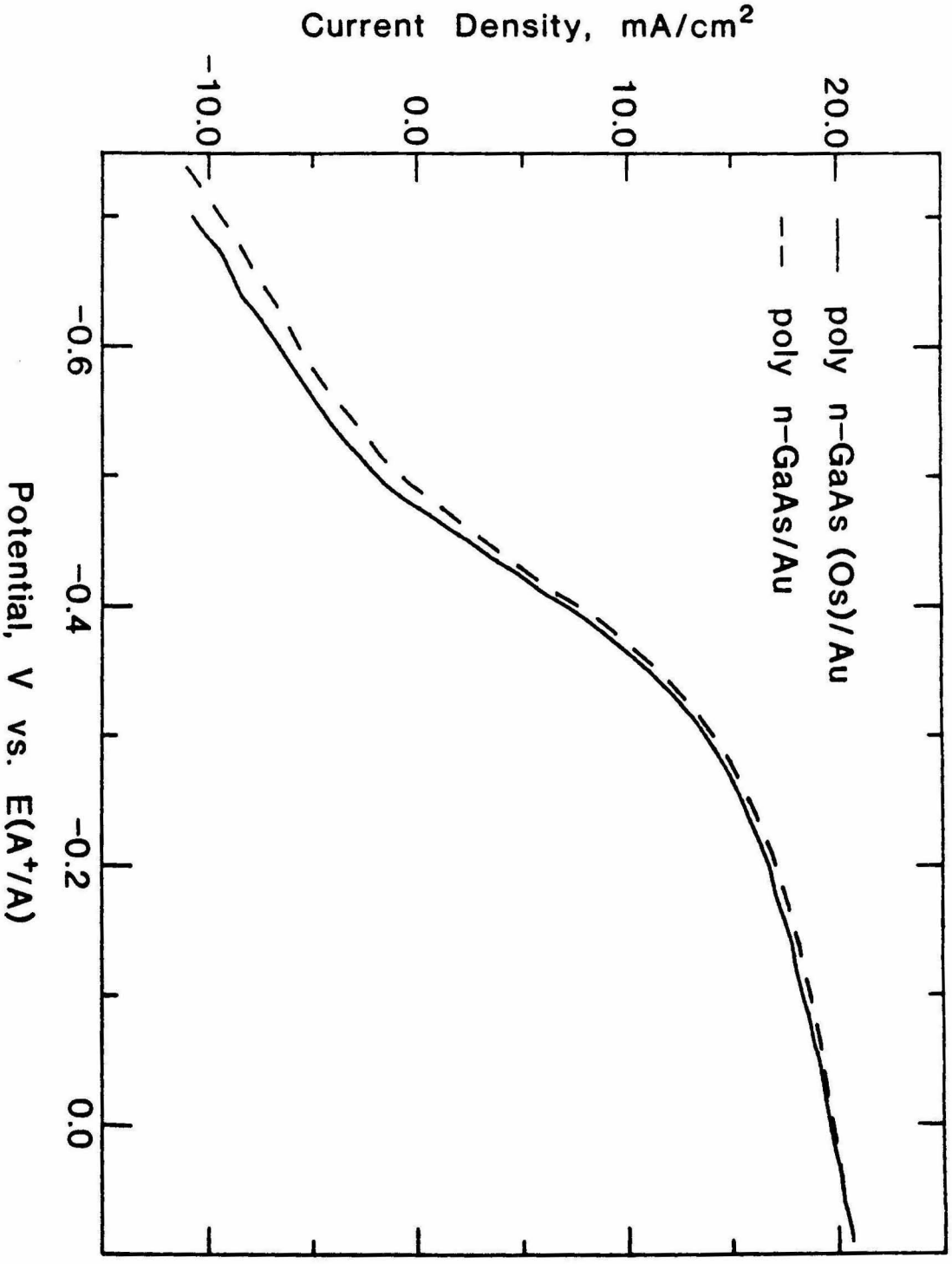
Current Density, mA/cm²
20.0
10.0
0.0
-10.0
poly n-GaAs (Os)/Au
poly n-GaAs/Au
0.0
-0.2
-0.4
-0.6
Potential, V vs. E(A⁺/A)

junction;[22,23,24] thus, any change in I-V behavior of these interfaces should be primarily due to metal-ion induced changes in the recombination processes at the grain boundaries. Figure 2.4 compares the I-V properties of polycrystalline n-GaAs(Os^{III})/Au and polycrystalline n-GaAs/Au samples. Similar curves were also obtained using Rh^{III} and Ru^{III} ions; Table 2.III gives the V_{oc} and J_{sc} for various metal-ion treated and untreated junctions. Exposure to KOH-$Se^{-/2-}$ solution before metal-ion treatment was also tried in the Ru^{III} case and there was no change in the I-V behavior.

Table 2.III. Electrochemical data for polycrystalline n-GaAs/Au junctions where the GaAs was treated for 60 s with the given metal-ion complex before evaporation of Au. The concentration for each metal-ion was 0.01 **M** in water at pH=1.

Metal Ion Complex	Open-Circuit Voltage (mv ± 20)	Short-Circuit Current (mA/cm^2)	Fill Factor
blank	-530	20	0.36 - 0.45
$RhCl_3$	-450	17.7	0.39
$OsCl_3$	-490	18.7	0.43
blank	-424	13.4	0.50
$RuCl_3$ (after KOH-$Se^{-/2-}$)	-410	13.4	0.49

The diode I-V curves showed only very small changes as a result of the metal-ion treatment, but all diodes displayed an improvement in the open-circuit voltage and fill factor over the untreated n-GaAs/KOH-$Se^{-/2-}$ semiconductor/liquid junction. These results further support an electrocatalytic mechanism for the improvement in polycrystalline, n-GaAs-based, surface barrier devices after metal-ion treatment. The lower open-circuit voltage of the polycrystalline n-GaAs/Au Schottky barrier as compared to that of the polycrystalline n-GaAs/CH_3CN-$Fc^{+/0}$ junction is also consistent with our previous

observations that GaAs/liquid junctions suffer less severe recombination losses than would be predicted, given the measurements of GaAs/metal Schottky barrier heights and thermionic emission recombination currents.[11b,c]

III.3 Spectral Response Properties of Polycrystalline GaAs Samples

Another prominent feature of the n-GaAs(M^{III})/KOH-$Se^{-/2-}$ interface is the increased short circuit photocurrent obtained after metal-ion chemisorption. This could arise either from a grain boundary recombination effect or from other surface-related processes. To elucidate the origin of this effect, spectral response data were collected for various n-GaAs(M^{III}) systems. Figure 2.5 compares the short circuit quantum yield vs. wavelength for single crystal n-GaAs/KOH-$Se^{-/2-}$, polycrystalline n-GaAs/KOH-$Se^{-/2-}$, polycrystalline n-GaAs(Ru^{III})/KOH-$Se^{-/2-}$, and polycrystalline n-GaAs/CH_3CN-$Fc^{+/0}$ junctions. As we found to be the case for the polycrystalline n-GaAs/KOH-$Se^{-/2-}$and n-GaAs/CH_3CN-$Fc^{+/0}$ I-V data, the spectral response in acetonitrile was independent of prior electrode history in KOH-$Se^{-/2-}$ and immersion in CH_3CN did not affect the spectral response of the various n-GaAs photoanodes in the KOH-$Se^{-/2-}$ system.

The polycrystalline n-GaAs/KOH-$Se^{-/2-}$ electrode displayed a rapid rise in quantum efficiency near the band gap, but reached a saturation value that was much less than that observed for a mirror-finished, (100) oriented, single crystal, n-GaAs surface in the same electrolyte. The metal-ion treated samples exhibited a similar rapid rise near the band edge, but reached a limiting quantum yield that was greater than the untreated n-GaAs samples. The untreated n-GaAs/CH_3CN-$Fc^{+/0}$ interface displayed a spectral response that was similar to that of the treated n-GaAs (M^{III})/KOH-$Se^{-/2-}$ junction, though the quantum yield was slightly higher. For wavelengths shorter than 800 nm, all of the junctions exhibited a slight decline in external quantum yield with decreasing photon wavelength, which is due to optical scattering from the polycrystalline GaAs samples.[25] The sharp declines at wavelengths shorter than 500 nm were due to solution absorptions.

Figure 2.5. Short-circuit quantum yield vs. wavelength data for several semiconductor/liquid junctions. a) polycrystalline n-GaAs/KOH-$Se^{-/2-}$; b) polycrystalline n-GaAs(Ru^{III})/KOH-$Se^{-/2-}$; c) polycrystalline n-GaAs/CH_3CN-$Fc^{+/0}$; d) single crystal n-GaAs/KOH-$Se^{-/2-}$.

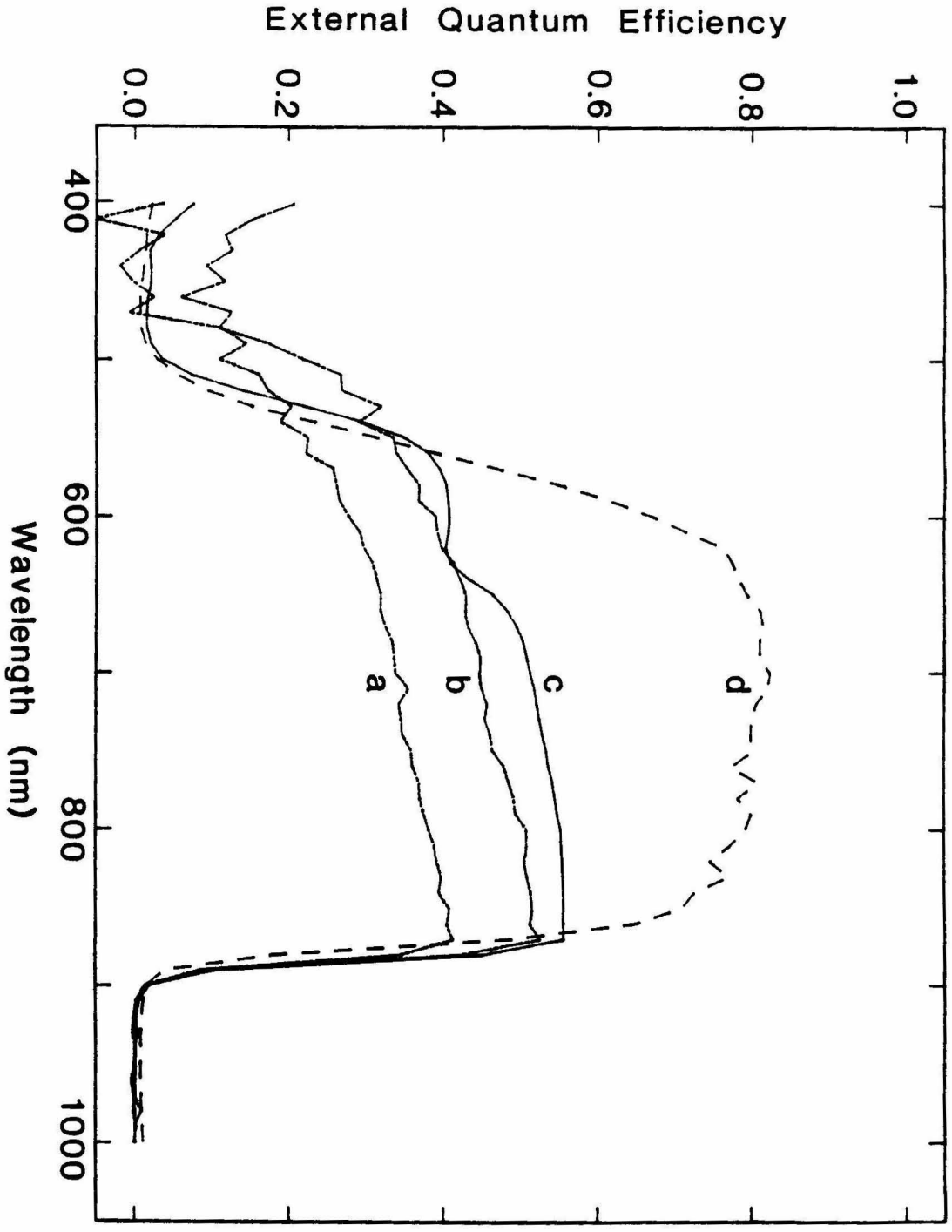
External Quantum Efficiency
0.0
0.2
0.4
0.6
0.8
1.0
400
600
800
1000
Wavelength (nm)
a
b
c
d

All of the spectral response data can be understood by consideration of the competing effects of minority-carrier recombination at the grain boundaries and minority-carrier injection into the solution. If the grain boundaries are active minority carrier recombination sites, then any carriers created within a diffusion length of the grain boundary will be effectively scavenged by the boundary. Thus, only those carriers that are created near the semiconductor/liquid junction and far from the grain boundaries will lead to a photocurrent. Extensive theoretical modeling of this process has been discussed for polycrystalline Si homojunction solar cells,[16,26] and our data are consistent with the extension of this treatment to the polycrystalline n-GaAs/liquid junction systems. For the KOH-$Se^{-/2-}$ system, there is a sharp rise in photocurrent, but an abrupt plateau at less than unity external quantum yield. This behavior can be explained by recombination losses at the grain boundaries. An increased rate of minority-carrier injection into the solution is expected to increase the effective collection volume for the minority carriers, and should produce an increase in the maximum quantum yield of the sample. This is consistent with the improvement in spectral response for the polycrystalline n-GaAs(M^{III})/KOH-$Se^{-/2-}$ systems when M is an electrocatalyst for Se^{2-} oxidation. It is also consistent with the high quantum efficiencies observed for untreated polycrystalline n-GaAs samples in contact with the electrochemically reversible CH_3CN-$Fc^{+/0}$ electrolyte system.

Previous work by Johnston and Heller et. al[6,27] using electron beam induced collection microscopy (EBIC) yielded improved short-circuit current collection in polycrystalline n-GaAs Schottky barriers that were exposed to Ru^{III} ions. EBIC on our samples (primary beam energy at 20 kV) showed very little difference in collected current between a Schottky barrier fabricated using a sample that had just been etched, and one that had also been exposed to selenide and Ru^{III} ion treatment before the gold deposition. Samples used for EBIC differed from the Schottky barriers used to obtain I-V properties only in that 400 Å of gold were deposited. In our studies, a comparison of short-circuit photocurrent densities for polycrystalline n-GaAs/Au Schottky barriers with and without

Ru^{III} treatment showed only a very small change in J_{sc}, implying that the magnitude of the grain boundary passivation effect is much smaller than the electrocatalytic effect of the metal ions in the KOH-$Se^{-/2-}$ medium. This is also consistent with the observation that the quantum yields of the polycrystalline n-GaAs/CH_3CN-$Fc^{+/0}$ system were comparable to those of the n-GaAs(M^{III})/KOH-$Se^{-/2-}$ junctions. Furthermore, an inspection of the entire I-V data for the Schottky barriers indicates that the grain boundary passivation effect is rather small for the solid-state systems.

IV. Conclusions

This chapter has discussed a series of experiments designed to determine the mechanism responsible for the observed improvement in I-V properties of polycrystalline n-GaAs/KOH-$Se^{-/2-}$ junctions. A series of metal ions was tested in the KOH-$Se^{-/2-}$ electrolyte, and the improvement in the I-V properties of the semiconductor/liquid junction paralleled the known electrocatalytic properties of a specific metal ion for selenide oxidation. The introduction of the polycrystalline electrodes into the CH_3CN-$Fc^{+/0}$ electrolyte system, which exhibits much faster electron-transfer kinetics, resulted in no noticeable improvement of junction properties after metal-ion treatment. Au Schottky barriers showed a similar lack of dependence on whether the polycrystalline GaAs had been exposed to metal ions prior to device fabrication. Spectral response measurements are also consistent with an increased rate of carrier injection into the solution after treatment as opposed to a decrease in trapping efficiency of grain boundary or surface states. We therefore conclude that although electrocatalytic effects of certain chemisorbed metal ions are an effective method of obtaining efficiency improvements in the polycrystalline n-GaAs/KOH-$Se^{-/2-}$ cell, other chemical procedures must be identified if substantial grain boundary passivation effects, and the resultant device efficiency improvements, for these polycrystalline n-GaAs samples in contact with most surface barrier systems are to be obtained.

References

1. A. L. Fahrenbruch and R. H. Bube, *Fundamentals of Solar Cells* (Academic Press, New York, 1983).

2. a) P. Allongue, H. Cachet, P. Clechet, M. Froment, J. R. Martin, and E. Verney, *J. Electrochem. Soc.* **134**, 620 (1987). b) L. F. Schneemeyer and B. Miller, *J. Electrochem. Soc.* **129**, 1977 (1982). c) K. C. Chang and A. Heller, *Science* **196**, 1097 (1977). d) A. B. Ellis, J. M. Bolts, S. W. Kaiser, and M. S. Wrighton, *J. Am. Chem. Soc.* **99**, 2848 (1977).

3. H. J. Lewerenz, D. E. Aspnes, B. Miller, D. L. Malm, and A. Heller, *J. Am. Chem. Soc.* **104**, 3325 (1982).

4. A. Heller, H. Leamy, B. Miller, and W. D. Johnston, *J. Phys. Chem.* **87**, 3239 (1983).

5. B. A. Parkinson, A. Heller, and B. Miller, *J. Electrochem. Soc.* **126**, 954 (1979).

6. W. D. Johnston, Jr., H. J. Leamy, B. A. Parkinson, A. Heller, and B. Miller, *J. Electrochem. Soc.* **127**, 90 (1980).

7. M. P. Dare-Edwards, A. Hamnett, and J. B. Goodenough, *J. Electroanal. Chem.* **119**, 109 (1981).

8. a) I. L. Abrahams, L. G. Casagrande, M. D. Rosenblum, M. L. Rosenbluth, P. G. Santangelo, B. J. Tufts, and N. S. Lewis, *Nouv. J. Chim.* **11**, 157 (1987). b) B. J. Tufts, I. L. Abrahams, P. G. Santangelo, G. N. Ryba, L. G. Casagrande, and N. S. Lewis, *Nature* (London) **326**, 861 (1987).

9. R. J. Nelson, J. S. Williams, H. J. Leamy, B. Miller, B. A. Parkinson, and A. Heller, *Appl. Phys. Lett.* **36**, 76 (1980).

10. a) A. Heller, *Accts. Chem. Res.* **14**, 154 (1981). b) A. Heller, B. Miller, S. S. Chu, and Y. T. Lee, *J. Am. Chem. Soc.* **101**, 7633 (1979).

11. a) C. M. Gronet, N. S. Lewis, G. Cogan, and J. Gibbons, *Proc. Natl. Acad. Sci., U.S.A.* **80**, 1152 (1983). b) N. S. Lewis, *Ann. Rev. Mater. Sci.* **14**, 95 (1984). c) L. G. Casagrande, N. S. Lewis, *J. Am. Chem. Soc.* **107**, 5793 (1985).

12. H. Van Ryswyk, A. B. Ellis, *J. Am. Chem. Soc.* **108**, 2454 (1986).

13. a) S. S. Chu, T. L. Chu, and H. T. Yang, *IEEE Photovolt. Spec. Conf.* **13**, 956 (1978). b) S. S. Chu, T. L. Chu, and H. T. Yang, *Appl. Phys. Lett.* **32**, 557 (1978).

14. C. M. Gronet and N. S. Lewis, *J. Phys. Chem.* **88**, 1310 (1984).

15. M. L. Rosenbluth and N. S. Lewis, *J. Am. Chem. Soc.* **108**, 4689 (1986).

16. a) C. H. Seager, in *MRS Symp Ser. 5(Grain Boundaries in Semiconductors)*, G. E. Pike, C. H. Seager, H. J. Leamy, Eds., 1982 pp. 85-98.

17. a) C. H. Seager, D. S. Ginley, and D. J. Zook, *Appl. Phys. Lett.* **36**, 831 (1980). b) D. S. Ginley and D. M. Haaland, *Appl. Phys. Lett.* **39**, 271 (1981). c) C. H. Seager, and D. S. Ginley, *Appl. Phys. Lett.* **34**, 337 (1979).

18. K. P. Pande, D. H. Reep, S. K. Shastry, A. S. Weiner, J. M. Borrego, and S. K. Ghandi, *Proc. 14th IEEE Photovoltaic Specialists Conf.*, 1324 (1980)

19. I. L. Abrahams, B. J. Tufts, and N. S. Lewis, *J. Am. Chem. Soc.* **109**, 3472 (1987).

20. B. J. Tufts, I. L. Abrahams, L. G. Casagrande and N. S. Lewis, *J. Phys. Chem.* **93**, 3260 (1989).

21. M. L. Rosenbluth, L. G. Casagrande, B. J. Tufts, and N. S. Lewis, *Proc. 18th IEEE Photo. Spec. Conf.* **18**, 1405 (1985).

22. a) L. M. Peter, *Electrochemistry* **9**, 66 (1984). b) H. Reiss, *J. Electrochem. Soc.* **125**, 937 (1978). c) W. J. Albery, P. N. Bartlett, A. Hamnett, and M. P. Dare-Edwards, *J. Electrochem. Soc.* **128**, 1492 (1981). d) D. Haneman and J. F. McCann, *J. Electrochem. Soc.* **129**, 1134 (1982). e) J. J. Kelly and R. Memming, *J. Electrochem. Soc.* **129**, 170 (1982).

23. S. M. Sze, *Physics of Semiconductor Devices, 2nd Ed.* (John Wiley and Sons, New York, 1981).

24. S. J. Fonash, *Solar Cell Device Physics* (Academic Press, New York, 1981).

25. Measurement of the reflectivity of the polycrystalline n-GaAs/air interface was performed with a diffuse reflectance attachment for a Cary 17 spectrophotometer. Use of this data to calculate the reflectivity losses at the n-GaAs/liquid interfaces yielded excellent agreement with the observed decline in external spectral response.

26. a) A. Neugroschel and J. A. Mazer, *IEEE Trans. Elect. Dev.* **ED-29**, 225 (1982). b) T. H. DiStefano, and J. J. Cuomo, *Appl. Phys. Lett.* **30**, 351 (1977). c) A. K. Ghosh, C. Fishman, and T. Feng, *J. Appl. Phys.* **51**, 446 (1980). d) H. P. Maruska, A. K. Ghosh, A. Rose, and T. Feng, *Appl. Phys. Lett.* **36**, 381 (1980).

27. a) A. Heller, *ACS Symp. Ser.* **146**, 57 (1981). b) A. Heller, *J. Vac. Sci. Technol.* **21**, 559 (1982).

Chapter 3. X-ray Photoelectron Specstroscopy and Extended X-ray Absorption Fine Structure Studies of Cobalt, Ruthenium, and Chromium Ammines Adsorbed on (100) n-GaAs

I. Introduction

Chapter 2 discussed the behavior of metal-ion exposed polycrystalline n-GaAs electrodes in $Se^{-/2-}$ - KOH electrolytes and the electrocatalytic properties of the various metal ions for selenide oxidation. This chapter discusses some studies performed to elucidate the mechanism for surface binding of transition metals to GaAs surfaces. While the transition metals unfortunately do not directly affect electronically active surface sites, the study of the fundamental chemistry of GaAs surfaces exposed to transition metal complexes is still important in understanding basic reaction pathways available for binding true surface-state passivants.

There are several possible binding modes for a complex to a GaAs surface. The metal complex can bind to unsaturated "dangling" bonds, to surface oxide species, or to the surface through electrostatic interactions. In this work, GaAs surfaces were reacted with a series of metal pentaammine complexes that are well characterized and well studied, so that their reaction chemistry with the semiconductor surface can provide insight into the chemical nature of the reactive surface species.

This chapter discusses the chemistry of three types of ammine complexes: $Ru(NH_3)_5H_2O^{2+}$, $Co(NH_3)_5X^{3+}$ ($X=NH_3$, H_2O, N_3), and $Cr(NH_3)_5CF_3SO_3^{3+}$. The semiconductor substrate was single crystal, (100) n-type GaAs and, in the case of the Ru complex, GaP, and InAs. The surface coverage of the metal, and the question of whether the starting complex remained intact during the course of exposure to the semiconductor, were monitored through x-ray photoelectron spectroscopy (XPS). The structure of the bound metal complex on the GaAs surface was studied by surface and powder extended

x-ray adsorption fine structure (EXAFS) measurements. Observations made by XPS on the reactivity of GaAs with $[Rh(CO)_2Cl]_2$ are discussed in the Appendix.

II. Experimental

A. Chemicals and Etches

The GaAs wafers used in the XPS studies were (100) oriented 10^{17} doped n-type single crystal bulk material (Wacker), and the EXAFS studies were 10^{18} Si-doped 6° off-axis substrates. n-type, (100) oriented 3° off-axis GaP wafers were supplied by Sematech, and n-type (unintentionally doped), (100) InAs was grown by MBE by Dr. T. Hasenberg of Hughes Research Laboratories.

$[Ru(NH_3)_5H_2O](PF_6)_2$ was synthesized from $Ru(NH_3)_5Cl_3$ as per the literature.[1] $[Cr(NH_3)_5CF_3SO_3](CF_3SO_3)_2$ was synthesized by stirring $Cr(NH_3)_5Cl_3$ for 3.5 days in tenfold molar excess of trifluorosulfonic acid under N_2. The reaction was worked up by adding an excess of diethylether while stirring, then filtering the salmon-pink precipitate in air and washing with ether. This compound is moisture sensitive and should be stored under N_2.

Model compounds used for EXAFS studies of $Co^{III}(NH_3)_5X$ on GaAs powders were: $Co(OH)_2$,[2] Co(OOH),[3] $Co(H_2O)_6(ClO_4)_2$ (GFS Chemicals), $CoSe_2$,[4] and $CoAs_3$.[5] Models used for $Ru(NH_3)_5H_2O^{2+}$ on single crystal GaAs were: $Ru(NH_3)_6Cl_3$ (Strem), $Ru(NH_3)_6Cl_2$ (Strem), $Ru(H_2O)_6$(p-tosylate)$_3$,[6] $Ru(H_2O)_6$(p-tosylate)$_2$[6] and $RuSe_2$ (prepared by grinding a stoichiometric amount of Ru and Se powders together in a mortar and pestle, sealing in an evacuated quartz tube and heating at 650 C for 4 days. Identity of the compound was confirmed via a powder pattern).[7]

All EXAFS experiments done on fine GaAs powders (400 mesh) were exposed to 0.01 **M** solutions of the cobalt complex ($Co(NH_3)_5H_2O^{3+}$, $Co(NH_3)_5N_3^{3+}$, or $Co(NH_3)_6^{3+}$) in either the chloride, bromide or perchlorate salts at pH > 10 (0.01 **M** KOH) for 5 minutes, washed with H_2O, then CH_3OH, and dried with N_2. The loading was calculated to be 30-40 mg Co/g GaAs. The experiments were usually done at 77 K and

10^{-6} torr, in order to minimize the thermal vibrational disorder introduced into the EXAFS. Other conditions are noted in the results section.

GaAs powder samples were also studied, that were exposed to 1**M** KOH-1**M** K_2Se after exposure to cobalt ion, in order to determine if any additional chemistry occurred after introduction of the GaAs surface into an electrochemical cell. Powders were prepared as above and then exposed to the selenide solution under N_2 for 5 minutes, washed with H_2O and dried.

Single crystal samples exposed to $[Ru(NH_3)_5H_2O](PF_6)_2$ were treated in a flowing Ar box, since the Ru complex is sensitive to N_2. For GaAs samples, a 1" x 1" square was etched for 10 s in 4:1:1 (conc. H_2SO_4:H_2O:30% H_2O_2), then exposed to a 0.01 **M** aqueous solution (pH = 1) of $Ru(NH_3)_5H_2O(PF_6)_2$ for 1 hour. The GaP samples were etched in 1:1 (H_2O:HF) for 10 s and the InAs samples in 0.05% Br_2 in methanol (15 s), 1 **M** KOH (15 s), and then rinsed with water, repeated 3 times, before exposure to the Ru complex. It should be noted that XPS spectra of InAs after exposure to acidic etches (e.g., 4:1:1), showed a marked decrease in As at the surface; however, the repetitive bromine methanol/KOH etch preserved the surface stoichiometry.

B. X-ray Photoelectron Spectroscopy

XPS spectra reported in this work were taken on three different XPS instruments. High resolution spectra were obtained on a Surface Science Instruments system with a Model 100 Top Hat mononchromatic Al-K_α x-ray source (SSI). Lower resolution spectra were taken with either an Al (1486.6 eV) or Mg (1254. eV) x-ray source on a VG Mark II system (Mark II) or a heavily modified VG HP580 system (VG). The FWHM of the Au $4f_{5/2}$ line was 0.95 eV on the SSI instrument and was 1.61 eV on the VG instrument. The base pressure was at least $1x10^{-9}$ torr in the first two instruments and $5x10^{-9}$ in the VG. Samples were transported to the instruments in N_2 or Ar filled vials and, in the case of the SSI and Mark II systems, were introduced into the chamber through a flowing N_2 box or an Ar drybox.

Data workup was performed by fitting the appropriate peaks using software provided with the various instruments, and then calculating coverages through the relation:

$$d_a = \lambda_a \cdot \cos\theta \cdot ln((I_a \sigma_b n_b \lambda_b)/(I_b \sigma_a n_a \lambda_a)+1), \qquad (1)$$

where d is the thickness in angstroms, λ_x is the escape depth of the species of interest, n_x is the number density, I_x is the peak area, θ is the angle between the surface normal and the detector, σ_x is the Scofield cross section;[8] the layer designated as "a" is on top of the layer designated as "b", and the transmission functions are assumed to be equal for both phases. The escape depth was calculated via the method of Seah and Dench.[9] The values used for all complexes in this chapter are given in Table 3.I. The angle between the surface normal and the detector was 42° for the SSI machine and 15° for the VG and Mark II instruments,

Table 3.I. Cross sections (σ), escape depth (λ) and atomic density (n) used for calculation of Ru and Cr coverages and mole ratios on GaAs, GaP, and InAs substrates.

Element Region	σ	λ (Å)	n (atom/cm^3) (x10^{-22})
GaAs:			
Ga (3d)	1.085	25	2.22
As (3d)	1.821	25	2.22
As_2O_3 (As 3d)	1.821	36	2.27
GaP:			
Ga (3d)	1.085	22	2.45
P (2p)	1.583	22	2.45
InAs:			
In	13.32	22	1.81
As	1.821	26	1.81
$Ru(NH_3)_5H_2O^{2+}$	7.39 (Ru)	19 (Ru)	0.74 (Ru)
(Ru $3d_{5/2}$)	1.87 (N)		
$Cr(NH_3)_5CF_3SO_3^{3+}$	7.6 (Cr)	30 (Cr)	0.17
(Cr $3d_{5/2}$)	1.87(N)		

unless otherwise noted. The concentration (moles/cm^3) was calculated by multiplying the calculated thickness by the density of the complex of interest.

All the initial XPS data on the $Cr(NH_3)_5CF_3SO_3^{3+}$/GaAs system were taken on the VG instrument. This instrument does not have the capability of introducing a sample anaerobically, so additional experiments were performed using the Mark II. A sample was etched with 4:1:1 in an Ar drybox so that no detectable oxide (~$1x10^{-10}$ moles/cm^2) was present on the surface by XPS, and this sample was run in parallel with another piece of GaAs, which had been etched for 30 s in 30% H_2O_2 to leave an oxidized surface.

C. EXFAS

EXAFS experiments were conducted at the Stanford Synchrotron Radiation Laboratory (SSRL) at beam lines II-3, IV-2, and VII-3 using a Si (220) crystal in the monochromator. Data for model compounds were taken by detection of the transmitted x-rays with a nitrogen-filled gas ionization detector. All model compound data were taken at the temperature of the GaAs unknown. Reference Co and Ru foil data for energy calibration were taken with an Ar gas-filled ionization detector

Powder spectra were obtained by packing the unknown or the model at ~10 wt% in BN. The powder was placed in a copper holder (1cm x 4 mm x 1mm), which was positioned in the x-ray beam either on the end of the refrigerated cold finger (Figure 3.1) or in a slot on the single crystal assembly (Figure 3.2). The slits were then closed so that the x-ray beam was not hitting any portion of the copper holder (~1 x 20 mm) and the Co x-ray fluorescence at 6.925 Kev was detected using an Ar gas ionization detector with an Fe filter. A schematic of this apparatus is shown in Figure 3.1. The data for GaAs powder samples were taken at 10 K using a helium refrigerator, or at 77 K using a home-built copper cold finger filled with liquid nitrogen.

The data for single crystal samples were all taken at room temperature, and the Ru K_α fluorescence line at 19.2 keV was detected using a 36 mm diameter, high-purity Ge

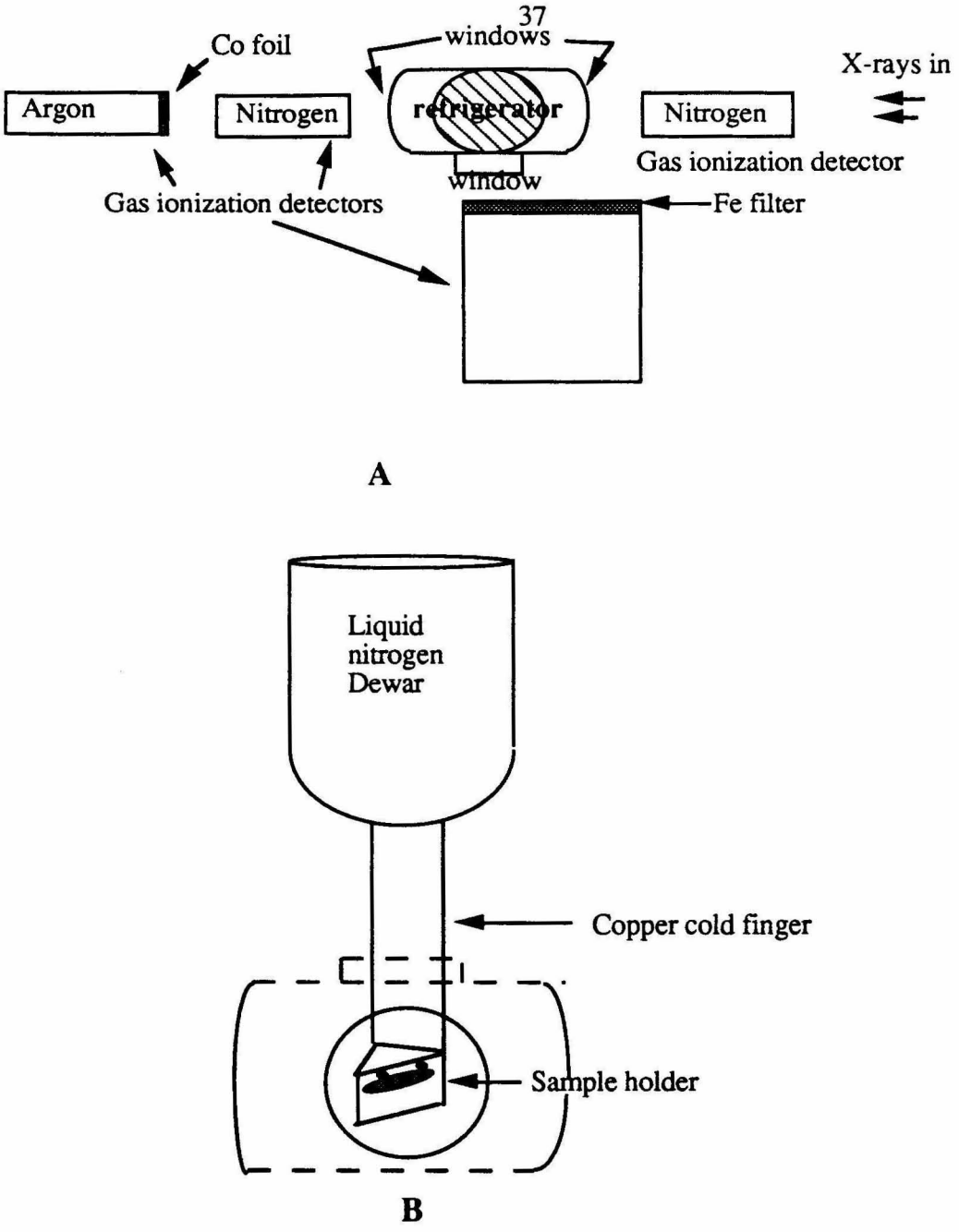

Figure 3.1. a) Schematic of apparatus used for collecting powder EXAFS data at low or ambient temperatures. b) Side view of refrigerator assembly. The refrigerator portion was evacuated to 10^{-6} torr by a diffusion pump (not shown) and the windows were fabricated out of mylar.

Figure 3.2. Schematic of apparatus used for collecting surface EXAFS data.

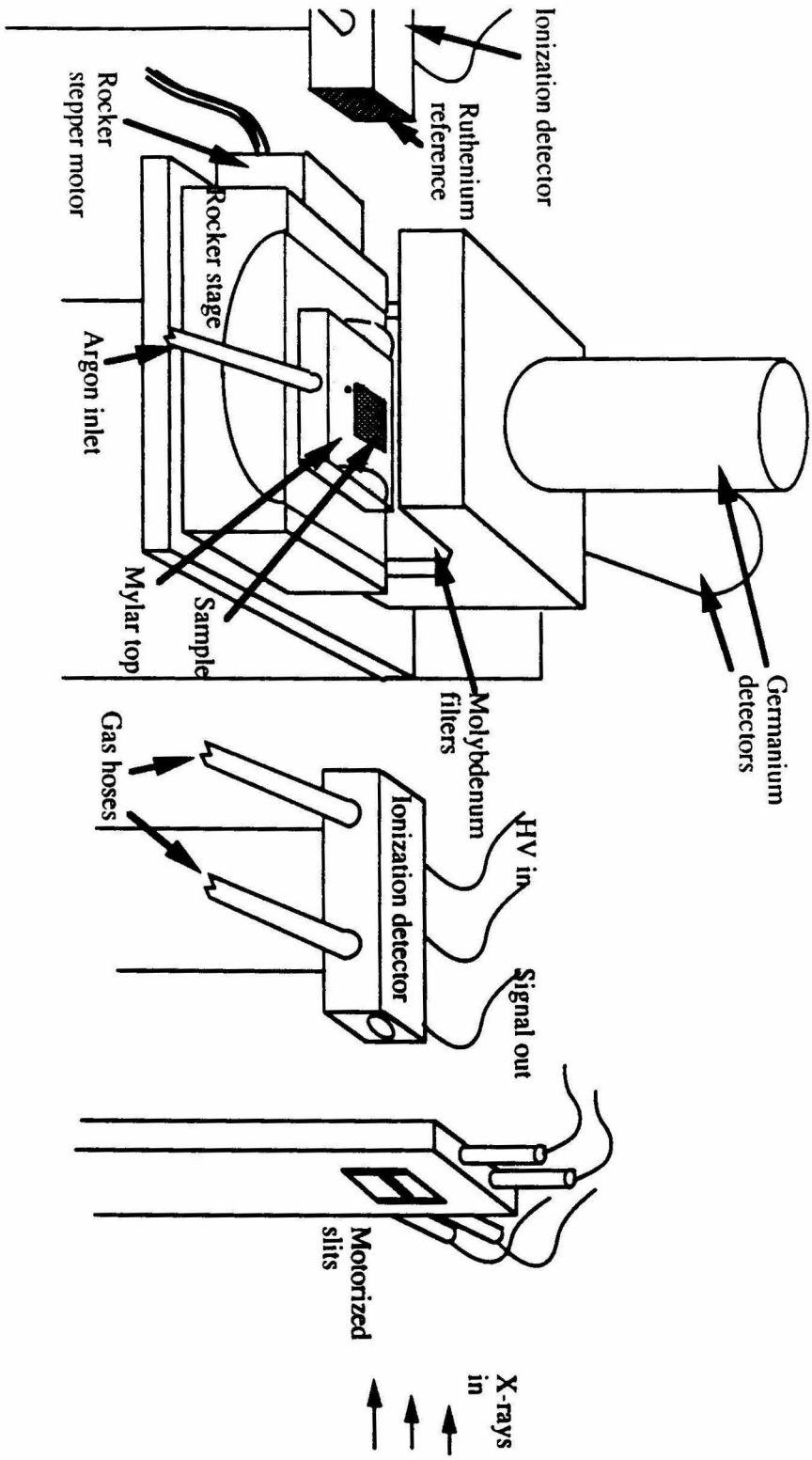
Ionization detector
Ruthenium reference
Rocker stepper motor
Rocker stage
Argon inlet
Mylar top
Sample
Molybdenum filters
Germanium detectors
Gas hoses
Ionization detector
HV in
Signal out
Motorized slits
X-rays in

solid-state detector (Ortec LOAX-36300/15), in conjunction with an amplifier (Tenelec TC244) and a single channel analyzer (Ortec 551).[10] A schematic of this setup is shown in Figure 3.2.

Data for SEXAFS experiments were obtained by positioning a 1" x 1" sample of (100) GaAs, GaP, or InAs so that the x-ray beam (slits were closed so that the beam was ~0.1-0.2 mm tall) was grazing the top of the sample. The sample was then rocked ~1° until total external reflection occurred, and the Ru K_α fluorescence became visible on a multichannel analyzer. The gating electronics on the single-channel analyzer was then adjusted so only the signal from the Ru fluorescence was counted and recorded by the computer.

Once the spectra were obtained, a complex analysis is needed in order to extract the desired structural data.[10] The process is illustrated in Figure 3.3. The general procedure is first to extract the EXAFS out of the full absorption spectrum by subtracting the background. The pre-edge background is approximated by a line (step 1). The post-edge background, which has contributions from processes other than the absorption (e.g. elastic scattering and beam harmonics), is approximated by a cubic spline (step 2). After subtraction of the background, the resulting EXAFS is weighted by a factor of k^3 to amplify the oscillations at higher energies (step 3). The EXAFS is then Fourier transformed (step 4), producing peaks corresponding to the different atomic shells. By back-transforming each peak, the contributions of each shell are separated (step 5). These oscillations are curve-fitted, using parameters from model compounds, to obtain the desired bond length and number of scatters (nearest neighbors). The bond length determinations have an error of about 0.05 Å. The error in the number of nearest neighbors is about 10-20%.[10a] The analysis was done using software procedures developed by R. A. Scott of the University of Illinois.

Figure 3.3. Illustration of data manipulation used to extract structural data from raw X-ray adsorption data.

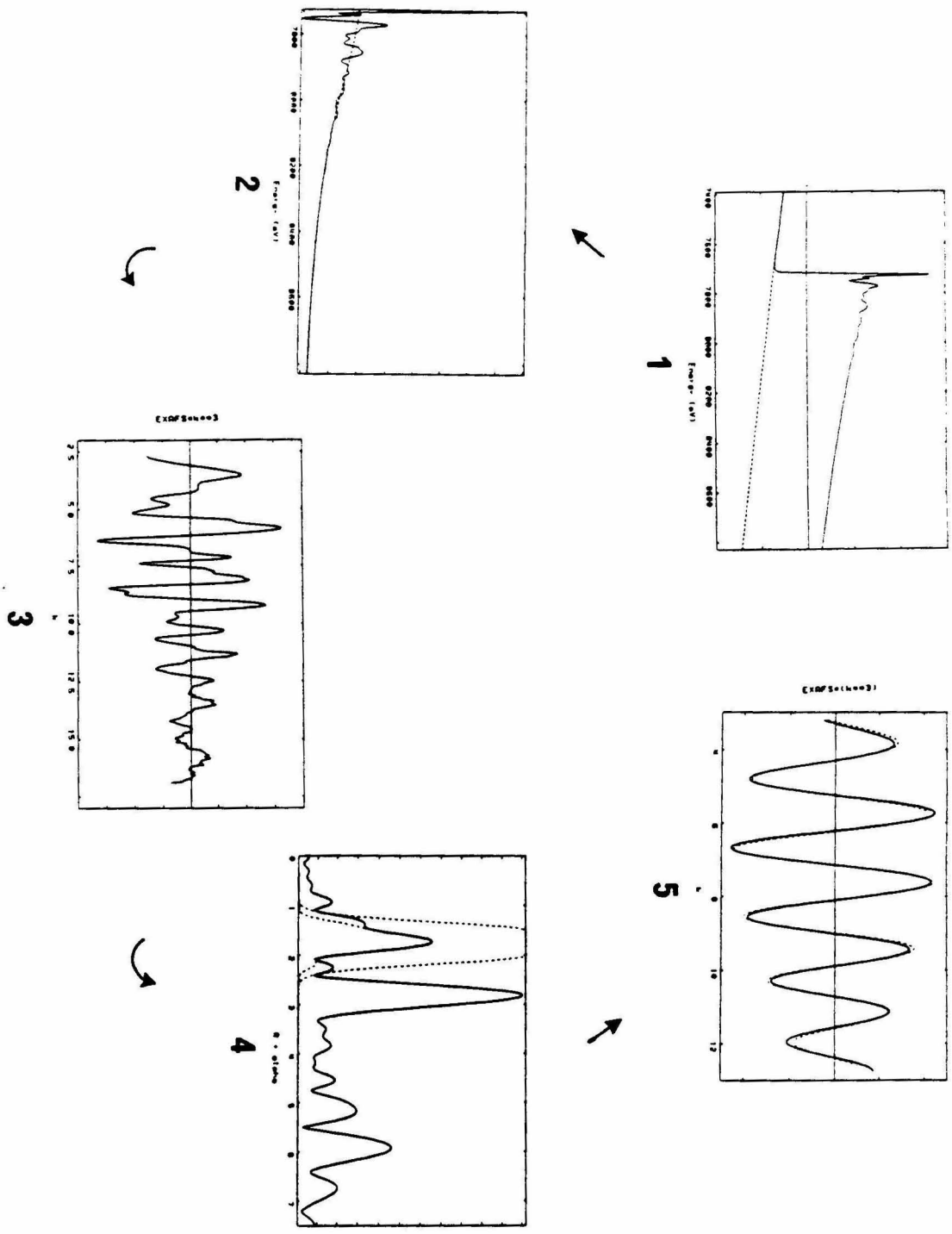
1
2
3
4
5

III. Results and Discussion

A. $Co(NH_3)_5X^{3+}$ on GaAs Powders

The XPS data for a variety of $Co(NH_3)_5X^{3+}$ complexes exposed to GaAs powders and single crystals have been reported earlier.[11] These data showed that Co complexes were reduced from Co^{III} to Co^{II} upon exposure to GaAs, that no ammine ligands were present on the surface, and that a thick film (~60 Å) of a Co-O phase was deposited on the surface. Also, exposure of GaAs to a solution of $Co(2,2\text{-bipyridyl})_3^{3+}$ resulted in the reduction of the Co, and the oxidation of the GaAs surface, but no adsorbed Co was observed by XPS, and no improvement in I-V properties of photoelectrochemical cells using $K_2Se^{-/2-}$ electrolyte.[11] The structure of the Co phase was studied through a series of EXAFS experiments on GaAs powder.

EXAFS and Fourier transforms of the model compounds used for GaAs exposed Co are shown in Figure 3.4 - 3.5. EXAFS of powders exposed to $Co(NH_3)_5H_2O^{2+}$, taken at room temperature and 10^{-6} torr, yielded a spectrum which was extremely similar to EXAFS data for bulk $Co(OH)_2$ (Figure 3.6, 3.4a). The edge absorption position and structure were also quite similar, lending further support to the assignment of the Co^{II} oxidation state to the species on the surface. Using $Co(OH)_2$ as a model compound, analysis of the EXAFS yielded the results given in Table 3.II. We cannot determine whether any of the second-shell atoms are Ga or As because of the very similar scattering properties expected for Co, Ga, and As. However, the high coverage of Co (approximately 10 monolayers by radioisotope and XPS analysis[11]) suggests that most of the Co is in the $Co(OH)_2$ environment.

Comparison of the EXAFS data in Figure 3.6 with that obtained obtained for a sample exposed to $Co(NH_3)_5H_2O^{3+}$ and measured at 10 K or 77 K, or in contact with 0.01 M KOH indicated no significant difference in the EXAFS data or Fourier transforms of these data (Figure 3.6, 3.7 and 3.8), implying that cooling and exposure to vacuum did not induce significant changes in the sample. Exposure of GaAs powder to the complex

Figure 3.4. EXAFS extracted from raw data of a) $Co(OH)_2$, b) $Co(H_2O)_6(ClO_4)_2$, and c) Co(OOH) taken at 77 K in transmission mode.

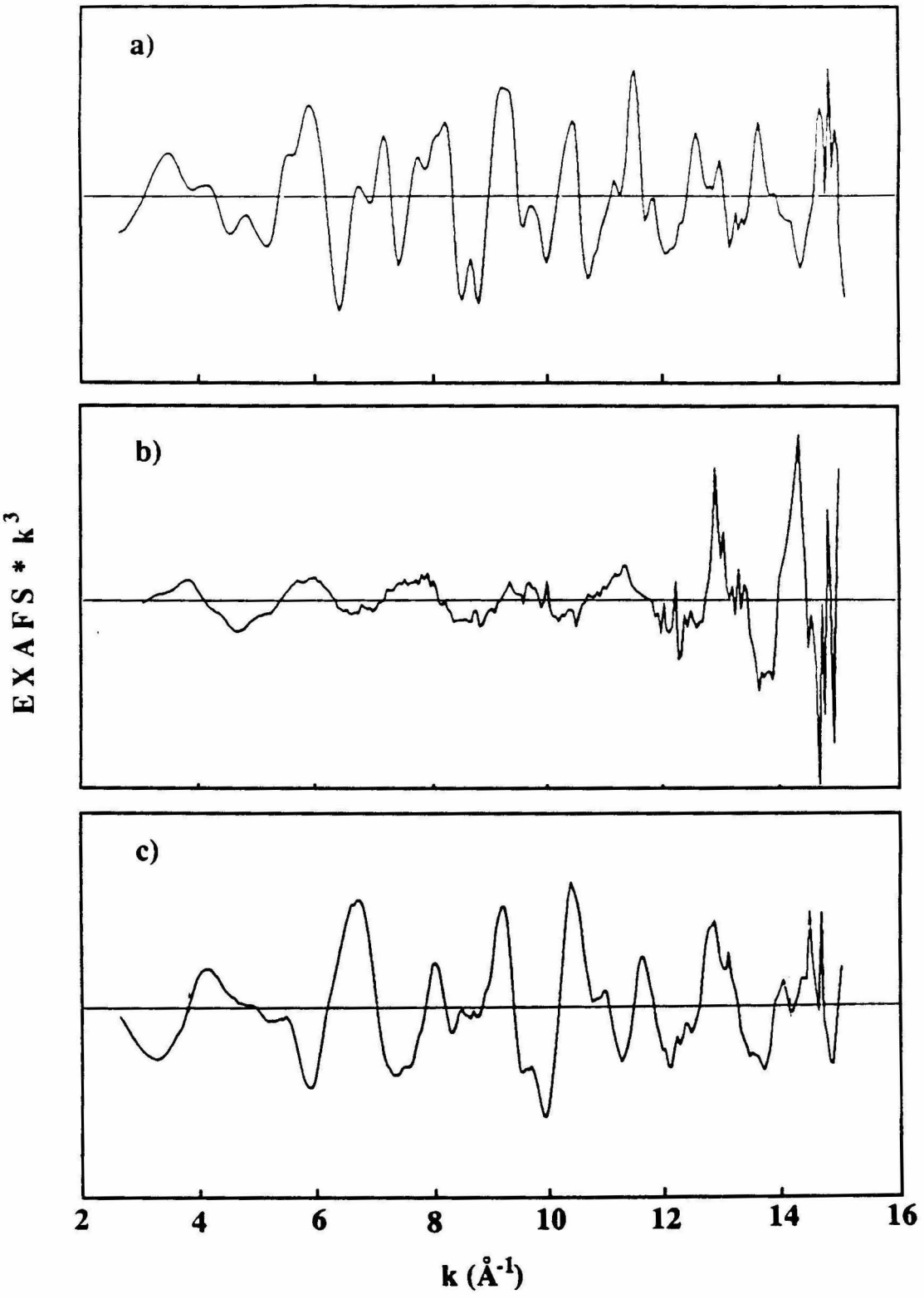
a)
b)
c)
EXAFS * k3
2
4
6
8
10
12
14
16
k (Å-1)

Figure 3.5. Fourier transforms of EXAFS shown in Figure 3.4.

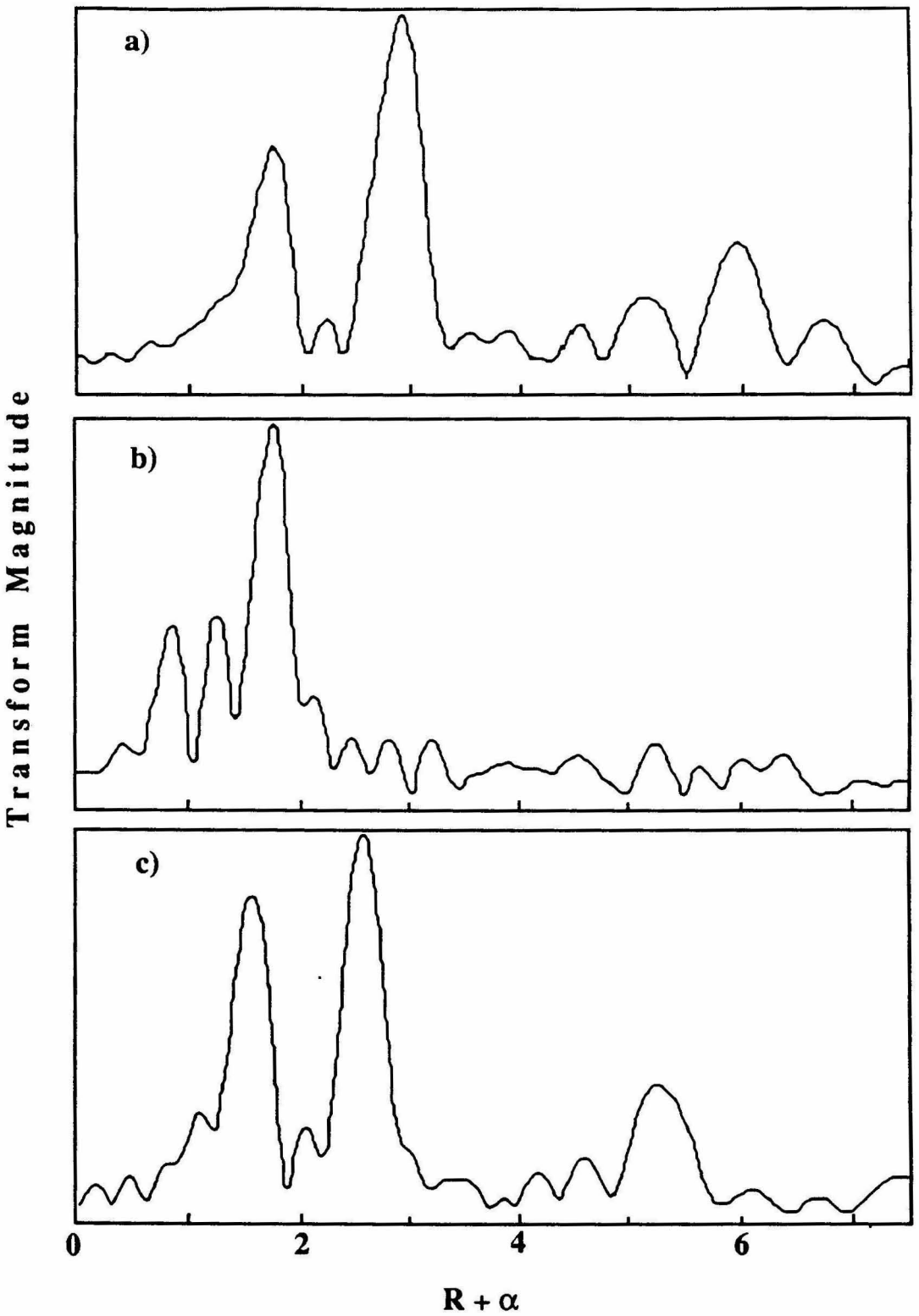
a)
b)
c)
Transform Magnitude
0
2
4
6
R + α

Table 3.II - Bond distances and edge energies for model compounds and best fit numbers for GaAs powders exposed to $Co(NH_3)_5X^{3+}$ using $Co(OH)_2$ as the model compound.

Compound	Bond Distance (Å) (Co-O)	Number of Nearest Neighbors	Bond Distance (Å) (Co-Co)	Number of Nearest Neighbors	Edge Energy (eV)
$Co(OH)_2$	2.097	6.0	3.17	6.0	7719.7
$Co(H_2O)_6(ClO_4)_2$	2.085	6.0			7720.1
Co(OOH)	1.90	6.0			7721.3
	2.69	4.0			
GaAs powder + $Co(NH_3)_5H_2O^{3+}$					
T = 10 K	2.08[a]	7[b]	3.13[a]	7[b]	7720.7
T = 77 K	2.08[a]	8[b]	3.13[a]	8[b]	7720.3
T = 298 K	2.08[a]	7[b]	3.14[a]	7[b]	7720.8
slurry, T = 298 K	2.09[a]	6[b]	3.13[a]	8[b]	7720.7
GaAs powder +					
Co^{II} (aq)[c]	2.08[a]	6[b]	3.13[a]	8[b]	7720.3
$Co(NH_3)_5N_3^{3+}$[d]	2.08[a]	7[b]	3.12[a]	6[b]	7720.7

[a]The error on the bond distances is ± 0.05 Å.

[b]The error on the number of nearest neighbors is ± 1. The numbers are slightly higher than expected because of interference from the Cu sample holder.

[c]Data taken at 10 K.

[d]Data taken at 77 K.

$Co(NH_3)_5N_3^{3+}$ (77 K), and aqueous Co^{II} ions also yielded an x-ray absorption spectrum that was also extremely similar to $Co(OH)_2$ (Figure 3.9).

The fact that similar EXAFS, bond distances, and number of nearest neighbors were obtained in the case of GaAs powders exposed to the azide and aquo ammines as well as aqueous Co^{II} ions (Figures 3.6-3.9, Table 3.II) is consistent with a mechanism whereby the Co^{III} complex is reduced by the GaAs substrate, loses its ligands, and forms $Co(OH)_2$,

Figure 3.6. a) Raw x-ray fluorescence data; b) EXAFS, and c) Fourier Transform for GaAs powder exposed to $Co(NH_3)_5H_2O^{3+}$. Data were taken at 10^{-6} torr at room temperature in the fluorescence mode. The dashed line in part b) is the two shell fit of the filtered EXAFS using $Co(OH)_2$ as the model compound.

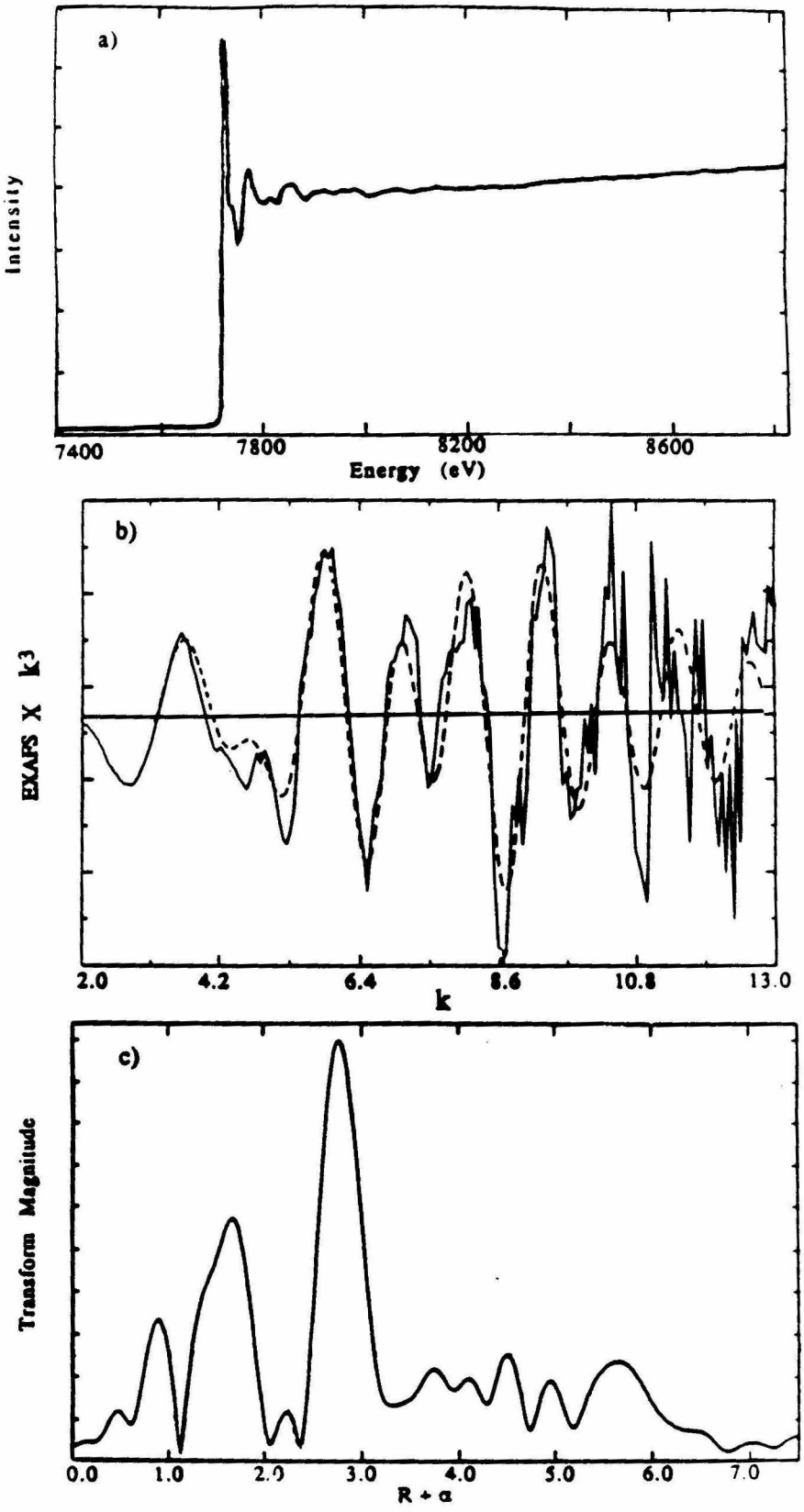
a)
Intensity
7400
7800
8200
8600
Energy (eV)
b)
EXAFS X k3
2.0
4.2
6.4
8.6
10.8
13.0
k
c)
Transform Magnitude
0.0
1.0
2.0
3.0
4.0
5.0
6.0
7.0
R + α

Figure 3.7 EXAFS of GaAs exposed to $Co(NH_3)_5H_2O^{3+}$. Data taken at a) room temperature, b) T = 77 K, c) T= 10 K, d) in contact with 0.01 **M** KOH. a) and b) were taken at a pressure of 10^{-6} torr.

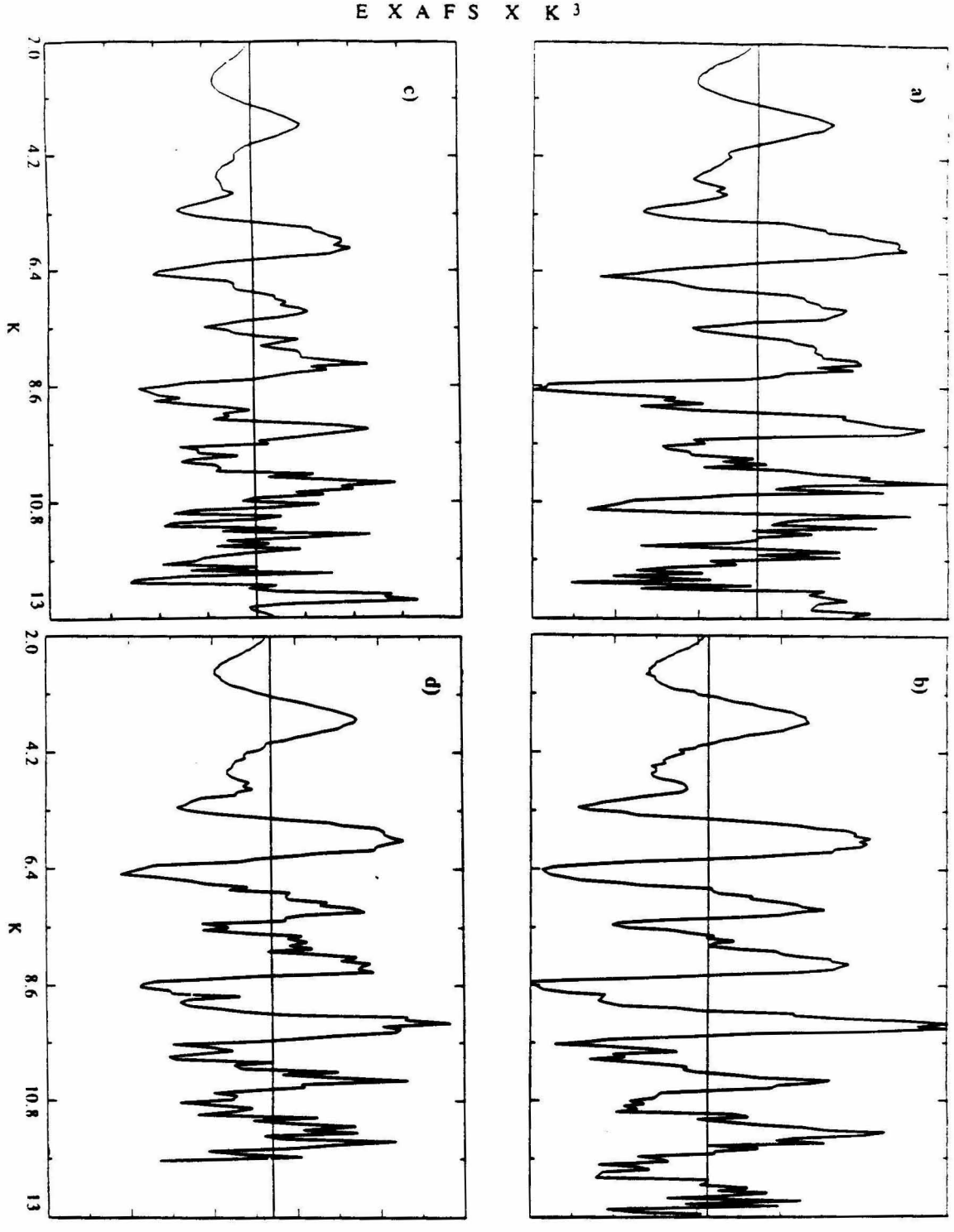
EXAFS X K3
a)
b)
c)
d)
2.0
4.2
6.4
8.6
10.8
13
K

Figure 3.8. Fourier transforms of EXAFS in Figure 3.7.

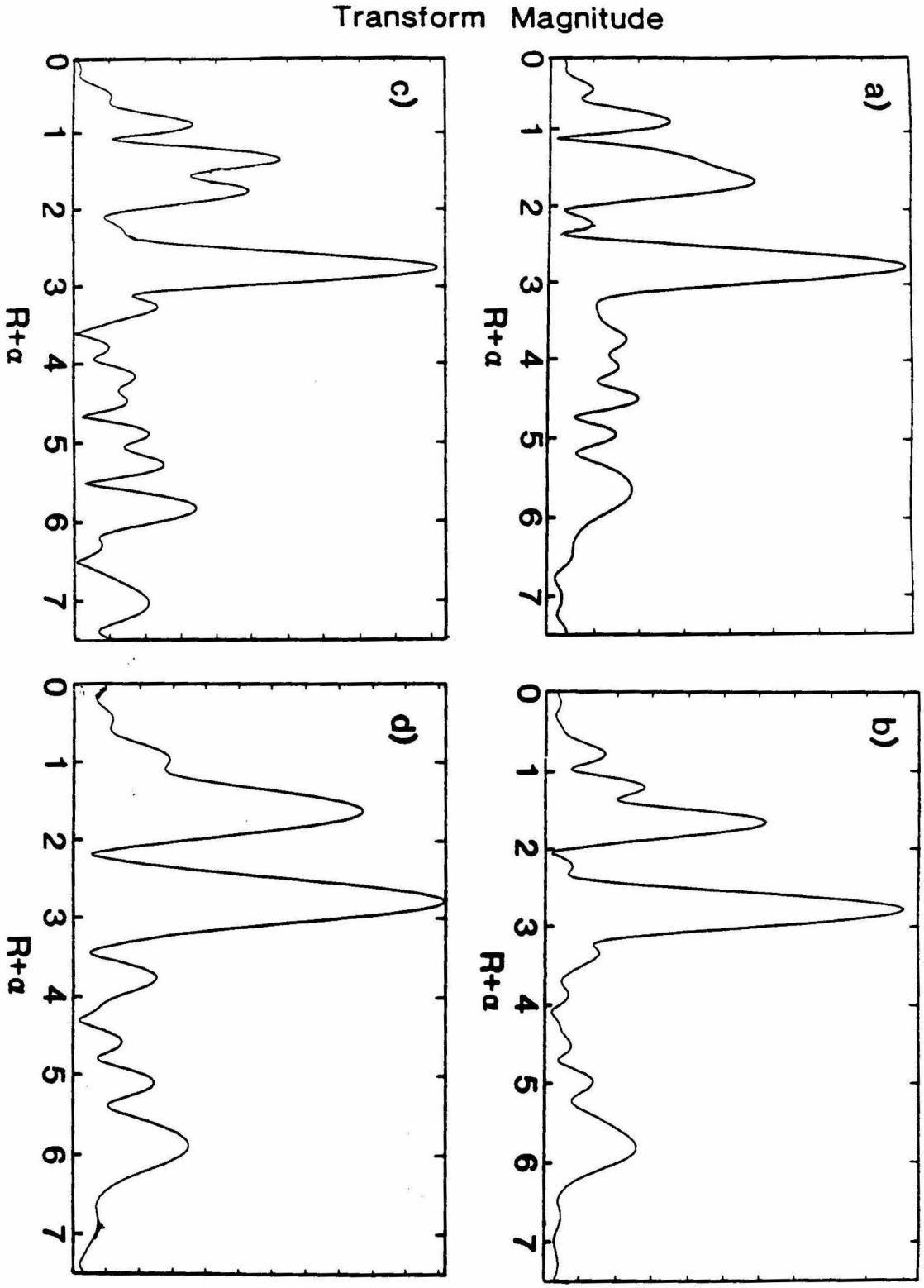
Transform Magnitude
a)
b)
c)
d)
R+α
0
1
2
3
4
5
6
7

Figure 3.9. a) EXAFS for GaAs powder treated with $Co^{II}(H_2O)_6$ at pH 12, b) Fourier transform of EXAFS in part a). c) EXAFS of GaAs powder treated with $Co(NH_3)_5N_3^{2+}$ at pH 11, d) Fourier transform of EXAFS in part c). The dashed line in a) and c) is the two-shell fit of the filtered EXAFS, using $Co(OH)_2$ as the model compound. Data were taken at T= 77K, p= 10^{-6} torr.

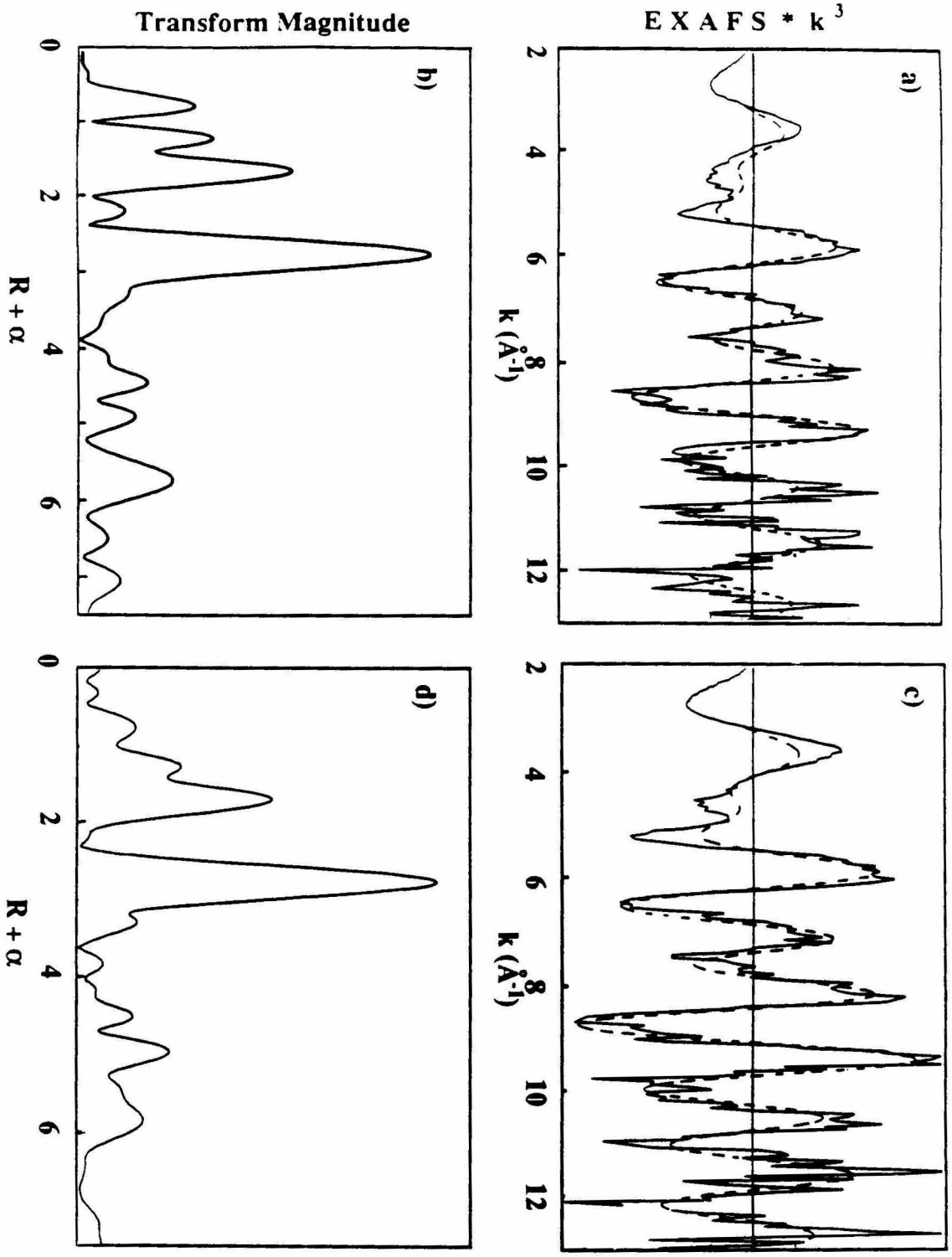
EXAFS * k 3
Transform Magnitude
a)
b)
c)
d)
k (Å-1)
R + α
2
4
6
8
10
12
0
2
4
6

which is insoluble at a high pH. This conclusion is further supported by the observation that electrochemical studies using aqueous Co^{II} ions without the ammines as the starting complex showed that there was an improvement in I-V properties of GaAs in the KOH-$Se^{-/2-}$ test electrolyte, though the improvement was not as great as that from treatment by Co^{III} ammine complexes.[11] Also, at lower pH, the $Co(OH)_2$ dissolved off the surface and no beneficial effect on the I-V behavior of the semiconductor/liquid junction was observed.[11]

The analysis of the EXAFS of GaAs powders exposed to cobalt ions in basic solution shows conclusively that a $Co(OH)_2$ surface phase is formed, but this is most likely not the phase that is present on the surface after exposure to the KOH-$Se^{-/2-}$ used for electrochemical studies. When GaAs powder was exposed to $Co(NH_3)_6^{3+}$, then selenide solution, the EXAFS shown in Figure 3.11b was obtained.

A comparison of the edge and EXAFS of the treated GaAs samples to the $CoSe_2$ model compound shows some dissimilarities. The edge of the $CoSe_2$ is at lower binding energy, implying that the cobalt in $CoSe_2$ is in a nominally lower oxidation state. However, the edge structure of the Co-treated GaAs samples are very similar with and without exposure to Se. The near edge or XANES region is a good indicator of the geometry of the scatterer[12] and thus indicates that the complex is still predominantly in the same octahedral geometry before and after selenium exposure. The Fourier transforms of the model and GaAs spectra both show a single shell at about the same R value (Figure 3.10c, 3.11c). Best-fit values using the $CoSe_2$ model for the hexaammine, and pentaammineaquo complexes are given in Table 3.III.

The above data for GaAs powders exposed to cobalt ions and then selenide solution indicate that the selenium becomes incorporated into the inner shell. EXAFS is an average over all the contributing absorber atoms, and a mixed oxide-selenide layer may be present; since selenium will dominate the backscattering, any residual oxygen will not be visible. A fit of the $Co(NH_3)_5H_2O^{3+}$ with $CoAs_3$ as the model gave a significantly worse fit to the

Figure 3.10. a) Normalized x-ray transmission data; b) EXAFS, and c) Fourier transform for $CoSe_2$ diluted with BN. Data were taken at 77 K and 10^{-6} torr.

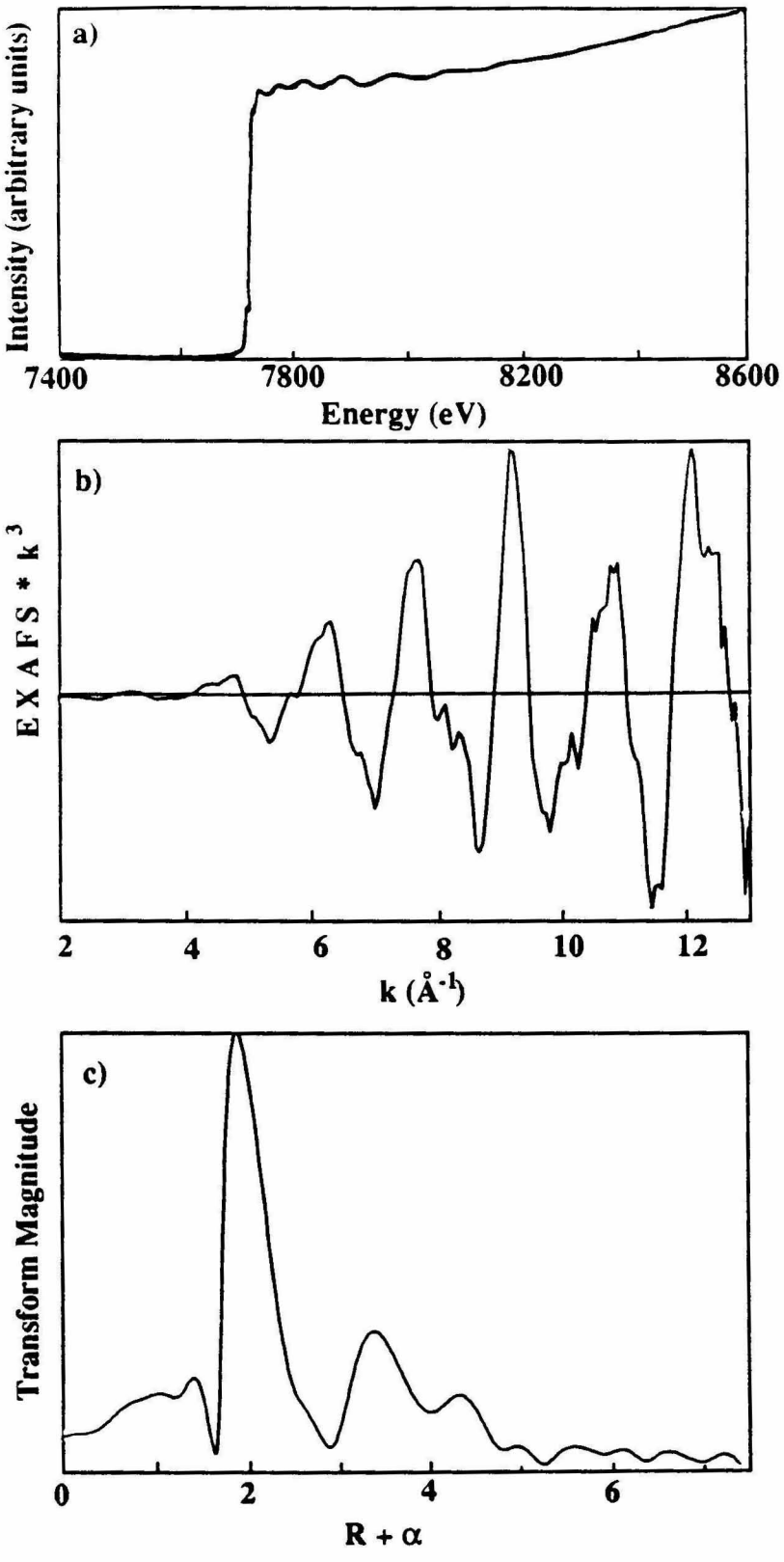
a)
Intensity (arbitrary units)
7400
7800
8200
8600
Energy (eV)
b)
E X A F S * k 3
2
4
6
8
10
12
k (Å-1)
c)
Transform Magnitude
0
2
4
6
R + α

Figure 3.11. a) Raw x-ray fluorescence data for GaAs powder treated with $Co(NH_3)_6^{3+}$ at pH 11 and exposed to $Se^{-/2-}$ - KOH; b) EXAFS and single-shell fit (dashed line) of filtered EXAFs data using $CoSe_2$ as a model. c) Fourier transform of EXAFs in b). Data were taken at 77 K and 10^{-6} torr.

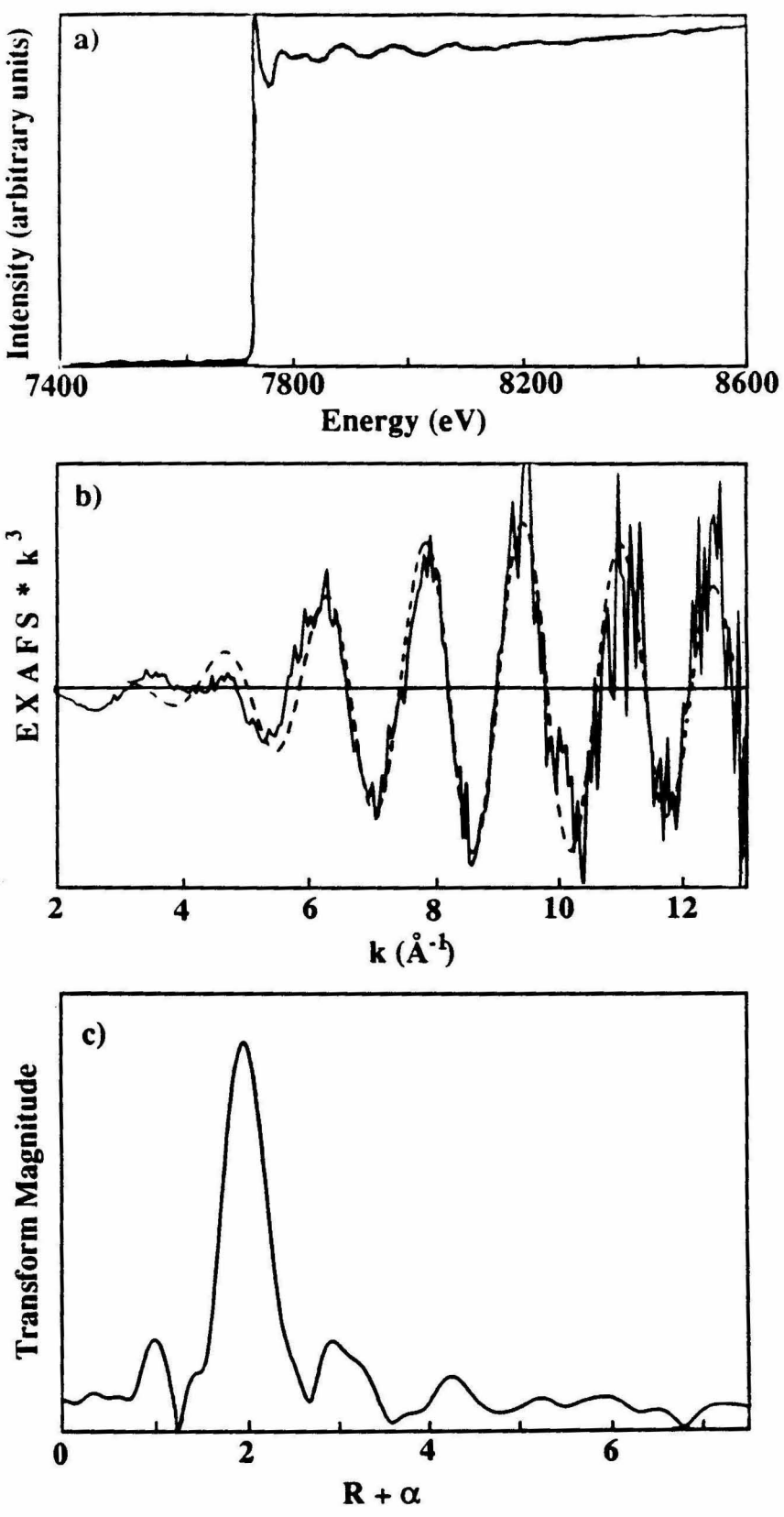
a)
Intensity (arbitrary units)
7400
7800
8200
8600
Energy (eV)
b)
EXAFS * k 3
2
4
6
8
10
12
k (Å-1)
c)
Transform Magnitude
0
2
4
6
R + α

Table 3.III Bond distances and edge energies for model compounds and best-fit numbers for GaAs powders exposed to $Co(NH_3)_5X^{3+}$ + KOH-$K_2Se^{-/2-}$ using $CoSe_2$ as the model compound.

Compound	Bond Distance (Å) (Co-Se)	Number of Nearest Neighbors	Edge Energy (eV)
$CoSe_2$	2.42	6.0	7716.2
$CoAs_3$	2.34	6.0	7717.0
GaAs+1.0 **M** $K_2Se^{-/2-}$ - 1.0 **M** KOH+			
$Co(NH_3)_5H_2O^{3+}$ (T = 10 K)	2.36[a]	5[b]	7717.1
$Co(NH_3)_6^{3+}$ (T = 77 K)	2.34[a]	5[b]	7719.0

[a]The error on the bond distances is ± 0.05 Å.

[b]The error on the number of nearest neighbors is ± 1.

data, and along with XPS studies,[11] lends further support to the proposal that Se is the heavy scatterer incorporated into the inner shell. The electrocatalytic effects of the cobalt and selenium overlayer are consistent with work done by Hodes, Manassen, and Cahen on CoS electrodes.[13] They studied several electrodes in sulfide solutions (e.g., CuS, PbS, CoS) and found that CoS showed a decrease in overpotential for sulfides compared to a platinum electrode.

B. $Ru(NH_3)_5H_2O^{2+}$ on GaAs, GaP and InAs

The Co results showed that redox chemistry can be important in the interaction of metal ions with GaAs surfaces. Unfortunately, the thickness of the $Co(OH)_2$ film formed from the reduction of cobalt ammines precluded the observation of the surface bound metal ion for that system. Other metal ammine complexes ($Ru(NH_3)_5H_2O^{2+}$, $Cr(NH_3)CF_3SO_3^{3+}$) have reduction potentials significantly negative of Co^{III}, and so would not be expected to undergo this type of reaction.[14] These complexes do indeed exhibit a

much lower surface coverage than Co and so offer an opportunity to observe directly the GaAs binding site.

Accurate XPS data of Ru are difficult to obtain, because of the interference of the C 1s and Ru 4d lines.[15] The XPS spectra for $Ru(NH_3)_5H_2O^{2+}$ on GaP, GaAs, InAs, and GaAs that had been deliberately oxidized prior to exposure, are shown in Figure 3.12. The observation of the ammine ligands is hindered by the overlap of the Ga Auger lines on the GaAs and GaP sample; however, it can be clearly seen on the InAs substrate (Figure 3.12d). Estimated coverages and ratios are given in Table 3.IV. There does not appear to

Table 3.IV. XPS data for GaAs, InAs and GaP exposed to $Ru(NH_3)_5H_2O^{2+}$ for 1hr. Data were taken on the SSI system with a spot size of 300 μm for individual regions. All ratios are normalized using appropriate cross sections. Ga, As, Ru and N binding energies are reported with respect to C 1s = 285.0 eV. These samples were confirmed to have no oxide present (except for the intentionally oxidized sample) initially after treatment and prior to EXAFS experiments, but all showed a large amount of oxidation after the EXAFS experiments and it is on these surfaces that the Ru and N data were obtained.

Substrate	Ga 3d (eV)	As 3d (eV)	III / V	C 1s (eV)	Ru 3d (eV)	N 1s (eV)	Ru / As	N / Ru	Γ_{Ru} x10^9 (moles/cm^2)
GaAs	19.5	41.5	1.0	284.8	280.6	400.3	0.5	9	1.3
GaAs (oxidized)	19.8 21.4[a]	41.7 45.7[a]	1.0	284.6	279.4	399.6	0.3	13	1.8
GaP	19.6	129.1[b]	1.8	285.7	280.7	402.6	0.8[c]	9	2.5
InAs	17.8[d]	41.3	1.3	284.6	281.3	400.6	0.4	5	1.4

[a]Energies for substrate oxides.

[b]P 2p energy.

[c]Ratio taken with respect to P area.

[d]In $4d_{5/2}$ energy.

Figure 3.12. Ru 3d XPS regions for a) GaAs, b) InAs and c) GaP exposed to 0.01 **M** $Ru(NH_3)_5H_2O(PF_6)_2$ at pH=1. Also shown are the N 1s regions for d) GaAs, e) InAs and f) GaP. Data were taken on an SSI Model 100 system using monochromatic Al K_α X-rays.

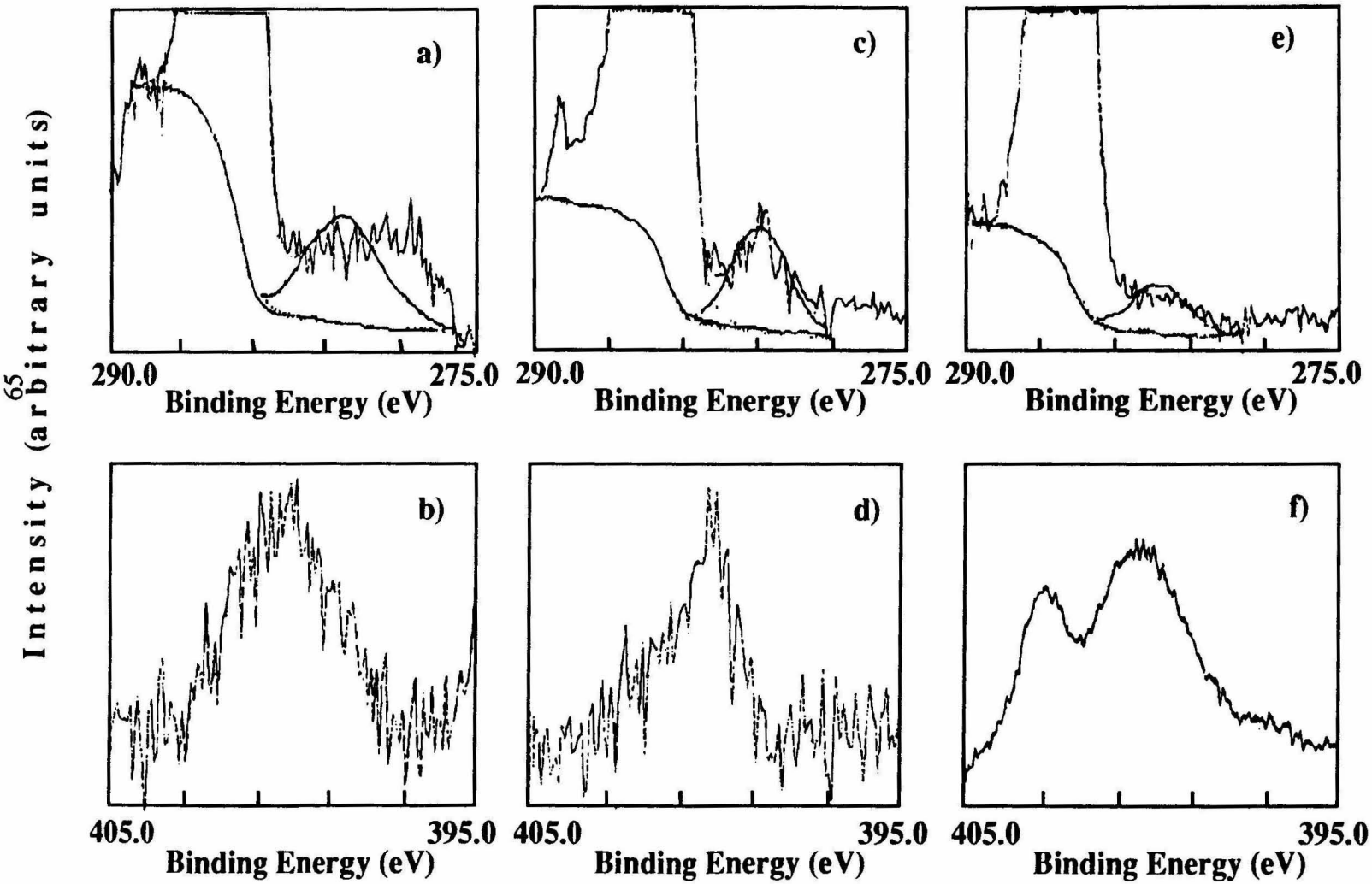
a)
c)
e)
b)
d)
f)
290.0
275.0
405.0
395.0
Binding Energy (eV)
Intensity (arbitrary units)

be a significant difference in coverage of chemisorbed metal on initially oxidized vs. cleanly etched GaAs surfaces. The ratio of N/Ru on InAs was in agreement with that expected for ruthenium pentaammine.

There is a large amount of spread of the data in Table 3.IV because of the low signal to noise ratio associated with the Ru peaks (Figure 3.12). This uncertainty also limits the accuracy of the coverage estimates. The presence of Ru on all substrates was confirmed by secondary ion mass spectrometry (SIMS).[16] While a quantitative estimation of the coverage cannot be obtained without several control experiments to determine cross sections, the relative intensity of the Ru signal was constant on all three types of substrates and indicates approximately the same metal coverage. SIMS data also confirm that there is approximately the same amount of Ru present whether or not the GaAs substrate had been oxidized or cleanly etched prior to exposure to $Ru(NH_3)_5H_2O^{2+}$.

Additional data on the coverage of Ru on GaAs and GaP surfaces were obtained from Rutherford backscattering (RBS) measurements. This technique provides a more accurate estimate of the coverage because the calculation relies on more well-known parameters.[17] The estimated coverage from RBS is ≤ 0.25 monolayer for GaAs and GaP. An exact coverage could not be obtained because this is the detectability level of the technique, and the signal was barely observable. This technique cannot be used on InAs because In is a heavier atom than Ru, and would obscure the Ru signal. The calculated coverages from XPS data are considerably higher (~1-2 monolayers, since 1 monolayer $\sim 1.4 \times 10^{-9}$ moles/cm^2), but this is most probably a function of the large number of assumptions that must be made in order to estimate photoelectron escape depths for unknown compounds. Cross sections are known to much better accuracy, and so the mole ratios of the constituents from XPS are much more reliable numbers.

EXAFS spectra were obtained for GaAs powder exposed to aqueous $RuCl_3$ (pH = 1), and the x-ray fluorescence data are shown in Figure 3.13. Better data was obtained by surface EXAFS (SEXAFS) of (100) GaAs exposed to $Ru(NH_3)_5H_2O^{2+}$, and it is

Figure 3.13. X-ray adsorption edge for GaAs treated with $RuCl_3$ (aq) at pH 1. X-ray fluorescence was taken at room temperature and detected by a Ge detector. The spectrum shown is an average of three scans.

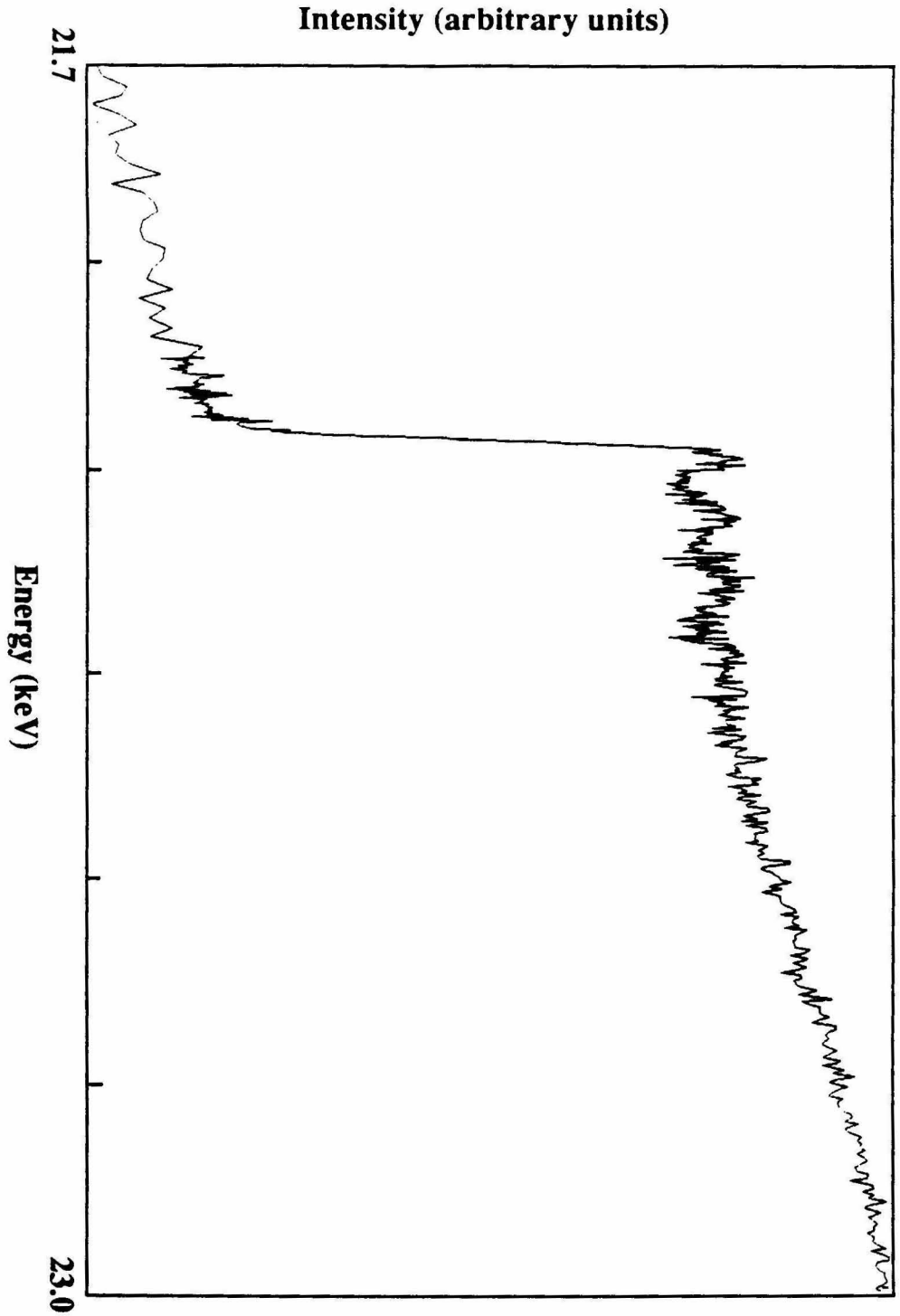
Intensity (arbitrary units)
21.7
23.0
Energy (keV)

Figure 3.14. a) X-ray absorbance data, b) EXAFS and c) Fourier transform of $Ru(NH_3)_6Cl_2$. The x-ray transmission was detected at room temperature using a N_2-filled ionization detector.

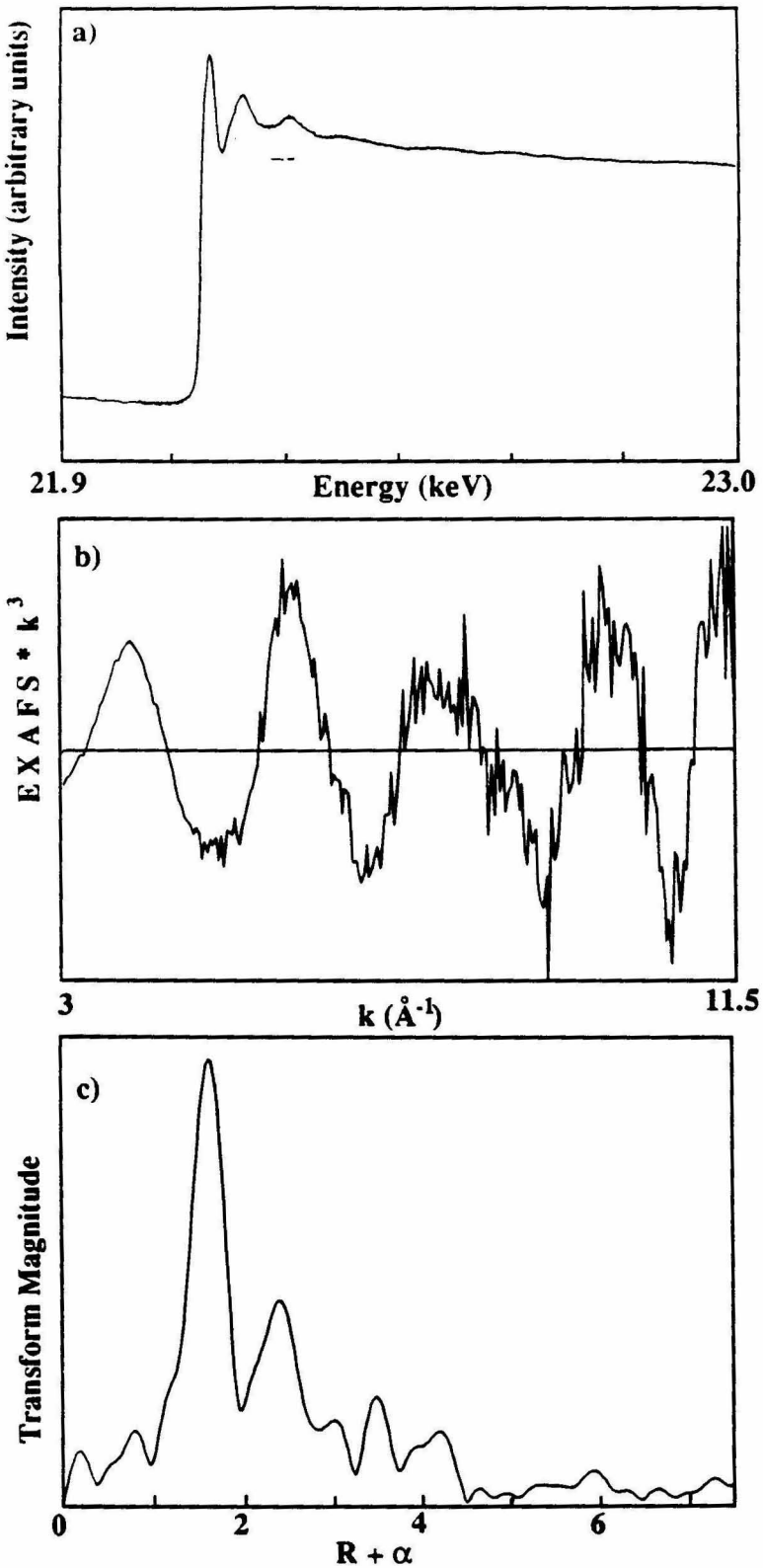
a)
Intensity (arbitrary units)
21.9
Energy (keV)
23.0
b)
E X A F S * k 3
3
k (Å-1)
11.5
c)
Transform Magnitude
0
2
4
6
R + α

Figure 3.15. a) Raw data, b) EXAFS and c) Fourier transform of $Ru(NH_3)_5H_2O^{2+}$ adsorbed on (100) GaAs. The Ru x-ray fluorescence was detected at room temperature using Ge detectors. The data shown are an average of twelve scans. The plain solid line in b) is the best fit obtained using $Ru(NH_3)_6^{2+}$ as a model compound.

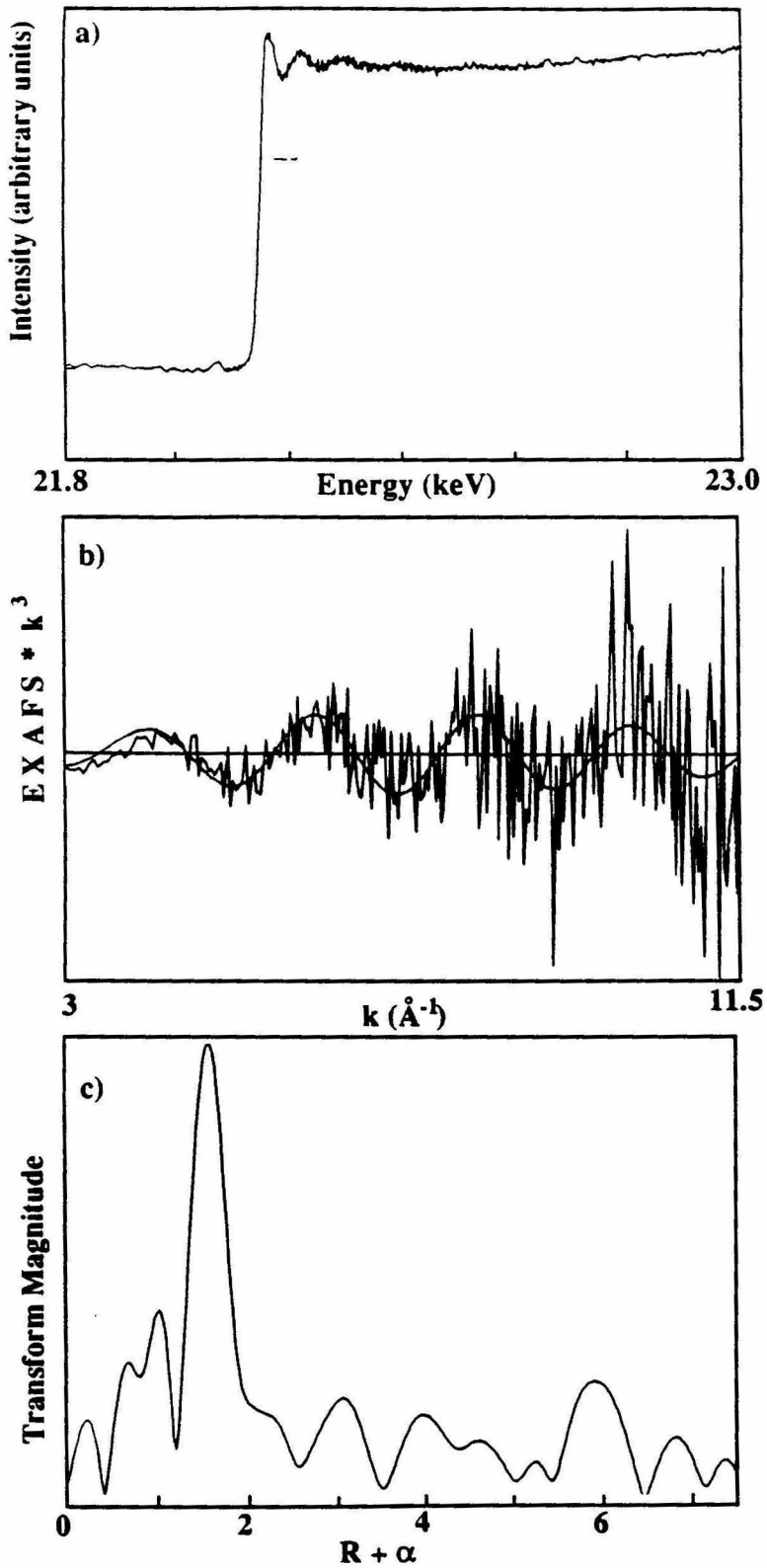
a)
Intensity (arbitrary units)
21.8
Energy (keV)
23.0
b)
EXAFS * k 3
3
k (Å-1)
11.5
c)
Transform Magnitude
0
2
4
6
R + α

Figure 3.16. X-ray adsorption edges of a) $RuCl_3$ on GaAs powder and b) $Ru(NH_3)_5H_2O^{2+}$ (dashed curves) on single crystal (100) GaAs compared to $Ru(NH_3)_6Cl_3$ (right-hand solid curve) and $Ru(NH_3)_6Cl_2$ (left-hand solid curve).

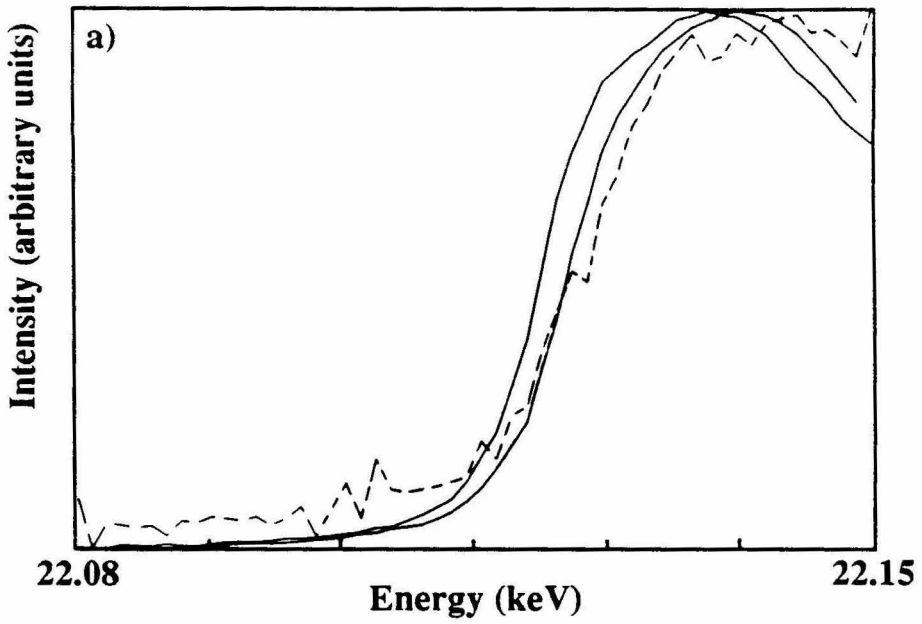
a)
Intensity (arbitrary units)
22.08
22.15
Energy (keV)

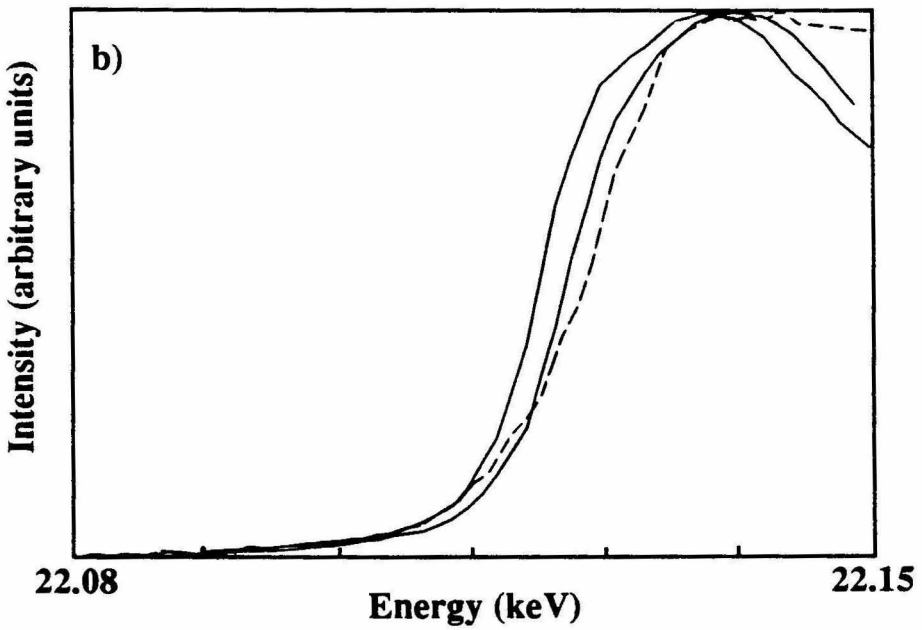
b)
Intensity (arbitrary units)
22.08
22.15
Energy (keV)

somewhat similar to data obtained from a sample of $Ru(NH_3)_6Cl_2$ (Figure 3.14 vs. Figure 3.15).

The position of the x-ray adsorption edge is indicative of the oxidation state and shows that the ruthenium is probably in the 3+ oxidation state for the $RuCl_3$ case (Figure 3.16a). Unfortunately, the signal-to-noise ratio is too low to allow the EXAFS to be reliably fit to obtain any structural data. The position of the adsorption edge for the $Ru(NH_3)_5H_2O^{2+}$ indicates that the Ru is also in the 3+ oxidation state (Figure 3.16b), which is not surprising, since XPS of the Ga and As regions taken after the SEXAFS was obtained clearly showed the presence of Ga and As oxides. The SEXAFS data were gathered over a period of > 24 hrs., and even under flowing Ar there apparently was sufficient leakage of O_2 to oxidize the surface.

EXAFS obtained from the raw spectra is shown in Figure 3.15b, as well as the best fit to the data using $Ru(NH_3)_6^{2+}$ as a model compound. The calculated values were number of nearest neighbors = 5 and bond distance = 2.07 Å. The calculated fit is very close to the actual data at lower **k** values, but diverges considerably at **k** > 9. The cause of the divergence could be either due to the presence of a heavy scatterer (e.g., As) incorporated in the first shell or due to excessive noise. The cross section for backscattering is dependent on the atomic number of the backscatterer as well as on the energy.[20] As can be seen from Figure 3.17, the backscattering amplitude for light scatters such as N or O would fall off sharply as a function of k, while Ga or As, which are very close to Ge, has a peak at ~8 k. A heavy scatterer, such as As, in the first shell would therefore be expected to increase the amplitude of the EXAFS at higher **k**, and the EXAFS of the $Ru(NH_3)_5H_2O^{2+}$ bound to an As or Ga on the surface should not fit well to a $Ru(NH_3)_6^{2+}$ model at higher **k** values. A lighter scatterer, such as O, would be expected to be very close to N as a scatterer, and so the EXAFS should be well modeled by $Ru(NH_3)_6^{2+}$.

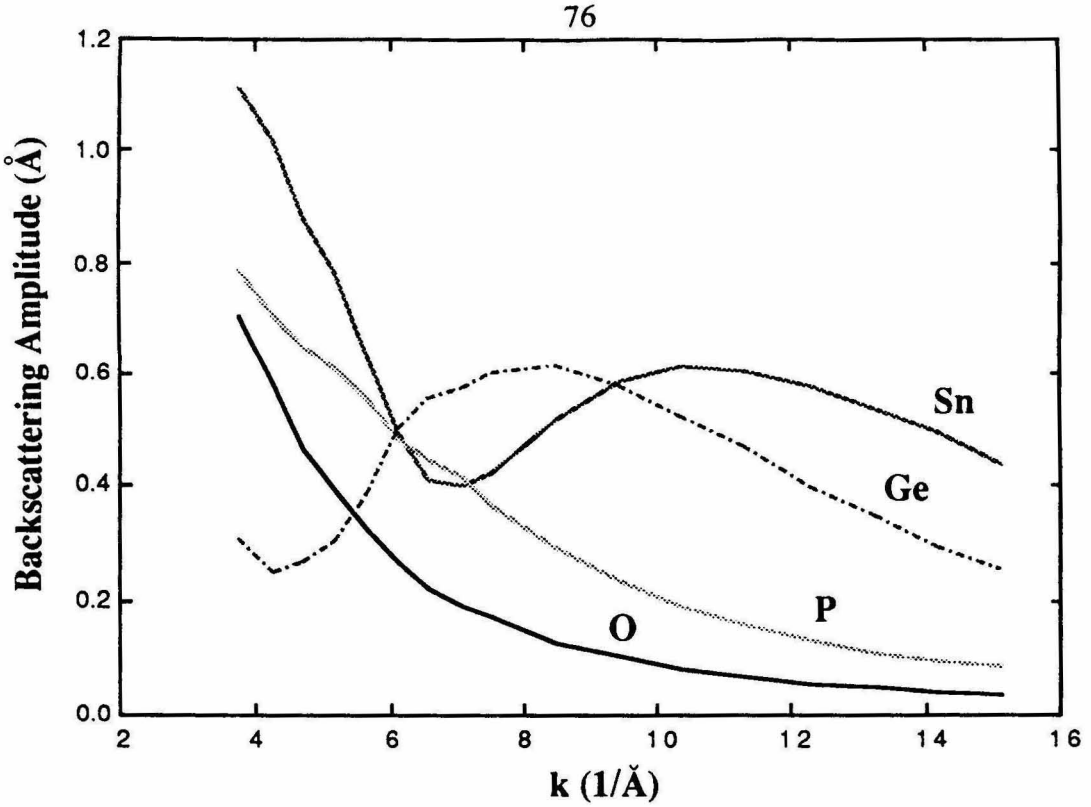

Figure 3.17. Calculated backscattering amplitude for representative atoms from Reference 18.

Separation of Ga from As as a scatterer can be achieved by comparing EXAFS data from InAs, GaAs and GaP, since In has a quite different envelope function than Ga, and P is different from As. If Ru is binding exclusively to As, EXAFS obtained from GaAs surfaces should be the same as that obtained from InAs surfaces, but different from that from GaP surfaces, especially at higher **k**. GaP and InAs SEXAFS have also been obtained (Figure 3.18); however, the large "humps" present in the background preclude the separation of the EXAFS from the background, and thus extraction of structural data. There does appear to be some difference in the near-edge region for the InAs surface, possibly because of the effects of secondary scattering from the much heavier In atom. Regardless, better data need to be gathered with better signal to noise and a more well-

Figure 3.18. Raw x-ray fluorescence data for $Ru(NH_3)_5H_2O^{2+}$ adsorbed on single crystal (100) a) GaP (average of eighteen scans) and b) InAs (average of twelve scans). X-ray fluorescence was taken at room temperature and detected by a Ge detector.

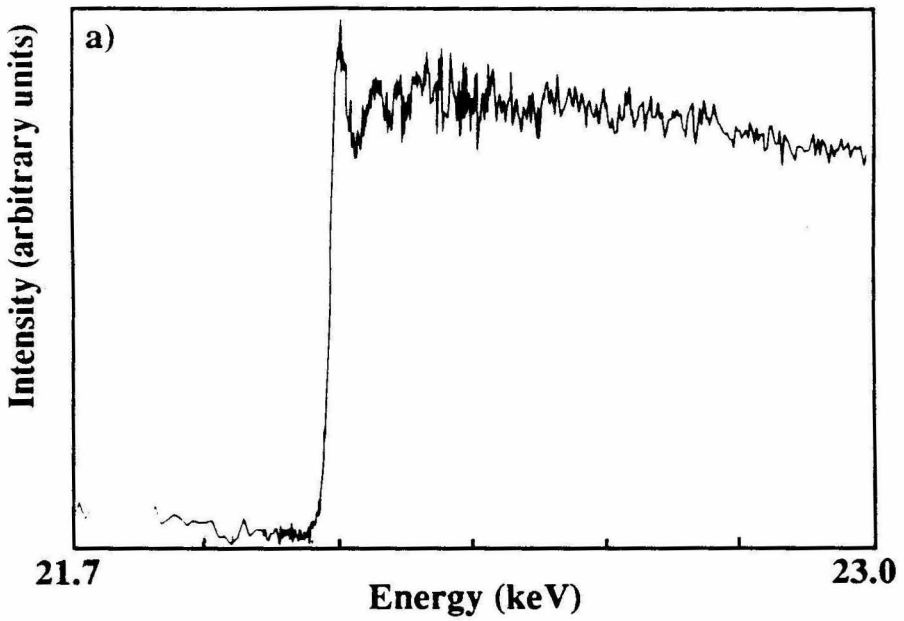
a)
Intensity (arbitrary units)
21.7
23.0
Energy (keV)

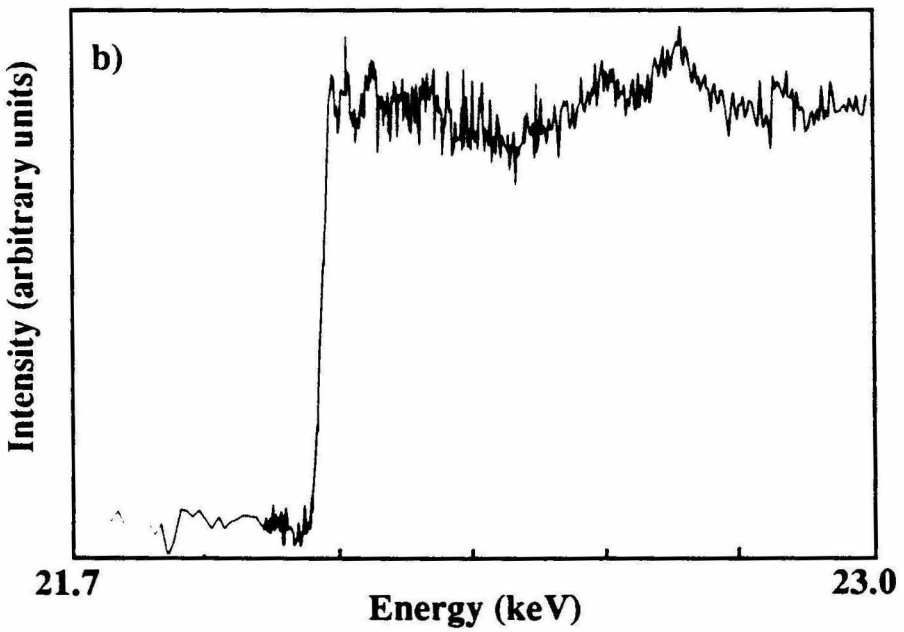
b)
Intensity (arbitrary units)
21.7
23.0
Energy (keV)

behaved background function before the question of the composition of the Ru inner shell can be answered definitively.

C. $Cr(NH_3)CF_3SO_3^{3+}$ on GaAs

Cr ammines have a much slower rate constant for substitution than the Ru or Co ammines;[19] therefore, the pentaammine triflate was used instead of the pentaammine aquo complex in order to decrease the time required to treat the samples. XPS data show that this Cr complex, like $Ru(NH_3)_5H_2O^{2+}$ adsorbs on GaAs surfaces at very low coverages (see Table 3.V, Figure 3.19), and that Cr was in the 3+ oxidation state. Unlike $Ru(NH_3)_5H_2O^{2+}$, there is a correlation between the amount of oxide on the surface and the adsorption of Cr. Also, a sample of etched GaAs which was place in a 0.01 **M** solution of substitutionally inert $Cr(bipyridyl)_3(ClO_4)_3$ showed no detectable Cr by XPS after 15 hours, indicating that the $Cr(NH_3)_5CF_3SO_3^{3+}$ is reacting with the surface.

The reaction is not completely selective, as a small amount of Cr was observed even on a sample that was cleanly etched in a drybox before exposure to $Cr(NH_3)_5CF_3SO_3^{3+}$ for 2 hrs., but about twice the level of Cr was observed on the heavily oxidized sample run in parallel (samples 1,2,3, a and b, Table 3.V). The coverages reported in Table 3.V are not changed if the observed Cr intensity is corrected for the thickness of the oxide surface layer. This is because the escape depth of the oxides is sufficiently large (33 Å for As_2O_3) and the coverage of oxide sufficiently small (~1-4 Å of effective thickness) that even for the thickest oxide surface layer, the attenuation of the As substrate signal is not enough to alter the calculation of Cr coverage to the accuracy reported here.

The main conclusion to be drawn from the data of Table 3.V is that while $Cr(NH_3)_5CF_3SO_3^{3+}$ will bind to clean GaAs surfaces, there is preferential reaction with surface Ga and/or As oxides. The observation that the $Cr(NH_3)_5CF_3SO_3^{3+}$ binds preferentially to an oxide, while there was no noticeable difference with $Ru(NH_3)_5H_2O^{2+}$, can be rationalized on the basis of the type of metal involved. Cr is a "harder" metal than

Table 3.V. XPS binding energies, calculated mole ratios and coverages for (100) n-GaAs exposed to 0.01 **M** $Cr(NH_3)_5(CF_3SO_3)_3$ in acetone for varying time periods. Also included are data taken for two Cr^{III} ammine complexes. Data were taken using a nonmonochromatic Mg K_α (1254 eV) x-ray source on a VG Mark II or VG HP580 system.

sample	As 3d (eV)	$\Gamma(As_2O_3)$ $\left(\frac{moles}{cm^3}\right)$	$\frac{As}{As_{ox}}$	Ga 3d (eV)	$\Gamma(Ga_2O_3)$ $\left(\frac{moles}{cm^3}\right)$	$\frac{Ga}{As}$	Cr 2p (eV)	ΔeV Cr 2p	N 1s (eV)	$\frac{N}{Cr}$	$\frac{Cr}{As}$	$\Gamma(Cr)$ $\left(\frac{moles}{cm^3}\right)$	C 1s
GaAs + $Cr(NH_3)_5(CF_3SO_3)_3$													
1a) clean etch, 1 week	41.5	0.5	0.13	19.5	1.0	1.1	578.2	9.8	400.8	3.0	0.12	0.6	285.2
	44.4			20.5			588.0						
2 a) , 24 hrs.	41.4	0.3	0.08	19.3	0.3	0.74	577.7	9.8	400.1	1.0	0.21	0.9	286.0
	44.2						587.5						
3) , 11 hrs.	41.9	0.4	0.11	19.7	0.7	1.0	578.5	9.8	400.9	1.4	0.27	1.1	--
	44.5			20.6			588.1						
4 a) etched	42.1	0.0	0.0	20.0	0.0	0.84							285.4
, 2 hrs.	41.7	0.0	0.0				578.5	9.2	400.3	4.0	0.05	0.3	
							587.7						
1 b)not etched, 1 week	42.1	0.8	0.21	20.3	NA	1.4	578.4	9.5	400.4	2.1	0.35	1.3	286.3
	45.2						587.9						
2 b)oxide etch, 24 hrs.	41.3	1.4	0.4	19.2	2.2	1.2	577.2	9.8	400.2	2.1	0.27	1.1	286.0
	45.2						587.0						
5) , 1.5 hrs.	42.2	1.7	0.5				578.5	9.6			0.39	1.3	
	45.1						588.1						
3 b) , 2hrs.	41.8	1.4	0.39	19.9	0.8	1.6							285.5
	45.4												
	42.0	1.4	0.39				578.5	9.2	400.3	2.5	0.17	0.6	
							587.7						
$Cr(NH_3)_5(CF_3SO_3)_3$							578.8	9.8	400.2	3.9			288.6
							588.6						
$[Cr(NH_3)_5H_2O]Cl_3$							578.6	9.4	400.7	2.4			384.8
							588.0						

Figure 3.19. a) Cr 2p and b) N1s XPS regions of GaAs exposed to 0.01 **M** $Cr(NH_3)_5CF_3SO_3^{3+}$ in acetone for two hours. The GaAs was etched to leave an oxidzed surface. Data were taken on a VG Mark II system using a nonmonochromatic Mg K_α (1254 eV) x-ray source.

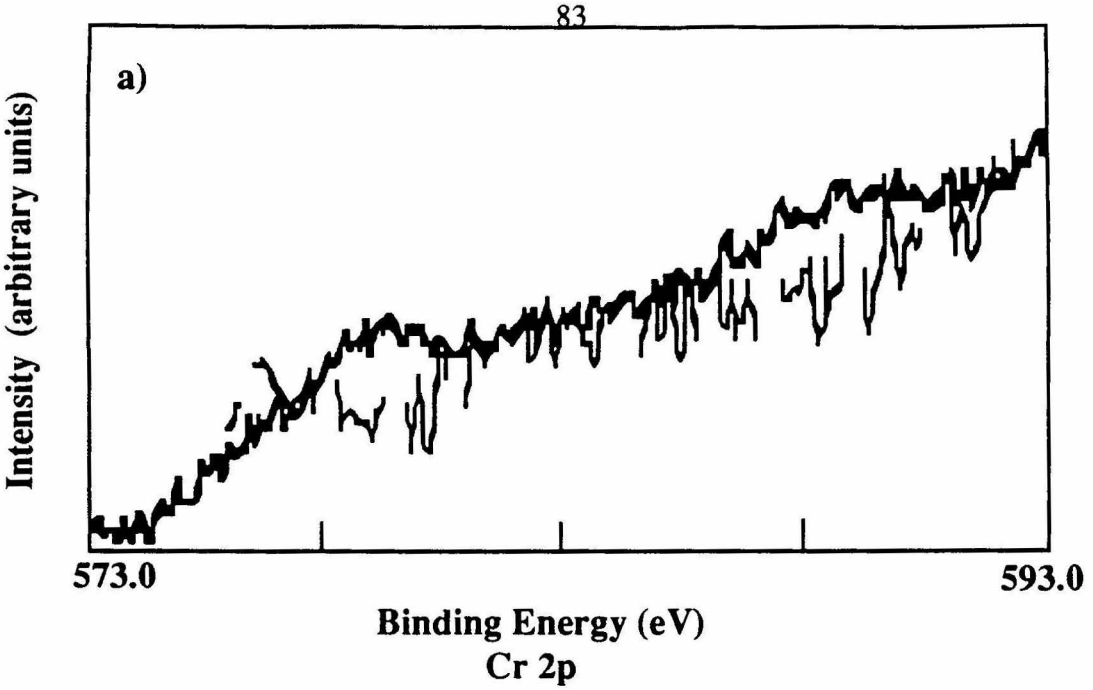
a)
Intensity (arbitrary units)
573.0
593.0
Binding Energy (eV)
Cr 2p

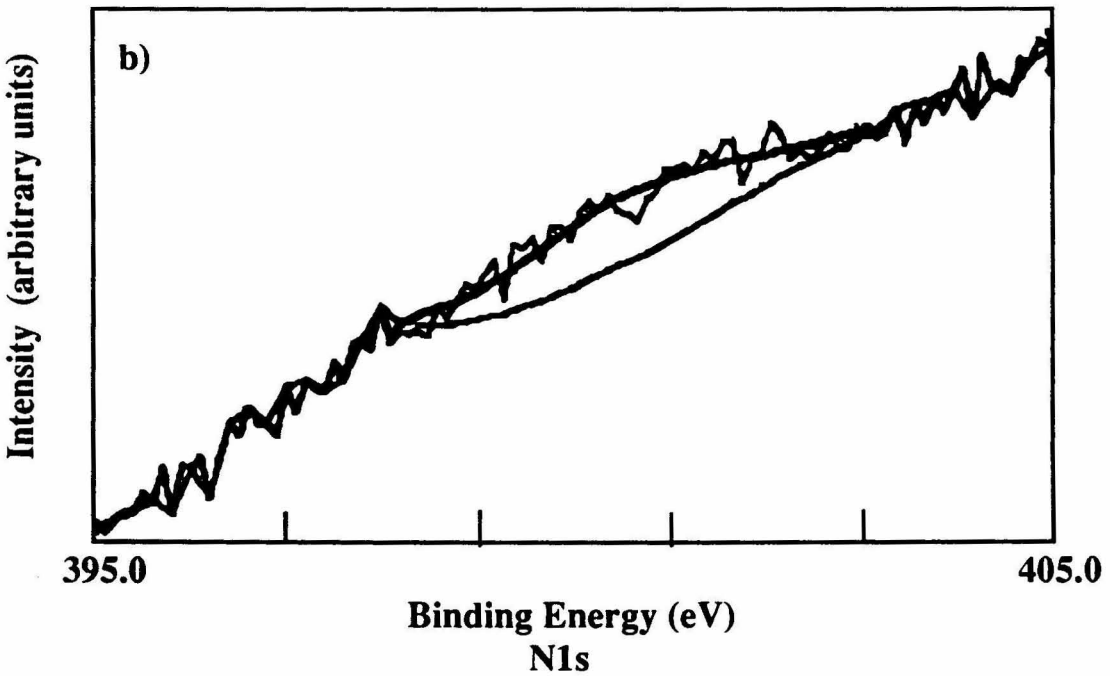
b)
Intensity (arbitrary units)
395.0
405.0
Binding Energy (eV)
N1s

Ru and so would be expected to be more likely to bond preferentially to O over As. EXAFS data are needed to confirm that the Cr has only lighter N or O atoms in the inner shell if some oxide is initially present on the III-V surface.

IV. Conclusion

The chemistry of the Co, Ru, and Cr ammine complexes on GaAs surfaces shows that several types of binding modes are relevant to (100) n-GaAs surfaces as Co, Ru and Cr ammines undergo rather different chemistries. $Co(NH_3)_5X^{3+}$ complexes ($X=H_2O$, NH_3, N_3) are reduced by the GaAs surface to Co^{II}, the ligands are lost, and a thick surface phase of $Co(OH)_2$ is formed.[11] This phase undergoes further reaction with K_2Se-KOH electrolyte solution and Se becomes incorporated into the inner sphere.

The $Ru(NH_3)_5H_2O^{2+}$ and $Cr(NH_3)_5CF_3SO_3^{3+}$ complexes adsorb at much lower coverages and XPS measurements indicate that the complexes remain intact. RBS measurements have put an upper limit on the Ru coverage at 0.25 monolayer and preliminary EXAFS data indicate that the $Ru(NH_3)_5H_2O^{2+}$ may bond to an As substrate atom, though further measurements are needed to confirm this hypothesis. $Ru(NH_3)_5H_2O^{2+}$ has also been shown by XPS, SIMS, and EXAFS to bind to both GaP and InAs surfaces.

$Cr(NH_3)_5CF_3SO_3^{3+}$, like $Ru(NH_3)_5H_2O^{2+}$, exhibits ≤ 1 monolayer surface coverages, but unlike $Ru(NH_3)_5H_2O^{2+}$, there is some selectivity of reaction with respect to a cleanly etched or oxidized GaAs surface, with oxide linkages apparently being preferred. XPS studies indicate that the coverage of Cr is about twice as high on an oxidized surface.

The studies presented in this chapter show that three different metal pentaammine complexes exhibit three different types of chemistry with the GaAs surface and indicate that many modes of binding are available for attachment of potential surface state passivants to GaAs surfaces. Much more data need to be collected, however, in order for correlations to be made between the binding mode of a complex to the surface and the effects of a molecule on the surface electronic properties.

Appendix

The reactivity of $[Rh(CO)_2Cl]_2$ (Strem) with the (100) GaAs surface has also been studied, and the following observations have been made by XPS:[20]

1. The Rh complex binds to GaAs in ~1 monolayer coverage with the Rh $3d_{5/2}$ peak at 308.3 eV (±0.2) and an average splitting of 4.4 eV between the $3d_{5/2}$ and $3d_{3/2}$ peaks. There is no detectable Cl on these surfaces.

2 When these surfaces are exposed to K_2Se-KOH electrolyte, Se is also detected on the surface in ~2:1 ratio to Rh, and the Rh coverage is about 85% of the selenide unexposed surface.

4. Triphenyl phosphine does not react with the Rh complex on the GaAs surface; 0.05% Br_2 in methanol decreases the coverage of Rh by 67% and leaves a small amount of Br_2 on the surface. Exposure of the $[Rh(CO)_2Cl]_2$ treated GaAs surface to 1.0 **M** KOH also appears to etch the Rh off the GaAs surface and to decrease the coverage by 50%.

3. Rh has also been detected after exposure of GaP to $[Rh(CO)_2Cl]_2$.

References

1. C. C. Kuehn and H. Taube, *J. Am. Chem. Soc.* **98**, 689 (1976).

2. G. Brauer, *Handbook of Preparative Inorganic Chemistry, 2nd. ed.*, Vol. 2 (Academic Press, New York, 1965) p. 1521.

3. W. Feitknecht and W. Bédert, *Helv. Chem. Acta* **24**, 683 (1941).

4. H. van der Heide, R. Hemmel, C. F. van Bruggen, and C. Haas, *J. Solid State Chem.* **33**, 17 (1980). Material was verified by powder diffraction.

5. Provide by Stanford University Geology Department.

6. P. Bernhard, H.-B. Bürgi, J. Hauser, H. Lehmann, and A. Ludi, *Inorg. Chem.* **21**, 3936 (1982).

7. J. J. Murray and R. D. Heyding, *Can. J. Chem.* **45**, 2675 (1967).

8. J. H. Scofield, *J. Electron. Spectrosc. Relat. Phenom.* **8**, 129 (1976).

9. M. P. Seah and W. A. Dench, *Surf. and Interface Anal.* **1**, 2 (1979).

10. a) M. J .Fay, A. Proctor, D. P. Hoffmann, and D. M. Hercules, *Anal. Chem.* **60**, 1225 A (1988). b) D. Norman, *J. Phys. C* **19**, 3273 (1986).

11. B. J. Tufts, I. L. Abrahams, C. E. Caley, S. R. Lunt, G. M. Miskelly, M. J. Sailor, P. G. Santangelo, N. S. Lewis, A. L. Roe, and K. O. Hodgson, *J. Am. Chem. Soc.* **112**, 5123 (1990).

12. D. C. Koningsberger and R. Prins, Eds., *X-ray Absorption* (John Wiley and Sons, New York, 1988) pg. 594.

13. G. Hodes, J. Manassen, and D. Cahen, *J. Electrochem. Soc.* **127**, 544 (1986).

14. a) P. C. Ford, *Coor. Chem. Rev.* **5**, 75 (1970). b) L. Meites, P. Zuman, A. Narayanan, *CRC Handbook Series in Inorganic Electrochemistry, Vol. II.* (CRC, Boca Raton, 1981), pp. 24-31BE.

15. C. D. Wagner, W. M. Riggs, L. E. Davis, J. F. Moulder, and G. E. Muilenberg, *Handbook of X-ray Photoelectron Spectroscopy* (Perkin Elmer, Eden Prairie, MN, 1979).

16. SIMS data obtained by Dr. J. Vajo of Hughes Research Laboratories.

17. L. C. Feldman, in *Chemistry and Physics of Solid Surfaces, Vol. III*. R. Vanselow and W. England, eds. (CRC Press, 1982), pp. 221-245.

18. B. K. Teo and P. A. Lee, *J. Am. Chem. Soc.* **101**, 2815 (1979).

19. F. Basolo and R. G. Pearson, *Mechanisms of Inorgnaic Reactions, 2nd. Ed.* (Wiley, New York, 1967) pp. 124-246.

20. Experiments done in collaboration with Dr. Michael J. Sailor.

Chapter 4. Steady-State and Time-Resolved Photoluminescence Studies of the Effects of Exposure to Aqueous Sulfides, and Nonaqueous Thiols and Alcohols on GaAs Surface Recombination Properties

I. Introduction

The use of $Na_2S \cdot 9H_2O$ has been reported recently by Skromme, Sandroff, Yablonovitch, and co-workers to decrease surface recombination rates at GaAs/air interfaces and to improve the electrical characteristics of GaAs bipolar transistors.[1] This system is notable because the surface recombination velocity under high-level injection of Na_2S-treated (100) GaAs surfaces is 10^3 cm sec^{-1} as opposed to the 10^6-10^7 cm sec^{-1} value that is characteristic of unpassivated GaAs/air interfaces.[1a,2] The application of the sulfide has been done in a variety of different ways, and apart from the observation that reductions in surface recombination velocity (S) can be obtained with Na_2S, $(NH_4)_2S$ and other salts that yield aqueous sulfur species,[1,3,4,5,6,7,8,9] little is known about the chemical reactivity of the GaAs surface sites.

Additionally, although numerous spectroscopic and electrical studies of Na_2S-coated GaAs surfaces have been performed, there is still controversy over the mechanism of surface passivation in the GaAs-$Na_2S \cdot 9H_2O$ system. Sandroff and coworkers showed that there was an increase in gain in bipolar transistors fabricated from sulfide-treated surfaces[1b] and that an As-S was present on the surface.[7] Work by Carpenter, et al. showed that Schottky barriers fabricated with sulfide-treated surfaces exhibited a slightly more ideal electrical behavior than untreated GaAs surfaces.[8a] Both groups of workers have associated the improvements in surface recombination rates with the bonding and/or etching of electrical traps by the basic aqueous sulfide solutions.[1,8] Other investigators have suggested that the traps might be associated with excess elemental As, which is presumably etched away by the Na_2S solution.[1,8,10]

Another theory is that a slight shift in the surface, Fermi level pinning position towards the GaAs valence band edge is responsible for the improved photoluminescence signals, and that passivation effects that are due to a decrease in the surface trap density and/or cross section are a secondary effect.[9,10] Support for this latter hypothesis has been obtained from deep-level, transient spectroscopy,[9b] from valence band shifts in vacuum photoemission experiments,[11] and from field effect measurements of the equilibrium band bending at Na_2S-treated GaAs surfaces.[9a] However, measurements of the surface Fermi level position under dark, equilibrium conditions are not sufficient to define the surface carrier concentrations under strong illumination,[6,12] so other data must also be obtained to understand the electrical effects of the GaAs surface modifications.

To address this issue, the next two chapters present studies of surface electrical and chemical properties of (100)-oriented GaAs that has been exposed to a variety of sulfur, nitrogen, and oxygen donors. Many of these treatments yielded improved GaAs surface recombination properties, demonstrating that a general class of chemical reactivity can be exploited to obtain information on the GaAs surface state properties. In this work, we have used steady-state, low-level injection, photoluminescence (PL) methods and time-resolved, high-level injection, photoluminescence methods[13] to probe the electrical recombination properties of various GaAs surfaces. Radiative lifetime data obtained under high-level injection conditions are relatively insensitive to the position of the dark, equilibrium surface Fermi level;[12,14] therefore, chemically induced changes in surface recombination rates can be probed unambiguously in such experiments. High resolution, x-ray photoelectron spectroscopy experiments done on these systems to determine how changes in recombination rates correlate with changes in surface stoichiometry are discussed in Chapter 5.

II. Experimental

A. Samples and Chemicals

All experiments in this work were performed with n-type, (100)-oriented GaAs,

which varied in dopant density from 10^{14} cm^{-3} to 10^{18} cm^{-3}. Some steady-state PL measurements were also performed on the $N_d=10^{17}$ cm^{-3} bulk GaAs samples; however, in order to maximize the surface sensitivity of the photoluminescence signals, the majority of the steady-state experiments were performed with thin, lightly doped, GaAs epilayer structures. Except where otherwise noted, these samples consisted of a semi-insulating GaAs substrate, followed by a layer of $Al_{0.4}Ga_{0.6}As$ (1000 Å thick), a layer of GaAs (1.01 μm thick) doped at 10^{15} cm^{-3} (n-type), and then another layer of $Al_{0.4}Ga_{0.6}As$ (1000 Å thick).[15] For convenience, these samples will be designated as the 1.0 μm epilayer GaAs samples. For experiments that probed the effects of treatments on the GaAs surface, the top $Al_{0.4}Ga_{0.6}As$ cap layer was removed by etching the sample for 4 minutes in a solution of 0.05% Br_2 (by vol.) in methanol. The PL intensity was monitored during the etching process, and the etch was stopped when no further decrease in the PL signal was observed in response to a 15 sec immersion into the Br_2/methanol solution.

In order to confine carriers to a narrow region and thereby maintain high injection during the course of the photoluminescence measurements, time-resolved photoluminescence experiments were conducted on samples with a layered structure that consisted of a semi-insulating GaAs substrate, followed by a layer of $Al_{0.3}Ga_{0.7}As$ (1000 Å thick), a layer of GaAs (2.8 μm thick) and then a layer of $Al_{0.3}Ga_{0.7}As$ (1000 Å thick).[16] These samples will be designated as the 2.8 μm thick epilayer GaAs samples. When desired, the $Al_{0.3}Ga_{0.7}As$ cap was removed by etching the sample for 4 minutes in a 1:8:500 (volume ratio) of a H_2SO_4(con.):30% H_2O_2(aq):H_2O solution. The exposed GaAs layer was then etched and manipulated as described below for the bulk GaAs samples.

Three types of etches were used in this work.[17] In the first procedure, samples were etched sequentially in 0.05% Br_2-CH_3OH and 1.0 M KOH(aq) solutions, with each etch being 15 sec in duration. After the KOH etch, the sample was rinsed with deionized water and then dried under a stream of N_2(g). Before further use of the GaAs, this etching

procedure was performed three times on each sample, ending in KOH. This etch leaves a surface with minimal oxides and elemental As, and will be referred to as etch A (or the "near-stoichiometric" etch).[18] This etch was the one most commonly used to give a good starting GaAs surface, and was used as the initial treatment except where otherwise noted.

In some experiments, GaAs samples were subsequently etched in 1:1:100 (con. H_2SO_4:30% H_2O_2:H_2O) solutions for 30 sec, and were then rinsed with deionized water and dried under a stream of N_2(g). This procedure resulted in a nonstoichiometric surface with an excess of elemental As on the GaAs surface,[17,18,19] and will be referred to as etch B (or the As^0-rich etch). Etch C consisted of exposure of the GaAs surface to etch A followed by exposure to 30% H_2O_2 for 30 sec, and resulted in the formation of an oxidized GaAs surface layer.[17,18]

The organic reagents were used as received (99% or better purity) from Aldrich Chemical Co. The organic reagents were dissolved in diethylether or in carbon tetrachloride to make solutions of 1.0 **M**, unless otherwise noted. The sodium salts of several of the organic reagents were formed by addition of a 5% mole excess of sodium to a 1.0 **M** solution of the organic reagent in diethylether. $Na_2S{\cdot}9H_2O$(s) was obtained from Mallinckrodt in 98.38% purity, and NaHS(s) was obtained in 99% purity from Aldrich. The pH of the aqueous Na_2S and NaHS solutions was adjusted by addition of 12 **M** HCl(aq) or 1 **M** NaOH, as necessary.

Chemical treatments of the GaAs samples were performed by immersing the etched GaAs surface into a pyrex beaker containing a solution of the desired reagent (1.0 **M** concentration unless otherwise specified) for time periods of 1-60 minutes, with an immersion time of 30 minutes used for most experiments. Except where otherwise noted, all solutions were open to the ambient air while in contact with the GaAs samples. The samples were then removed from the beaker, allowed to dry under N_2(g), and then transferred either to the XPS instrument or to the PL apparatus.

B. Steady-State Photoluminescence Experiments

Steady-state photoluminescence (PL) data were obtained using either an Ar ion laser at 514 nm (100 mW) or a He-Ne laser at 632.8 nm (10 mW). Both lasers were focused to produce illuminated sample areas ≈1 mm in diameter. In preliminary experiments, the relative trends in PL intensity for surface treatments with aqueous sodium sulfide on either 2.8 μm GaAs epilayer samples or on 10^{17}-doped bulk GaAs samples were found to be independent of the choice of excitation wavelength (514 nm vs. 633 nm), so 633 nm excitation was used for the majority of the experiments described below.

For either excitation wavelength, the PL signal from the GaAs was directed through a monochromator (SPEX 1681B, 1.25 mm slits) that was equipped with a long pass filter (transmitting $\lambda > 740$ nm). Light detection was performed with a conventional photomultiplier tube (Hamamatsu R632-01). A scan of the PL intensity was recorded between 800 nm and 900 nm at a scan rate of 1 nm/s; the maximum PL signal was then recorded as the characteristic value for this sample. The wavelength of the peak maximum (874 nm) did not shift noticeably after any of the surface treatments.

In order to minimize oxidation of the GaAs,[20] all PL measurements were performed with the sample placed in a two-necked glass cell equipped with a stopcock. The cell was continuously purged with N_2(g). The samples were etched (in ambient air) as described above, placed in the cell, and a baseline PL measurement was obtained. The samples were then transferred in air to the appropriate solution, treated with the desired chemical reagent, reinserted into the N_2-purged cell, and the PL peak was then rescanned. Frequently, there was some increase in the PL intensity over a period of about 10 minutes, after which the PL signal level remained constant. The data were recorded after the peak had reached a constant intensity. This process was found to yield consistent trends in PL intensity for the various reagents studied in this work. The increase in PL with time was clearly due to a photochemical step,[4] because after the PL signal had reached a maximum value on a sample of GaAs, illumination of a different portion of the same GaAs surface resulted in an initially

low PL intensity and also produced a similar time-dependence of the PL signal. After re-etching treated GaAs surfaces with the repetitive Br_2-CH_3OH and 1.0 **M** KOH(aq) procedure (etch A), the PL intensity always returned to the baseline value. For all samples, exposure of the Na_2S films to air for more than a few minutes usually resulted in adsorption of water from the air; this process was readily identified because the water wetted the film and eventually reduced the PL intensity back to the baseline value of etched samples. Such long-term exposure to air was therefore avoided in the measurements reported herein.

Some experiments were performed to investigate the effects of spin-coating[1] *vs* the immersion and drying procedures described above. Using a bulk GaAs specimen (N_d=10^{17} cm^{-3}, etched with etch A) in contact with 1.0 **M** $Na_2S \cdot 9H_2O$(aq) solutions, essentially identical PL signals were obtained from the spin-coating method vs. the immersion and drying procedure. Most of our work was therefore performed using the more straightforward immersion/drying procedure, as described above.

Some experiments were also performed using solutions specifically prepared to minimize the amount of oxidized sulfur and to maximize the amount of sulfur in the -2 oxidation state. In these experiments, $NaHS \cdot (H_2O)_x$ was dissolved in deaerated water to produce a 1.0 **M** NaHS solution; 0.1 **M** NaN_3 was then added to this solution to reduce any residual polysulfide species. The pH was then adjusted by addition of either HCl or NaOH, as required. Re-oxidation of the HS^- was prevented by maintaining a stream of N_2(g) through the solution during the reduction with NaN_3 and through all subsequent manipulation steps. This procedure was found to minimize the oxidized sulfur content relative to that obtained from solutions made with commercial $Na_2S \cdot 9H_2O$(s) and no reductant present.

C. Time-Resolved Photoluminescence Studies

Time-resolved photoluminescence experiments were performed using time-correlated single photon counting instrumentation. The excitation source was a Coherent

Model 701-2 dye laser that was pumped by the mode-locked, second harmonic output of a Nd:YAG laser (Coherent Inc. "Antares" Laser System). The dye laser pulses were less than 10 ps in duration, the repetition rate was 152 kHz, and the power per pulse was 4.6 nJ at 620 nm or 13.1 nJ at 685 nm. All time-resolved PL studies were carried out under high-injection conditions. The beam was focused to a spot with a diameter of <100 μm on the plane of the sample, yielding an incident flux of 10^{14} photons cm^{-2} $pulse^{-1}$. The absorption coefficient for GaAs at 656 nm (1.89 eV) is 3.44×10^4 cm^{-1};[21] thus, after accounting for a 30% loss in power that was due to reflection at the GaAs/gas interface, this incident power resulted in an initial injection level in the first 0.10 μm of approximately 10^{19} cm^{-3}, and produced injection levels of 10^{18} carriers cm^{-3} after carrier diffusion through the 2.8 μm thick epilayer GaAs sample. All time-resolved PL experiments were performed on the sample with the 2.8 μm GaAs epilayer structure.

The time-correlated photon counting apparatus consisted of an EG&G Ortec Model 934 Quad Constant Fraction Discriminator, a Tennelec TC 864 Time-Amplitude Converter/Biased Amplifier and an EG&G Ortec Spectrum Ace-4K Multichannel Analyzer. Trigger pulses were generated by an FND-100 photodiode, and were amplified and inverted by a Hewlett Packard 8447F preamplifier. The room temperature GaAs bandgap luminescence at 880 nm was detected using an accelerated Hamamatsu R928 Photomultiplier.[22,23] Stray light was rejected using Hoya long pass cutoff filters at 740 nm that were placed in front of the Spex monochromator, and the monochromator was set to 880 nm with 1.25 mm slits. The system response was determined by scattering the incident beam off a strip of Teflon tape, with some scattered light directed into the photomultiplier tube. This procedure yielded a value of ≈350 ps for the full width at half-maximum of the system response; the full system-response function was recorded and used in the convolution procedure described below.

Analysis of the time-resolved PL data was performed using a digital simulation program.[13,14] In our simulation, photogenerated carriers were created in a delta time pulse

with the appropriate penetration depth into the sample, and were then allowed to diffuse, to recombine radiatively and nonradiatively in the bulk, and to recombine nonradiatively at the front and back GaAs surfaces. The high-injection levels of the experiment greatly simplified the simulation procedure, because the flat-band conditions established in the experiments justified neglect of drift terms in the simulation. Standard Shockley-Read-Hall trapping statistics were used to model the nonradiative processes,[12] and the known radiative recombination coefficient of 2×10^{-10} cm^3 s^{-1} was used for the GaAs luminescence rate constant.[24]

For the samples of interest, the low-level injection bulk minority carrier lifetime was sufficiently long that bulk nonradiative recombination processes were not important in determining the time-decay of the PL signal; thus, the major factors that determined PL decays were carrier luminescence, diffusion, and surface recombination. Because the carrier mobilities, sample thickness, injection levels, and GaAs radiative rate constants were known independently, the only adjustable parameter in the simulation was the surface trapping rate, which was varied from 10^1-10^7 cm s^{-1} in the simulations. The simulated PL response was then convoluted with the laser/photomultiplier tube/electronics system-response function, and the resulting time-dependent PL function was then compared directly with the experimental PL data. Simulations of PL data on the $Al_{0.3}Ga_{0.7}As$ capped, 2.8 μm thick GaAs samples yielded a value for S of 500 cm s^{-1}, which is in good agreement with literature values for this interface.[24a] PL decays for the other surface treatments were more rapid than that obtained with the $Al_{0.3}Ga_{0.7}As$ cap layer, and S was found to range from 10^3-10^6 cm s^{-1} for these systems.

III. RESULTS

A. Steady-State Photoluminescence

1. Aqueous Sulfide Solutions

The effects of various surface treatments on surface recombination rates were investigated through room-temperature photoluminescence (PL) measurements on (100)

oriented n-type GaAs samples. As expected, the absolute magnitude of the PL intensity was a function of the thickness and minority carrier lifetime of the sample,[12,25] with thin, epitaxially grown, GaAs layers of low dopant density, high bulk lifetime, and a passivated back surface (at the GaAs/$Al_xGa_{1-x}As$ contact), showing the greatest relative increase in PL intensity. Although some previous PL work has been performed using highly-doped bulk GaAs samples,[3,5,9a] the rather low dynamic range of the PL signal for our highly doped samples precluded accurate separation of the various chemical effects of interest in this work. Therefore, epilayer samples with a thin active region and a long minority carrier lifetime (specifically, the 1.0 μm epilayer GaAs samples) were used to obtain most of the quantitative PL intensity data for the surface treatments reported in this work.

1a) pH dependence of the Steady State Photoluminescence Intensity: HS^- vs S^{2-} Ions

Figure 4.1, Table 4.I and Table 4.II report the steady state, low level injection, GaAs PL data for various surface treatments. All steady-state PL data in Tables 5.I and 5.II are reported as the ratio of the PL signal for the surface of interest relative to that observed for an etched (etch A) GaAs surface under the same experimental conditions. Under these conditions, a 300-fold increase in PL intensity was obtained after immersion of the 1.0 μm thick epilayer GaAs sample into an unbuffered (pH≈14) 1.0 **M** $Na_2S{\bullet}9H_2O$(aq) solution (Table 4.I, section A and Figure 4.1). This PL increase is very similar to that reported by Sandroff et al., and indicates that our surface passivation procedures and GaAs sample properties were similar to those used in the previous work on this system.[1] Notably, as reported in Figure 4.1 and Table 4.I, Section A, a slight increase in PL intensity was observed when the GaAs sample was exposed to 1.0 **M** $NaHS{\bullet}(H_2O)_x$ (pH≈12). Similar PL intensities were observed even when the pH was lowered to <8 (Table 4.I, Section A). Since H_2S has pK_a values of 6.9 and 18,[26] the predominant species for 7<pH< 15 is therefore HS^-(aq) , with only extremely low levels of S^{2-}(aq) present in the pH=7.8 solutions. If S^{2-}(aq) were the only species involved in reaction with

Table 4.I. PL intensity (arbitrary units) at 874 nm for 1.0 μm thick epilayer (100) n-GaAs. Excitation source was a He-Ne laser at 632.8 nm. Time of treatment was 30 minutes and the nonaqueous solvent was diethylether. All intensities were scaled to the signal of a GaAs surface exposed to etch A.

Treatment	PL Intensity
Section A	
1.0 **M** $Na_2S{\cdot}9H_2O$ (pH 13-14)	270[a]
1.0 **M** $NaHS{\cdot}(H_2O)_x$ (aq)	410[a]
0.10 **M** $NaHS{\cdot}(H_2O)_x$ (pH 10.8)	120
0.10 **M** $NaHS{\cdot}(H_2O)_x$ (pH 7.8)	240
0.10 **M** $NaHS{\cdot}(H_2O)_x$ (pH 1.54)	26
Section B	
H_2O (*l*)	1
0.1 **M** NaOH (aq)	1
1.0 **M** KOH (aq)	40[a]
Section C	
1.0 **M** $Na_2S{\cdot}9H_2O$ (pH 13.7)	280
0.10 **M** $Na_2S{\cdot}9H_2O$ (pH 12.7)	220
0.010 **M** $Na_2S{\cdot}9H_2O$ (pH 12.5)	33
0.0010 **M** $Na_2S{\cdot}9H_2O$ (pH 12.5)	1
Section D	
Etch A, 1.0 **M** $Na_2S{\cdot}9H_2O$ (aq)	270
Etch B, 1.0 **M** $Na_2S{\cdot}9H_2O$ (aq)	270
Etch A, 1.0 **M** $Na_2S{\cdot}9H_2O$ (aq)	270
Etch C, 1.0 **M** $Na_2S{\cdot}9H_2O$ (aq)	280
Etch A, 1.0 **M** HSC_6H_4Cl	140
Etch B, 1.0 **M** HSC_6H_4Cl	96
Section E	
1.0 **M** $Na_2S{\cdot}9H_2O$ (aq)	240
1 drop H_2O	85
rinse	28
Section F	
$HSCH_2CH_2SH$ (*l*)	170[a]
CH_3SCH_3 (*l*)	2[a]

[a]Experiments used in Figure 4.1.

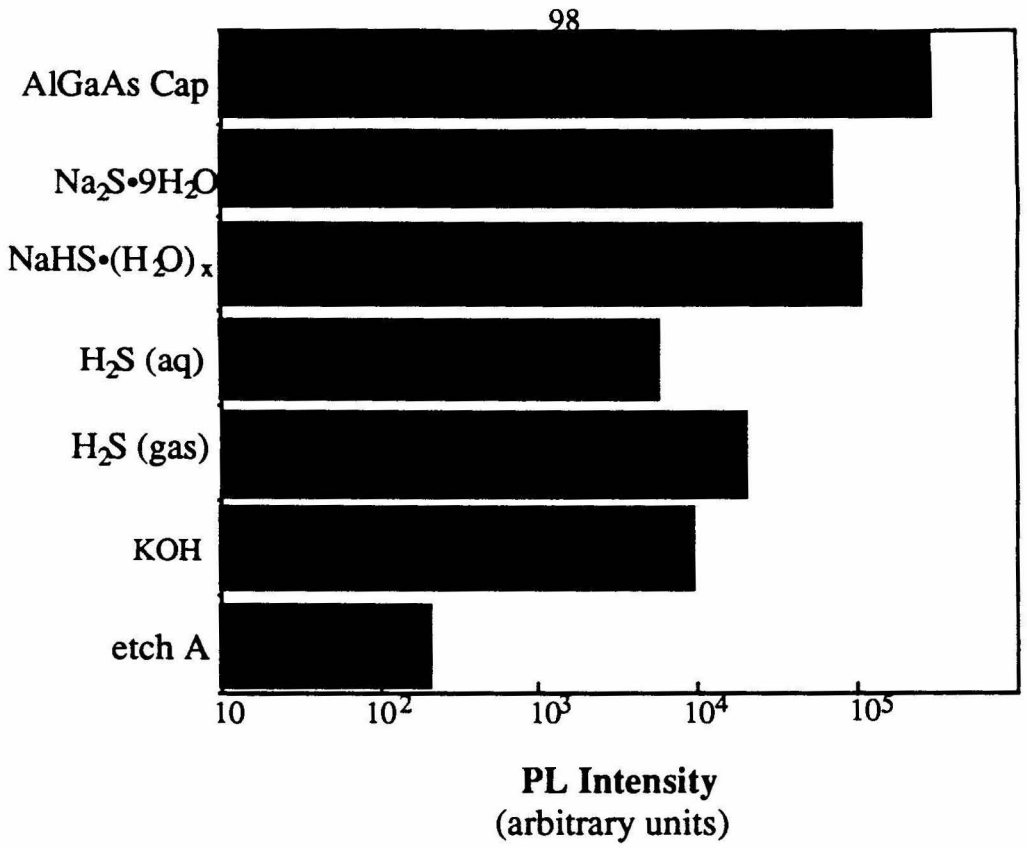

Figure 4.1. Bar graph of steady-state photoluminescence intensity at 874 nm for 1.0 μm thick epilayer (100) n-GaAs samples after exposure to various aqueous solutions. The excitation source was a He-Ne laser at 632.8 nm. The concentration of all species was 1.0 **M** with the exception of aqueous H_2S, which was 0.1 **M** in total sulfide (pH=1.5). The H_2S gas pressure was ~1 atm, and no H_2O was deliberately introduced into this environment.

GaAs, the steady-state PL increase would be expected to be pronounced only in the most basic aqueous solutions. The data of Table 4.I do not support this hypothesis, and therefore imply that the predominant reactive species is not S^{2-}(aq) but is HS^-(aq).

To determine if the GaAs surface recombination properties were influenced by the variation in proton activity from the unbuffered 1.0 **M** $Na_2S•9H_2O$(aq) (pH≈14) solution

to the pH=7.8, 0.1 **M** $NaHS\bullet(H_2O)_x$ solution, additional experiments were performed without any sulfides present in solution. Neutral water did not increase the PL signal over the value obtained from at etched GaAs surface (Table 4.I, section B). Also, exposure of the 1.0 μm epilayer GaAs samples to 0.1 **M** NaOH(aq) caused a very small enhancement in PL (~20% over baseline, which is a negligible increase in *S* for these low-doped samples), while exposure to 0.10 **M** $NaHS\bullet(H_2O)_x$ solutions resulted in a large PL signal. These experiments clearly indicated that the predominant surface passivation effects were related primarily to the sulfur component of the aqueous solutions. Exposure to 1.0 **M** KOH(aq) did yield modest improvements in the GaAs PL signal (Figure 4.1; Table 4.I, Section B), but these PL signals were transient in nature and were not of the same magnitude as those obtained after exposure to either the 0.10 **M** or 1.0 **M** aqueous sulfide solutions of $7 \leq pH \leq 14$.

Several control experiments were performed to determine whether S^{2-}(aq), which is present in extremely low concentrations in 0.10 **M** $NaHS\bullet(H_2O)_x$ (aq) solutions of pH<10, could influence the GaAs surface recombination rate. In 0.10 **M** NaOH(aq), when the total sulfur concentration (as HS^-, S^{2-}, etc.) was lowered to 1 m**M**, no increase in the GaAs PL intensity was observed relative to the etched and air-exposed GaAs surface (Table 4.I, section C). In contrast, as described above, a 200-fold increase in PL intensity was readily observed after immersion of 1.0 μm GaAs epilayer samples into a pH=7.8, 0.1 **M** $NaHS\bullet(H_2O)_x$ (aq) solution. Since the equilibrium concentration of S^{2-}(aq) in the 0.10 **M** NaOH(aq), 1.0 m**M** Na_2S(aq) solution was 1000 times *higher* than that in the 0.10 **M** total sulfur, pH=7.8 solution (where $S^{2-}(aq)=10^{-10}$ **M**), these data indicate that S^{2-}(aq) alone is not responsible for the passivation effect on GaAs surfaces.

1b) pH dependence of the Steady-State Photoluminescence Intensity: H_2S vs HS^-(aq)

Some prior work has reported the formation of robust Ga_2S_3 overlayers on GaAs after exposure to "activated" H_2S(g);[5] therefore, the activity of H_2S(g) and H_2S(aq) must

also be considered in evaluating the role of HS^-(aq). Exposure to 1 atm H_2S(g) (made from acidification of solid $NaHS\bullet(H_2O)_x$ or to 0.1 **M** H_2S(aq) (made from acidification of 0.1 **M** $NaHS\bullet(H_2O)_x$(aq)) produced some increase in the GaAs PL signal, but did not produce the 200-fold signal enhancements on 1.0 μm epilayer GaAs samples that were obtained from HS^-(aq) solutions (Table 4.I, Section A; Figure 4.1). When the GaAs samples were exposed to dry H_2S(g) from a lecture bottle, no PL signal increase was observed over timescales comparable to that used for the aqueous sulfide solutions. Longer exposure times to H_2S(g) in the presence of some water vapor did produce a modest PL signal increase over about a ten-minute time period, but again these signals were not of the magnitude obtained from immersion into the $Na_2S\bullet 9H_2O$(aq) or NaHS(aq) solutions. These experiments indicate that the predominant surface passivation effects of $Na_2S\bullet 9H_2O$(aq) solutions do not arise solely from H_2S chemisorption, but likely involve the aqueous HS^- ion, which is the dominant aqueous species over the $7 \leq pH \leq 14$ range in which the large PL enhancements are observed.

1c) Role of the Sulfur Oxidation State on the Steady-State Photoluminescence Intensity

The partial oxidation of aqueous chalcogenide anions by oxygen is well documented,[27] and must also be considered as a source of the surface-active sulfur species. Solutions of 1.0 **M** Na_2S(aq) prepared from commercial $Na_2S\bullet 9H_2O$(s) turned yellow upon acidification, indicating the formation of polysulfide species. This effect was minimized with the 0.10 **M** $NaHS\bullet(H_2O)_x$ solutions described above by using deaerated solutions and added NaN_3 as a reductant. This is relevant because most prior investigations of the GaAs-$Na_2S\bullet 9H_2O$ and GaAs-$(NH_4)_2S$ interfaces have not indicated that precautions were taken to exclude air from the aqueous solutions used as surface treatments or sample rinses, and even in basic solutions, oxidized sulfur could provide a facile reactant for transforming either lattice As_{GaAs} or As^0 into products such as As_2S_3.

Addition of elemental sulfur to 1.0 **M** $Na_2S \cdot 9H_2O$(aq) solutions was observed to yield only minor changes in the PL signal of bulk $N_d=10^{17}$ cm^{-3} GaAs (Table 4.II, Section A). This experiment suggested that either oxidized sulfur was not the source of the GaAs PL improvement, or trace levels of oxidized sulfur from the $Na_2S \cdot 9H_2O$(s) were sufficient to produce the maximum PL effect on GaAs surfaces. To test the latter possibility, a series of experiments was performed with solutions that contained minimal oxidized sulfur. Deaerated S^0-free solutions prepared from 1.0 **M** NaHS(aq) and NaN_3 (see Experimental Section B) yielded PL signals on 1.0 μm GaAs samples that were slightly higher than those obtained from 1.0 **M** $Na_2S \cdot 9H_2O$(aq) (Table 4.I, Section A). Another set of experiments with bulk $N_d=10^{17}$ cm^{-3} GaAs was performed in a glove bag that was purged with N_2(g). For these experiments, the etching and 1.0 **M** $Na_2S \cdot 9H_2O$(aq) solutions were deaerated before use, the GaAs samples were etched and manipulated anaerobically, and a polymer film was used to cover the Na_2S coating and to prevent oxidation during subsequent handling steps. Despite these precautions, no significant difference in the steady-state GaAs PL increase was observed relative to experiments performed when the sample was etched in air and exposed to air during transfer to the PL setup (Table 4.II, section A). These experiments seem to confirm the hypothesis that reduced sulfur in the -2 oxidation state (in the form of HS^-) is the key solution component in the aqueous GaAs surface passivation process.

1d) Role of GaAs Surface Composition on the Steady-State Photoluminescence Intensity

The effects of varying the initial surface composition are also of interest, because of a potential role of As^0 in GaAs surface recombination processes.[2,4] For two etches used in this study (the near-stoichiometric surface, etch A, or the As^0-rich surface, etch B), the relative change in PL intensity after exposure to 1.0 **M** $Na_2S \cdot 9H_2O$(aq) at pH=13 was found to be independent of the etching procedure. This somewhat surprising result was verified for the bulk $N_d=10^{17}$ cm^{-3} GaAs material, and for the 1.0 μm epilayer GaAs

Table 4.II. PL Intensity (arbitrary units) at 874 nm for bulk $N_D=10^{17}$ cm^{-3} (100) n-GaAs samples. The excitation source was an Ar-ion laser at 514 nm. The exposure time was 30 minutes and the nonaqueous solvent was diethylether. PL values are normalized to the value obtained for a surface that had been exposed only to etch A.

Treatment	PL Intensity
Section A	
1.0 **M** $Na_2S{\cdot}9H_2O$ (aq)	7
1.0 **M** $Na_2S{\cdot}9H_2O$ (aq) (in glove bag)	5
1.0 **M** $Na_2S{\cdot}9H_2O$ + 1 **M** S^o (aq)	9
Section B	
Etch A, 1.0 **M** Na_2S (aq)	1.7[a]
Etch B, 1.0 **M** Na_2S (aq)	1.7
Etch A, 1.0 **M** HSC_6H_4Cl	1.5
Etch B, 1.0 **M** HSC_6H_4Cl	1.5
Etch A, 1.0 **M** $HSCH_2CH_2SH$	1.5
Etch B, 1.0 **M** $HSCH_2CH_2SH$	1.5
Section C	
1.0 **M** Na_2S (30 min.) (aq)	5
rinse	3
Section D	
1.0 **M** KSCN (aq)	0.9
1.0 **M** KCN (aq)	1
Section E :	
$HSCH_2CH_2SH$ (*l*)	6
3-methyl thiophene (*l*)	1
DMSO (*l*)	1

[a]GaAs samples used for the experiments in section B were nominally the same dopant density, but had a lower bulk lifetime and were not from the same supplier as the GaAs used for all other experiments in this table.

samples (Table 4.I, section D; Table 4.II, Section B). Use of the oxidizing etch (etch C) also did not affect the magnitude of the PL increase for the 1.0 μm epilayer GaAs samples (Table 4.I, section D). In fact, we did not observe any systematic correlation with the initial GaAs surface composition for any of the aqueous $Na_2S \cdot 9H_2O$ solutions investigated in this study. The reasons for this insensitivity to initial GaAs surface composition are readily apparent from, and consistent with, the XPS results described in Chapter 5.

1e) Other Variables Affecting the GaAs Photoluminescence Intensity

A significant observation with respect to the XPS data is that the PL intensity resulting from all the aqueous treatments was observed to decrease after the GaAs surface was thoroughly rinsed with H_2O. To illustrate this observation, Table 4.I, section E and Table 4.II, Section C contain PL intensity data for two types of GaAs samples that had been a) immersed into 1.0 **M** $Na_2S \cdot 9H_2O$(aq) and dried, or b) immersed, dried and subsequently rinsed with one drop, or a large volume, of H_2O. Although the PL signal from a bulk $N_d=10^{17}$ cm^{-3} GaAs specimen that had been immersed in 1.0 **M** $Na_2S \cdot 9H_2O$(aq) declined by only a factor of 2 after an extensive H_2O rinse, the same procedure yielded a decrease in the PL signal by over an order of magnitude when the 1.0 μm GaAs epilayer sample was used. Similar behavior has been reported earlier for epilayer GaAs samples.[1]

The difference in PL behavior between the low-doped, thin epilayer and the highly doped bulk GaAs samples was due to the decreased bulk recombination rates, the longer radiative lifetime, and the increased ratio of surface to bulk present in the epilayer sample. The observation that the PL signal did not change substantially on a highly doped, bulk GaAs sample was not therefore sufficient to insure that the rinsing procedure did not affect the GaAs surface recombination velocity; such conclusions required the use of high purity, thin, low-doped, epilayer GaAs samples with low surface recombination velocities at the back AlGaAs/GaAs interface. This is especially relevant to a number of prior spectroscopic studies of bulk GaAs passivation chemistry on rinsed GaAs surfaces, in which increased

PL signals on bulk, highly doped GaAs samples have been used as a check that the passivation chemistry has not been altered during various aspects of the experimental procedure.

Aqueous solutions that contained ions other than sulfide were used to explore the possibility that a general class of large, negatively charged, aqueous ions might affect the steady-state PL intensity of GaAs surfaces. Exposure of bulk $N_d=10^{17}$ cm^{-3} GaAs to either 1.0 **M** KCN(aq) or 1.0 **M** KSCN(aq) produced no statistically significant increase PL intensity above the value for an etched GaAs sample (Table 4.II, Section D). This suggests that the large PL effects induced by the aqueous HS^- solutions were not dominated merely by an electrostatically driven adsorption process, but that specific S-based chemical interactions with the GaAs surface must be invoked to explain the large PL intensity change.

2. Organic Thiols and Sulfides

The significant surface passivation properties of HS^-(aq) prompted us to investigate the effects of organic thiols, thiolates, and other electron rich centers on the GaAs PL intensity. As depicted in Figure 4.2, exposure of the 1.0 μm GaAs epilayer sample to a variety of thiols (dissolved in diethyl ether solvent) yielded increases in PL that were comparable to the increase produced by 1.0 **M** $Na_2S{\cdot}9H_2O$(aq). The thiol-induced changes in PL intensity were identical for either etch A or etch B on the GaAs surface (Table 4.I, Section D). Similar trends in the general thiol PL behavior were evident in experiments performed on bulk $N_d=10^{17}$ cm^{-3} GaAs samples (Table 4.II, Section E), confirming that the surface passivation effects were not unique to low-doped, epilayer-type GaAs samples.

The efficacy of surface passivation was approximately the same for aromatic thiols, aliphatic thiols, and aliphatic dithiols, all of which showed on the order of a hundredfold increase in PL intensity for the 1.0 μm GaAs epilayer samples under our standard

Figure 4.2. Bar graph of steady-state photoluminescence intensity at 874 nm for 1.0 μm thick epilayer (100) n-GaAs samples after exposure to various nonaqueous solutions. The excitation source was a He-Ne laser at 632.8 nm. The result for a 1.0 **M** $Na_2S \cdot 9H_2O$ (aq) solution is given for comparison. Unless otherwise indicated, all species were 1.0 **M** in diethylether, except for the "wet" 1-butanethiol experiment, which was done in the pure liquid.

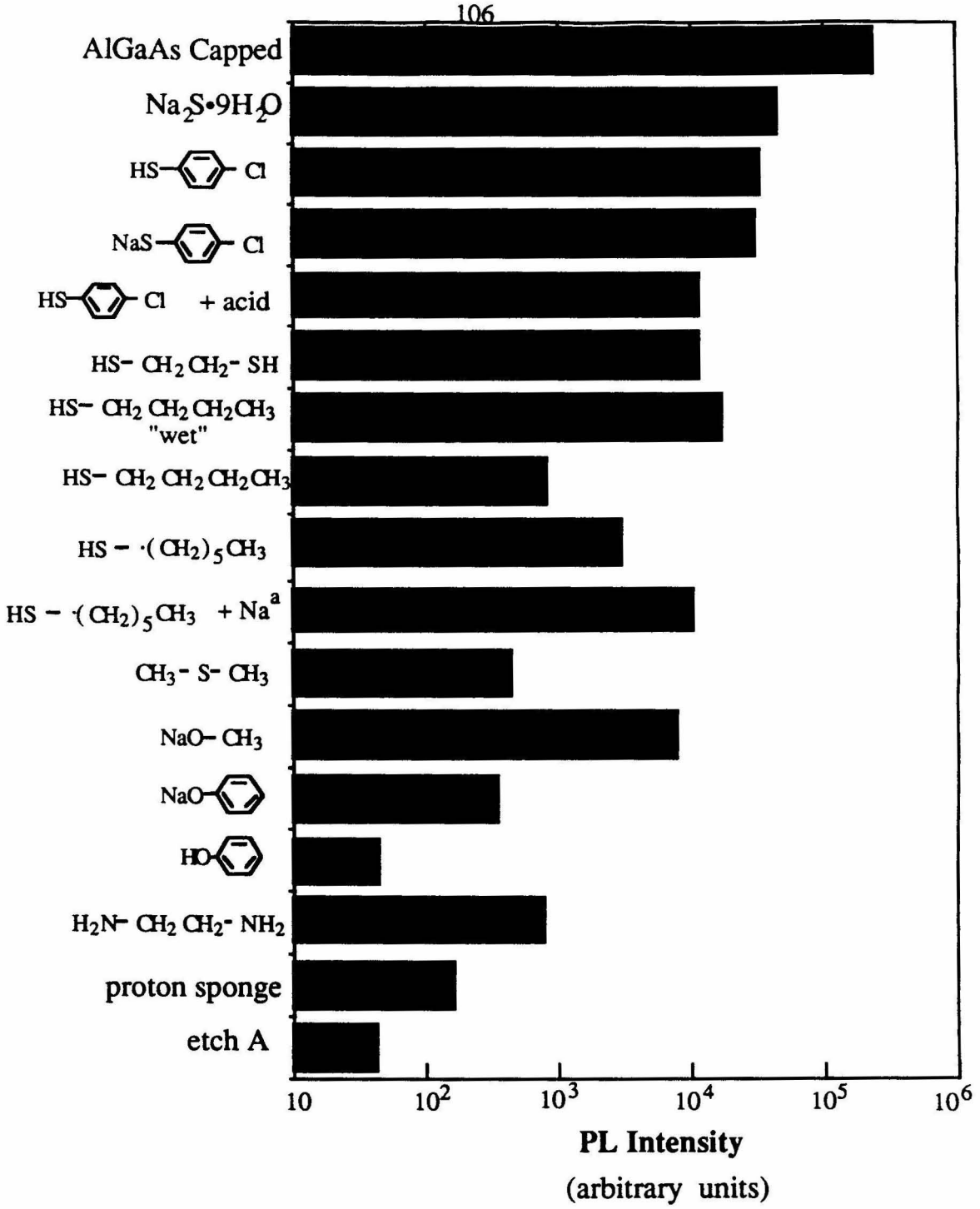

[a]Solvent was tetrahydrofuran.

experimental conditions. Although 1.0 **M** solutions of 1-butanethiol in diethylether did not yield an increase in PL comparable to that of the other thiols, this effect was readily explained by the volatility of the butanethiol (b.p. 98°); when the GaAs surface was kept in contact with the 1-butanethiol, either by continuous immersion in the liquid or by maintaining the sample above a volume of liquid 1-butanethiol, the expected PL increase was observed.

Other sulfur-containing compounds, including $(CH_3)_2SO$ and thiophene, were evaluated with respect to their surface passivation properties on bulk $N_d=10^{17}$ cm^{-3} GaAs (Table 4.II, Section E). These weak bases produced little or no change in the PL signal. Dimethylsulfide produced a larger PL increase than the weaker bases $(CH_3)_2SO$ or thiophene, but the magnitude of the $(CH_3)_2S$-induced PL increase was much smaller than that obtained with simple alkyl- or aryl-thiols (Figure 4.2 and Table 4.I, Section F). This trend is consistent with the ligation properties of these compounds towards various Lewis acid centers, as well as with trends in their equilibrium constants towards protonation.[28,29]

3. Other Organic Bases

Surprisingly, some nonsulfur Brønsted bases also produced substantial, persistent, increases in the GaAs PL signal. Methoxide and phenoxide both yielded significant PL increases, with the steady-state PL increase after exposure to OCH_3^- being comparable to that of the thiols and only slightly lower than that observed after contact with aqueous 1.0 **M** $Na_2S{\bullet}9H_2O$ solutions. The PL signal was also stable over time, unlike the behavior observed after exposure to 1.0 **M** KOH(aq) solutions. The beneficial effects of these oxygen bases were not anticipated in view of the previously proposed role for As-S (and/or Ga-S) species in the surface passivation mechanism.[7,10] A consistent explanation for the OCH_3^- and phenoxide PL response was obtained from time-resolved PL experiments that are discussed in the next section.

B. Time-Resolved Photoluminescence

To further understand the mechanism of surface passivation, time-resolved

photoluminescence studies were conducted under high-level injection conditions. Since the bands are flattened promptly after the laser excitation pulse, changes in the high-level injection PL signal should be due primarily to variation in the density and capture cross section of surface traps, with changes in the equilibrium band bending exerting only a minor effect on either the high-level injection PL intensity or the PL decay time. Because the low-level injection PL intensity is affected by changes both in S and in the equilibrium surface Fermi level,[30] the conversion of steady-state PL intensities into low-level S values is not straightforward; therefore, S was instead extracted from the high-injection, time-resolved data.[12,14,31]

Representative time-resolved PL data for several different GaAs surface treatments are shown in Figure 4.3. These data were taken at a higher injection level and over a shorter time period than the radio frequency decay measurements of Yablonovitch et al.[1c] Best fits of the PL decays are shown in Figure 4.4. The surface recombination velocity of the AlGaAs/GaAs interface has been previously determined to be 100-500 cm s^{-1};[1,25a,32] thus, in our experiments, the PL decay observed for an intact $Al_{0.3}Ga_{0.7}As$ capping layer (yielding a best fit to S=500 cm s^{-1} (Figure 4.4a) served as an excellent validation of our digital simulation method for these PL decay experiments. The most rapid PL decays were recorded for an etched, uncapped, air-exposed, GaAs surface, which gave a best-fit S of $2x10^5$ cm s^{-1} (Figure 4.4c). The GaAs/air interface has been previously shown to have a surface recombination velocity of $>10^5$ cm s^{-1},[1,2,32] which was consistent with both the qualitative and quantitative PL results obtained in this study (Figure 4.3). The low S value for the GaAs/$Al_{0.3}Ga_{0.7}As$ interface and high S value for the GaAs/air interface served as benchmarks for determining the surface recombination velocity of the other, chemically based, surface treatments.

As displayed in Figure 4.3, the various chemical treatments of GaAs surfaces yielded decay times that were between these two extremes of S. While none of the chemical surface treatments yielded PL decay times as long as those observed with the

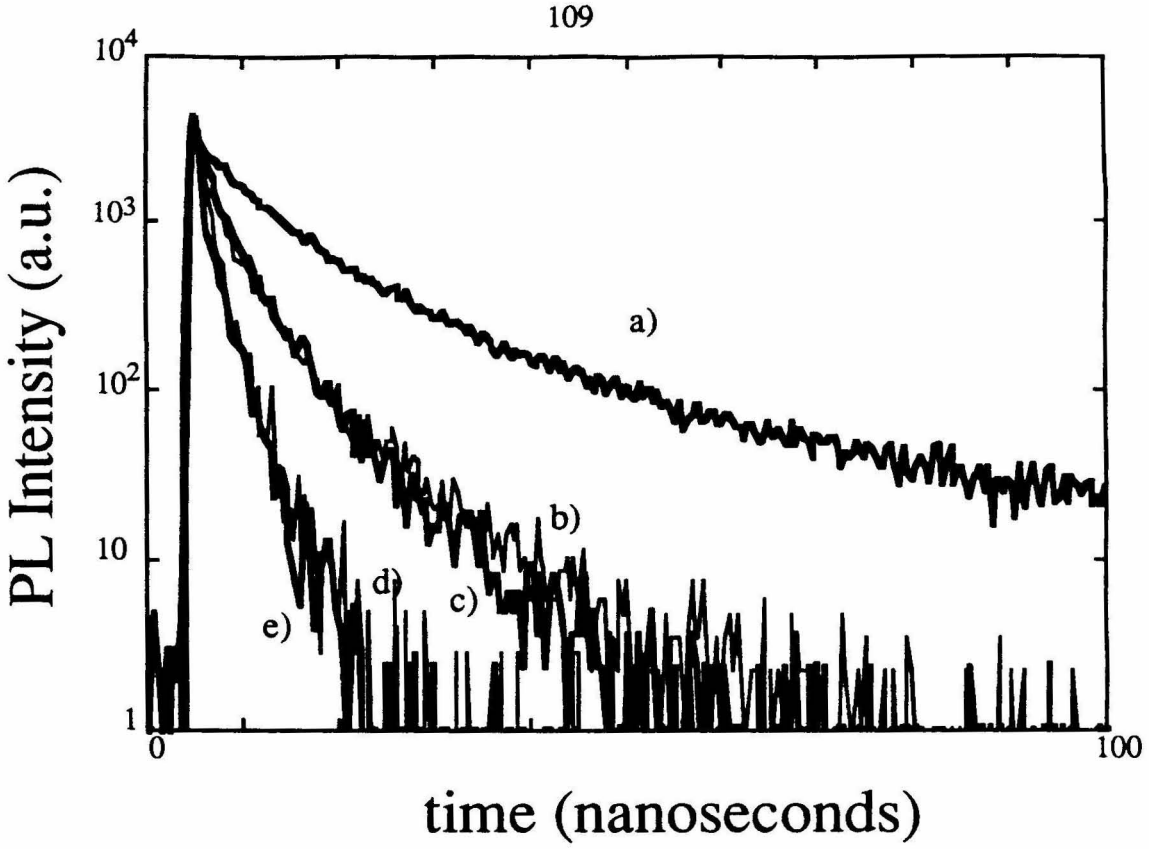

Figure 4.3. Time-resolved photoluminescence decay curves of 2.8 μm thick epilayer GaAs samples taken at 880 nm. The excitation source was a Nd:YAG pumped dye laser providing light at 685 nm. a) $Al_{0.3}Ga_{0.7}As$ capped GaAs sample, as grown. b) $Al_{0.3}Ga_{0.7}As$ cap etched off with 0.05% Br_2 in methanol and GaAs sample immersed into in 1.0 **M** $Na_2S{\bullet}9H_2O$ (aq) for 30 min.. c) Etched GaAs sample immersed into in 1.0 **M** 4-Cl-thiophenol in CCl_4 for 30 min.. d) Etched GaAs sample immersed into in 1.0 **M** $NaOCH_3$ in methanol for 30 min. e) GaAs sample exposed only to etch A (see text).

Figure 4.4. Theoretical fits to the data of Figure 4.3. a) $Al_{0.3}Ga_{0.7}As$ capped GaAs sample, as grown (———) and fit (- - - -) using an S of 500 cm s^{-1}. b) $Al_{0.3}Ga_{0.7}As$ cap etched off with 0.05% Br_2 in methanol and GaAs sample immersed into in 1.0 **M** $Na_2S{\cdot}9H_2O$ (aq) for 30 min. (——) and fit (- - - -) using an S of $7x10^4$. c) GaAs sample exposed only to etch A (——) and fit (- - - -) using an S of $2x10^5$ cm s^{-1}.

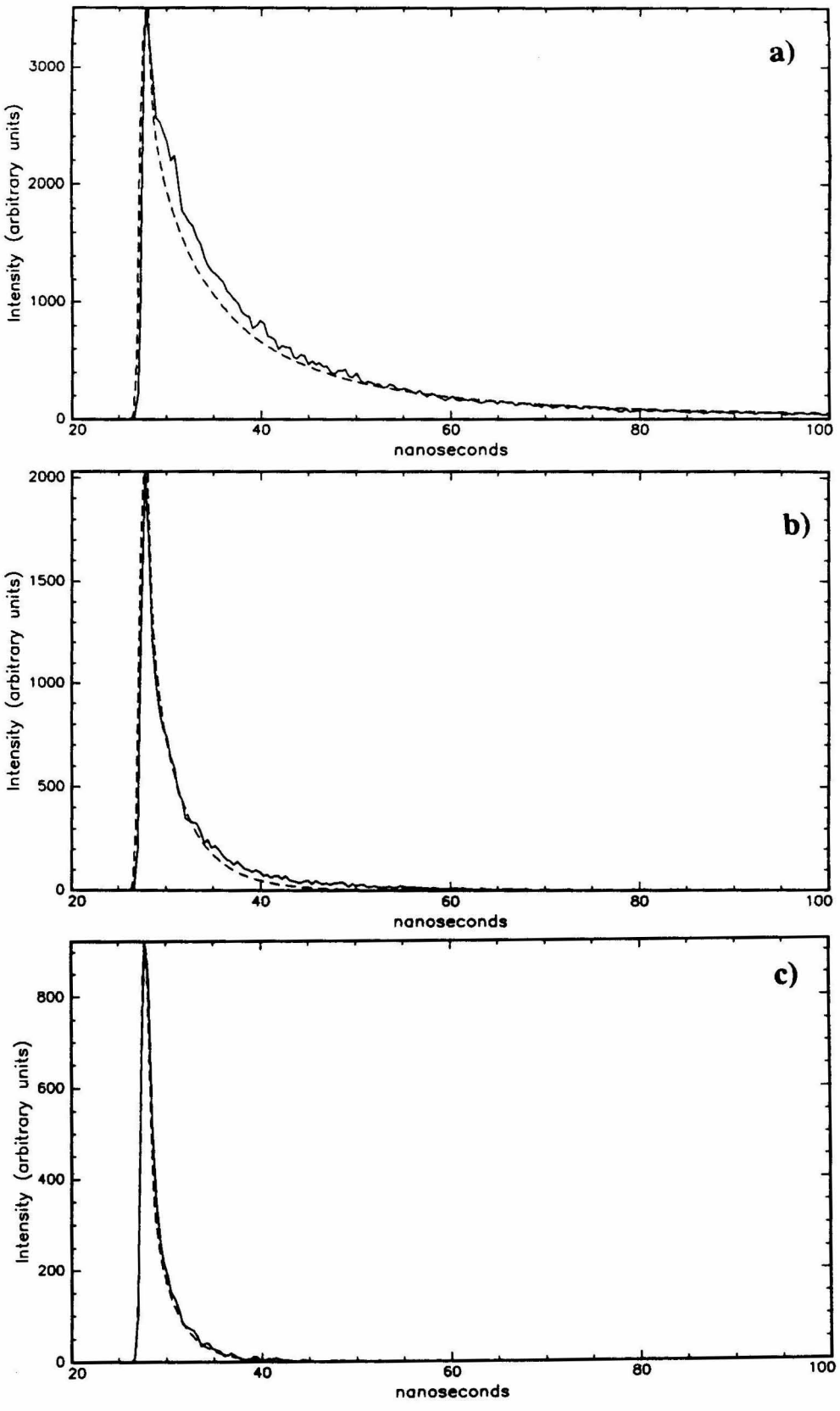
a)
Intensity (arbitrary units)
3000
2000
1000
0
20
40
60
80
100
nanoseconds
b)
Intensity (arbitrary units)
2000
1500
1000
500
0
20
40
60
80
100
nanoseconds
c)
Intensity (arbitrary units)
800
600
400
200
0
20
40
60
80
100
nanoseconds

$Al_{0.3}Ga_{0.7}As$ capping layer, exposure to 1.0 **M** $Na_2S{\cdot}9H_2O$ (aq) clearly produced an interface with a lower surface recombination velocity than that obtained from the unpassivated, air-exposed, GaAs surface (Figure 4.3b,e). The fit to the PL decay curve of a surface exposed to 1.0 **M** $Na_2S{\cdot}9H_2O$ (aq) yielded a surface recombination velocity of 7x104 cm s^{-1} for this interface (Figure 4.4b). Analysis of the PL decays after exposure to 4-Cl-thiophenol also yielded a value of $7x10^4$ cm s^{-1}. In contrast, exposure to 1.0 **M** $NaOCH_3$ in CH_3OH yielded essentially the same decay time as the air-exposed surface, ($S{\approx}2x10^5$ cm s^{-1}). These data clearly indicate that increases in the steady-state PL signal do not necessarily correlate with decreased surface recombination rates under high-injection conditions.

The time-resolved PL results reveal that the steady-state PL improvement from exposure to OCH_3^- was predominantly due to a shift in the equilibrium band bending, as opposed to a reduction in the inherent surface state recombination rates. This system therefore comprises a separate type of molecule that improves steady-state GaAs PL signals without concomitant decreases in high-level surface recombination velocity, and illustrates the variety of chemical mechanisms that can lead to changes in the GaAs steady-state PL intensity.

IV. Discussion

The photoluminescence experiments have shown that a series of chemical reagents can be utilized to reduce substantially recombination rates at GaAs surfaces. The resulting reductions in surface recombination velocity were quite large, and sulfur-containing molecules produced passivation effects that were apparent under both high-level and low-level injection conditions. This implies that a major contribution to the passivation process was a reduction in the surface trap density and/or trapping cross section. A second type of molecule (methoxide) showed a reduction in steady-state surface recombination velocity in the low-injection, steady-state experiments. The methoxide ion did not show an increase in

lifetime in the high-injection PL experiments, thus indicating a second mechanism whereby the steady-state PL yield increases through a shift in surface Fermi level.

In general, the increase in steady-state PL intensity followed the trend in the donor atom of S>O≈N. This is characteristic of a so-called "class b," or soft acid center,[29] as opposed to the behavior expected for the prototypical hard acid center of a proton. Arsenic sites would be expected to exhibit such chemical behavior, although Ga defects in a polarizable environment such as GaAs might also exhibit similar reactivity. It is unlikely, however, that oxides or hydroxides on the GaAs surface would show this order of binding or reactivity, so the PL observations suggest that these species are not the electrically important surface sites. The trends in reactivity certainly suggest that an electron-deficient site is present on the GaAs surface, and that this species is the key chemical site for recombination. Although this trend in reactivity is unfortunately not sufficient to identify unambiguously the chemical nature of the recombination sites, it should provide a useful guideline for choosing other potential surface passivating reagents on GaAs surfaces. A more quantitative analysis of the trends in surface ligation, specifically to address why the thiolates did not exhibit PL increases that generally were superior to those obtained with the thiols, would require determination of the binding constants and saturation coverages of the various ligands; however, the reduced magnitude of the PL effect on rinsed GaAs samples precludes the use of vacuum spectroscopic methods for this purpose. Equilibrium isotherm measurements[33] would be required to achieve these measurements, and these results will be the topic of a separate experimental study.

The general reactivity of donors with the GaAs surface is similar in many respects to recent observations on other semiconductor surfaces. Dunnhauser *et al.*[34] have observed that exposure to ethylenediaminetetraacetate yields a dramatic effect on the surface recombination properties of Cd-rich CdSe colloids, presumably through chelation of the Cd surface trap sites. Similar electron donor effects have also been observed by Ellis and co-workers in studies of the low-level PL intensity of CdSe surfaces,[35] where exposure to

strong nitrogen and oxygen donors and/or chelating reagents have been observed to produce large increases in the steady-state PL signal. These workers have proposed that the origin of this steady-state PL change arises from a modification of the equilibrium surface Fermi level position (i.e., a change in the so-called "dead layer" width) upon adsorption of the amine reagents, although the passivation of trap recombination cannot be explicitly ruled out without direct information on either the surface recombination velocity under high injection or on the absolute value of the equilibrium surface Fermi level position. Our results indicate that both mechanisms are relevant to the GaAs surface chemistry: species such as methoxide do not effect changes in the surface recombination velocity under high injection, but thiols and HS^-(aq) solutions do yield substantial reductions in the inherent surface recombination rates.

In our work, the real-time PL data clearly indicated that the methoxide treatment improved the steady-state PL intensity primarily through a change (increase) in the equilibrium band bending, without a significant reduction in the inherent surface state recombination rate. The high-level injection PL data of Figure 4.3 also confirmed that the Na_2S (aq) and 4-Cl-thiophenol treatments significantly affected the surface recombination properties. This conclusion is supported by previous high-level injection rf decay signals obtained with GaAs surfaces exposed to 1.0 **M** $Na_2S{\cdot}9H_2O$(aq), but does not support the hypothesis of Spindt et al. [9,10] that increased band bending is the primary cause of the steady state PL improvement. In fact, increased band bending should increase the dead layer width[35], which should produce a decrease in the steady-state luminescence intensity that is due to enhanced charge separation. This effect would be opposed only by a band-bending induced reduction in effective surface recombination velocity for certain specific conditions of the surface Fermi level position and of the (majority carrier/minority carrier) capture cross section ratio for the important trap sites.[12] Thus, explanations invoking increased band bending as the source of the PL effect are inconsistent with the experimental

behavior of the GaAs/sulfide system and with general expectations based on conventional carrier trapping statistics at depleted, uninverted, semiconductor interfaces.

V. Conclusions

The photoluminescence experiments described in this chapter demonstrate several important properties of the interaction of sulfides, thiols, and other organic electron donors with GaAs surfaces. The steady-state PL measurements indicated a correlation between the electron donating ability of a species and the improvement in PL. The improvement in PL with methoxide, phenoxide, and ethylenediamine, and the transitory improvement with hydroxide indicated that other strong electron donors beside sulfides can exhibit beneficial effects on GaAs surface recombination rates. The increase in PL followed the trend S > O≈N, which is characteristic of a soft acid center. Charge alone was not sufficient to effect an improvement in steady state PL, as several ionic species did not produce any decrease in the observed surface recombination rate.

The time-resolved PL studies showed that there was an increase in carrier lifetime, in the GaAs flat-band condition, after treatment with 4-Cl-thiophenol or with aqueous sulfides. Therefore, these surface treatments decreased the cross section or density of the important surface traps. Other reagents, such as sodium methoxide, yielded substantial increases in the steady-state PL intensity, but did not affect the inherent GaAs surface carrier trapping rates. GaAs surfaces exposed to sodium methoxide did not exhibit a change in the high-level injection PL lifetime, and therefore this reagent produced an increase in the steady-state PL intensity by effecting a change in the surface Fermi level position.

Although both types of reagents (OCH_3^- and thiols) produced a change in the observed low-level, steady-state PL intensity, the time-resolved PL results show that both types of systems do not coordinate to GaAs surface traps. It is this type of interaction that is the desired target of our work because of its more general relevance to the reduction of surface recombination processes in a variety of device configurations and under a variety of

carrier injection levels. Future work targeting reagents with the chemical properties of sulfides (electron donating, strong base), but having greater stability in air may result in even better passivants.

References

1. a) B. J. Skromme, C. J. Sandroff, E. Yablonovitch, and T. Gmitter, *Appl. Phys. Lett.* **51**, 2022 (1987). b) C. J. Sandroff, R. N. Nottenburg, and J. C. Bischoff, R. Bhat, *Appl. Phys. Lett.* **51**, 33 (1987). c) E. Yablonovitch, C. J. Sandroff, R. Bhat, and T. Gmitter, *Appl. Phys. Lett.* **51**, 439 (1987).

2. A. Heller, in *Photoeffects at Semiconductor-Electrolyte Interfaces*, edited by A. Nozik, ACS Symposium Series 146 (ACS, Washington DC, 1981), pp. 57-77.

3. a) H. Hasegawa, T. Saitoh, S. Konishi, J. Ishii, and H. Ohno, *Jap. J. Appl. Phys.* **27**, L2177 (1988). b) H. Hasegawa, H. Ishii, T. Sawada, T. Saitah, S. Kanishi, Y. Liu, and H. Ohno, *J. Vac. Sci. Technol. B* **6**, 1184 (1988).

4. a) G. D. Pettit and J. M. Woodall, J. Vac. Sci. Technol. *B* **6**, 1180 (1988). b) C. W. Wilmsen, P. D. Kirchner, and J. M. Woodall, *J. Appl. Phys.* **64**, 3287 (1988).

5. a) K. M. Geib, J. Shin, and C. W. Wilmsen, *J. Vac. Sci. Technol. B* **8**, 838 (1990). b) J. Shin, K. M. Geib, C. W. Wilmsen, and Z. Lilliental-Weber, *J. Vac. Sci. Technol. A* **8**, 1894 (1990). c) T. Tiedje, K. M. Colbow, D. Rogers, Z. Fu, and W. Everhardt, *J. Vac. Sci. Technol. B* **7**, 837 (1989).

6. E. Yablonovitch, B. J.Skromme, R. Bhat, J. P. Harbinson, and T. J. Gmitter, *Appl. Phys. Lett.* **54**, 555 (1989).

7. C. J. Sandroff, M. S. Hegde, L. A. Farrow, C. C.Chang, and J. P. Harbison, *Appl. Phys. Lett.* **54**, 362 (1989).

8. a) M. S. Carpenter, M. F. Melloch, and T. E. Dungan, *Appl. Phys. Lett.* **53**, 66 (1988). b) M. S. Carpenter, M. R. Melloch, M. S. Lundstrom, and S. P. Tobin, *Appl. Phys. Lett.* **52**, 2157 (1988).

9. a) R. S. Besser, C. R. Helms, *Appl. Phys. Lett.* **52**, 1707 (1988). b) D. Liu, T. Zhang, R. A. LaRue, J. S. Harris, and T. W. Sigmon, *Appl. Phys. Lett.* **53**, 1059 (1988).

10. C. J. Spindt and W. E. Spicer, *Appl. Phys. Lett.* **55**, 1653 (1989).

11. C. J. Spindt, R. S. Besser, R. Cao, K. Miyano, C. R. Helms, and W. E. Spicer, *J. Vac. Sci. Technol. A* **7**, 2466 (1989).

12. A. Many, Y. Goldstein, and H. B. Grover, *Semiconductor Surfaces* (North-Holland, New York, 1965).

13. M. Evenor, S. Gottesfeld, Z. Harzion, D. Hupert, and S. W. Feldberg, *J. Phys. Chem.* **88**, 6213 (1984).

14. S. W. Feldberg, M. Evenor, D. Huppert, S. Gottesfeld, *J. Electroanal. Chem.* **185**, 209 (1985).

15. Material grown by organometallic vapor phase epitaxy by Hugh MacMillan of Varian Associates, Palo Alto, CA.

16. Material grown by molecular beam epitaxy, and kindly supplied by C. Sandroff of Bellcore, Red Bank, NJ.

17. H. J. Stocker and D. E. Aspnes, *Appl. Phys. Lett.* **42**, 85 (1983).

18. B. J. Tufts, L. G. Casagrande, N. S. Lewis, and F. J. Grunthaner, *Appl. Phys. Lett.* **57**, 2262 (1990).

19. R. P. Vasquez, B. F. Lewis, and F. J. Grunthaner, *J. Vac. Sci. Technol. B* **1**, 791 (1983).

20. a) M. Fukuda and K. Takahei, *J. Appl. Phys.* **57**, 129 (1985). b) D. Guidotti, E. Hasan, H. J. Hovel, and M. Albert, *Appl. Phys. Lett.* **50**, 754 (1987). c) T. Suzuki, and M. Ogawa, *Appl. Phys. Lett.* **31**, 473, 1977.

21. D. E. Aspnes, S. M. Kelso, R. A. Logan, and R. Bhat, *J. Appl. Phys.* **60**, 754 (1986).

22. D. V. O'Conner and D. Phillips, *Time-Correlated Single Photon Counting* (Academic, London, 1984).

23. a) S. Canonica J. Forrer, and U. P. Wild, *Rev. Sci. Instrum.* **56**, 1754 (1985). b) W. R. Ware, M. Pratinidhi, and R.K. Bauer, *Rev. Sci. Instrum.* **54**, 1148 (1983).

24. a) R. J. Nelson and R. G. Sobers, *J. Appl. Phys.* **49**, 6103 (1978). b) G. W. t'Hooft, *Appl. Phys. Lett.* **39**, 389 (1981).

25. a) R. J. Nelson and R. G. Sobers, *J. Appl. Phys.* **49**, 6103 (1978). b) G. W. t'Hooft, *Appl. Phys. Lett.* **39**, 389 (1981).

26. S. Licht, F. Forouzan, and K. Longo, *Anal. Chem.* **62**, 1356 (1990).

27. a) J. C. Bailor, H. J. Emeleus, R. Nyholu, and A. F. Trotman-Dickenson, *Comprehensive Inorganic Chemistry Vol. I* (Pergamon, Oxford, 1973), pp. 430-431, b) *ibid., Vol. II*, p. 837

28. A. Streitwieser and C. H. Heathcock, *Introduction to Organic Chemistry* (McMillan, New York, 1976), p. 1188.

29. J. E. Huheey, *Inorganic Chemistry, 3rd Ed.* (Harper & Row, New York, 1983), pg. 313.

30. a) B. Smandek, G. Chmiel, and H. Gerischer, *Ber. Bunsenges. Phys. Chem.* **93**, 1094 (1989). b) G. J. Meyer, G. C. Lisensky, and A. B. Ellis, *J. Am. Chem. Soc.* **110**, 4914 (1988).

31. Full details of the modeling program used in our laboratory will be provided elsewhere: G. N. Ryba and N. S. Lewis, to be published.

32. R. J. Nelson and R. G. Sobers, *Appl. Phys. Lett.* **32**, 761 (1978).

33. A. Wieckowski, in *Modern Aspects of Electrochemistry*, R. E. White, J. O'M. Bockris, B. E. Conway, Eds. (Plenum, New York, 1990), pp. 65-119.

34. T. J. Dunnhauser, M. O'Neil, K. Johnasson, D. Whitten, G. McLendon, *J. Phys. Chem.* **90**, 6074 (1986).

35. a) C. J. Murphy and A. B. Ellis, *J. Phys. Chem.* **94**, 3082 (1990). b) G. J. Meyer, L. K. Leung, J. C. Yu, G. C. Lisensky, and A. B. Ellis, *J. Am. Chem. Soc.* **111**, 5146 (1989).

Chapter 5. X-ray Photoelectron Spectroscopy Studies of the Surface Chemistry of (100) n-GaAs Exposed to Thiols and Aqueous Na_2S

I. Introduction

In the previous chapter, steady-state and time resolved PL experiments were described which demonstrated that sulfur-containing inorganic salts and organic thiols were effective in reducing the cross section of surface recombination sites. In addition, we have used high-resolution x-ray photoelectron spectroscopy[1] to investigate the elemental As stoichiometry and to study the formation of arsenic sulfides after the GaAs surface has been exposed to the desired chemical reagent. Previous photoemission studies of GaAs exposed to aqueous Na_2S and $(NH_4)_2S$[2,3,4,5,6,7] have shown that an As-S phase, and possibly a Ga-S phase are formed on the surface. The As-S phase has been assigned to As_2S_3 by several different authors,[2,6] on the basis of the position of the As peaks. The Ga-S phase is rather difficult to resolve because of the small chemical shift of this species.

In this chapter, the correlation between changes in surface stoichiometry and the PL changes described in Chapter 4 is investigated. These studies have been performed in a rigorously anaerobic environment, so that the effects of native oxide growth on the formation of As_2S_3 and Ga_2S_3 precipitates (from a chemical reaction with the Na_2S(aq) solutions) can be minimized and investigated systematically. The GaAs surface was also exposed to a variety of etches in order to obtain a stoichiometric surface, an As^0-rich surface, or an oxidized surface. These experiments have enabled us to probe correlations between the initial surface chemical composition and the stoichiometry of the modified GaAs interface.

II. Experimental

Most bulk GaAs samples used in XPS experiments were performed on (100)-oriented GaAs single crystals with donor densities (N_d) of 10^{17} cm^{-3} (Morgan Semiconductor, Inc. or Wacker Inc.) or on nominally undoped GaAs samples. XPS

studies were performed using a high resolution Surface Science Instruments Model 100 top hat monochromator (Al x-rays, 1486.6 eV) or using a VG Mark II ESCAlab, nonmonochromatic, x-ray source (Mg x-rays, 1254 eV). The FWHM of the Au $4f_{7/2}$ line was 0.95 eV on the SSI instrument and was 1.61 eV on the VG instrument. The base pressure was at least $1x10^{-9}$ torr in both instruments. The monochromatic x-rays from the SSI machine were used to obtain chemical information in the As 3d and 2p regions, while the use of the Mg source from the VG instrument eliminated interference from the As Auger lines (≈232 BeV in Al XPS) and allowed the observation of signals in the S 2s 229 BeV region. All peaks are reported with respect to C 1s= 285.0 eV, but the actual measured value of the carbon peak for each spectrum is also reported in the tables. XPS data were analyzed using standard, peak-fitting routines to obtain peak areas. For analysis of the As 3d regions, two sets of doublets, each constrained to a ratio of 1.5:1 and to a separation of 0.7 eV, were used to obtain fits for substrate As and elemental As. The separation between the substrate and elemental As doublets was constrained to 0.7-0.8 eV.[8] The amorphous As-S component was fit with a broad singlet without any constraints. Overlayer coverages were calculated from the XPS signal intensities as described in Chapter 2 and the values for σ, λ, and n used in this chapter are given in Table 5.I.

The etching procedure for samples studied by XPS was the same as for steady-state PL measurements in Chapter 4. However, to avoid interference from surface oxides, the etching solutions and all chemical reagent solutions were deaerated, and etching was performed either in a glove bag or in an N_2-purged glove box. Except where otherwise noted, after immersion into aqueous solutions, the GaAs samples were rinsed thoroughly with deaerated H_2O; after immersion into organic solvents, the samples were rinsed with methanol. Dried and treated samples were transported to the XPS instrument, or between the two XPS machines, in glass vials that were sealed under N_2 or Ar. The vials were opened in a glove box that was attached to the desired XPS instrument, and the GaAs

Table 5.I. Cross sections (σ), escape depth (λ) and atomic density (n) used for calculation of coverages and mole ratios on GaAs surfaces exposed to various etches and sulfur-containing compounds. Numbers in parentheses are for Mg x-rays.

Surface species	σ	λ (Å)	n (atom/cm^3) (x10^{-22})
As 3d region:			
GaAs substrate	1.821(1.972)	25(22)	2.22
As^o	"	23	4.6
As_2O_3	"	36(33)	2.27
As_2S_3	"	42	2.52
As 2p region:			
GaAs substrate	27.19	8	2.22
As^o	"	8	4.6
As_2O_3	"	12	2.27
As_2S_3	"	14	1.68
Ga 3d region:			
GaAs substrate	1.085(1.193)	25(22)	2.22
Ga_2O_3	"	28(25)	3.97
Ga 2p region:			
GaAs substrate	21.4	12	2.22
Ga_2O_3	"	14	2.52
S 2s region:			
As_2S_3	(1.25)	(36)	2.52
HS-(C_6H_6)-Cl	"	(31)	0.52
Cl 2p (HS-(C_6H_6)-Cl)	2.245	31	0.52
C 1s	1.00	36(29)	13.1

samples were then introduced into the vacuum chamber of the instrument without deliberate exposure to oxygen.

Spin-profiling experiments were performed using the following procedure. Bulk, low-doped GaAs samples were exposed to etch B in a dry box containing flowing N_2(g). These samples were analyzed by XPS, and were then returned to the dry box for subsequent exposure to 1.0 **M** $Na_2S{\cdot}9H_2O$ (aq). After a 10 min exposure, the GaAs samples were spun-dried and transferred back into the high vacuum chamber and another set of XPS data (which showed only sodium, oxygen, carbon and sulfur) was taken. The sample was then removed, rotated on a spin coater, exposed to one drop of water, and

spun to dryness. The XPS spectrum was then reexamined, and the spin/etch/dry process was repeated until no further changes in the XPS spectrum were noted. This procedure is very similar to that described earlier for profiling oxide films on Si and GaAs.[1,9]

III. RESULTS

A. Etched GaAs Surfaces

The high-resolution, small-spot XPS instrument described in the experimental section was used to obtain chemical information on the GaAs surface composition. (100)-oriented GaAs samples were exposed to three different etching procedures (etch A, B or C) in order to obtain a range of initial surface stoichiometries. The As 3d regions of the XPS spectra for these three surfaces are displayed as the dashed lines in Figures 5.1a-c,[10] and the corresponding As 2p regions are the dashed lines in Figures 5.1d-f. These spectra were normalized relative to the intensity of the As_{GaAs} lattice peak in the As 3d region. To provide background for the changes observed after exposure to the various chemical reagents, the important features of the XPS spectra for each etch are discussed below.

1. XPS Spectra of the Br_2-CH_3OH/KOH Etched GaAs Surface

Etch A has been studied previously by Stocker and Aspnes using spectroscopic ellipsometry[11] and by Tufts et al.,[12] using XPS. If exposure to air is minimized, this etching procedure has been shown to leave a minimally oxidized, near stoichiometric, GaAs surface. This behavior was apparent in the data depicted in Figure 5.1a (dashed curve). As_{GaAs} signals in the As 3d region were apparent as the As $3d_{5/2}$ peak at 41.2(±0.3) eV, with a doublet splitting of 0.7 eV, and As_{GaAs} $2p_{3/2}$ signals were apparent as a peak at 1322.9(±0.2) eV. The Ga 3d region (not shown) displayed the expected peak for Ga_{GaAs} at 19.3(±0.3) eV. Although the calculated elemental ratio of As_{GaAs} to Ga_{GaAs} was not precisely unity (Table 5.II), no oxidized Ga, little oxidized As, and no other significant impurities (other than adventitious carbon and oxygen from adsorbed water) were detected on this surface. Specifically, the lack of detectable peaks at 20.3 eV in the Ga 3d region and at 44.3 eV in the As 3d region (Figure 5.1a, Table 5.II) indicated that the

Figure 5.1. As 3d and 2p XP spectra for bulk 10^{17} doped (100) n-GaAs. The dashed lines are the spectra for the freshly etched sample, and the solid lines are after immersion into 1.0 **M** $Na_2S \cdot 9H_2O$ (aq) for 30 min. and extensive rinsing with H_2O. Panel a) displays the As 3d region for a sample that had been exposed to etch A (dashed line), and for another sample that had been etched and then exposed to 1.0 **M** $Na_2S \cdot 9H_2O$ (solid line). Panel b) displays the As 3d region for a sample that had been exposed to etch B (dashed line), and for another sample that had been etched and then exposed to 1.0 **M** $Na_2S \cdot 9H_2O$ (solid line). Panel c) displays the As 3d region for a sample that had been exposed to etch C (dashed line), followed by subsequent exposure of this same sample to 1.0 **M** $Na_2S \cdot 9H_2O$ (solid line). Panel d) shows the As 2p region for the samples of Panel a). Panel e) shows the As 2p region for the samples of Panel b). Panel f) shows the As 2p region for the samples of Panel c). All spectra were collected with a monochromatic XPS source under rigorously anaerobic conditions, except for the spectra in panels c) and f).

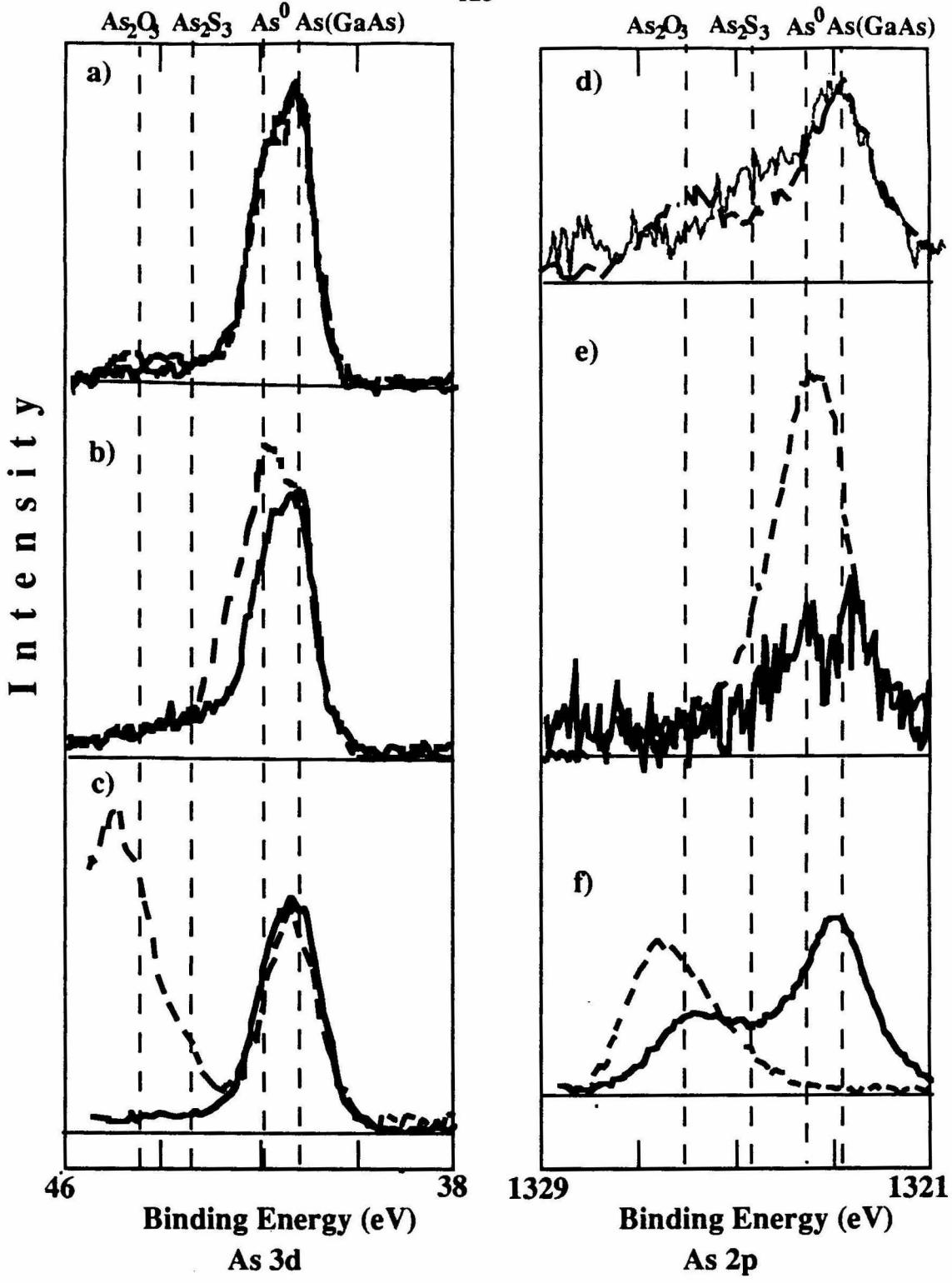
As2O3 As2S3 As0 As(GaAs)
a)
b)
c)
Intensity
46
38
Binding Energy (eV)
As 3d
As2O3 As2S3 As0 As(GaAs)
d)
e)
f)
1329
1321
Binding Energy (eV)
As 2p

Table 5.II. XPS data for GaAs exposed to aqueous sodium sulfide solutions. All coverages were calculated relative to the As 3d GaAs substrate peak. A value of 0.0 indicates that the level was less than 0.1 X 10^{-9} moles/cm^2. "--" indicates that the peaks were undetectable because of either sensitivity or resolution.

Sample	x-ray[a] source	Ga 3d			Ga 2p		
		Ga (GaAs) eV	Ga (Ga_2O_3) eV	Γ (Ga_2O_3) moles/cm^2 X 10^9	Ga (GaAs) eV	Ga (Ga_2O_3) eV	Γ (Ga_2O_3) moles/cm^2 X 10^9
Etch A[c]	Al	19.5	20.5	0.5			
+ 1.0 M Na_2S (30 min)	Al	18.7	–	0.0	1116.4	–	0.0
Etch A	Al/Mg	19.4	–	0.0	1117.0	–	0.0
+ 1.0 M Na_2S (30 min)	Al/Mg	19.5	–	0.0	1117.1	–	0.0
Etch B	Al	19.5	–	0.0	1117.2	1118.3	0.8
+ 1.0 M Na_2S (60s) fresh film	Al						
+ 1 drop H_2O	Al				1116.3	–	0.0
+ 2 drops H_2O	Al				1116.5	–	0.0
+ H_2O rinse	Al	18.8	19.8	0.3	1116.5	–	0.0
Etch B	Al	19.3	–	0.0			
+ 1.0 M Na_2S (60s)	Mg	19.0	–	0.0			
	Al	19.3	20.3	0.4			
Etch B	Al	19.2	–	0.0			
+ 1.0 M Na_2S (1hr)	Mg	19.2	–	0.0			
Etch B	Al	19.0	20.6	0.2			
+ 1.0 M Na_2S pH 7 (1 hr)	Mg	19.2	–	0.0			
	Al	19.2	–	0.0			
Etch C	Al/Mg	19.5	20.6	5.3	–	1118.2	
+ 1.0 M Na_2S (30 min)	Al/Mg	19.9	–	0.0			
Etch C	Al/Mg	20.1	21.5	2.4			
+ 1.0 M NaHS pH 7 (15 min)		19.5	–	0.0			

[a]Al=Data taken with monochromatic Al K_α x-rays (1486.6 eV) on a Surface Science Instruments Model 100.
Mg=Data taken with Mg K_α x-rays (1254 eV) on a VG Mark II.
Al/Mg=Data taken primarily with Al K_α x-rays on a VG HP 580, except for S regions.
[b]The Ga/As ratio is based on substrate peaks and does not include oxides.
[c]Etch A=1.0 M KOH (15s), 0.5% Br_2/Methanol (15 s), repeated 3 times and ending in KOH.
Etch B= Etch A + 30s 1:1:100 (H_2SO_4:30% H_2O_2:H_2O).
Etch C= Etch A + 10 s 30% H_2O_2.
[d]Binding energy for S 2p region.

Table 5.II. Continued

As 3d							As 2p		
As (GaAs) eV	As (As_2O_3) eV	Γ (As_2O_3) moles cm^2 X 10^9	As (As^o) eV	Γ (As^o) moles cm^2 X 10^9	As (As_xS_y) eV	Γ (As_xS_y) moles cm^2 X 10^9	As (GaAs) eV	As (As_2O_3) eV	Γ (As_2O_3) moles cm^2 X 10^9
41.3	44.6	0.3	–	0.0	–	0.0	1323.1	1326.0	0.5
40.5		0.0	–	0.0	42.4	0.2	1322.1	–	0.0
41.4	44.0	0.2	–	–	–	0.0	1322.4	1325.4	0.7
41.5	–	0.0	–	–	–	0.0	1322.6	–	0.0
41.5	–	0.0	42.3	5.1	–	0.0	1323.1	–	0.0
							1321.7	–	0.0
40.7	–	0.0	41.5	2.9	–	0.0	1321.8	–	0.0
40.7	–	0.0	41.5	1.7	43.0	0.1	1322.1	–	0.0
41.1	–	0.0	42.0	2.9	–	0.0			
40.8	–	0.0	–	–	--	0.0			
41.2	–	0.0	41.9	0.9	43.4	0.2			
41.1	–	0.0	42.0	2.1	–	0.0			
41.2	–	0.0	–	–	–	0.0			
41.0	44.3	0.3	41.7	5.0	–	0.0			
41.0	–	0.0	–	–	–	0.0			
41.0	–	0.0	41.8	0.8	43.4	0.3			
41.3	45.7	3.8	–	–	–	0.0	–	1326.9	
41.9	44.7	0.3	–	–	–	0.0	1322.9	1326.0	0.6
42.1	46.5	1.9	–	–	–	0.0	–	1328.6	
41.4	–	0.0	–	–	–	0.0	1323.4	–	0.0

Table 5.II. Continued

As 2p				Ga/As		S 2s		C 1s
As (As^O) eV	Γ (As^O) moles cm^2 X 10^9	As (As_xS_y) eV	Γ (As_xS_y) moles cm^2 X 10^9	3d region	2p region	eV	Γ (S) moles cm^2 X 10^9	eV
–	0.0	–	0.0	1.5	–			284.9
–	0.0	1323.6	0.7	2.0	5.7			285.9
		–	0.0	1.1	1.4			286.0
		1324.3	0.4	1.4	2.4	225.8	0.2	286.2
1323.8	4.2			0.7	1.3			284.9
						162[d]	>10.4	285.6
1322.4	0.9	1324.0	0.1			162[d]		285.6
1322.5	0.2	1323.9	0.3					285.4
1322.9	1.1	1323.7	0.2	0.9	1.6			285.5
				1.6				284.9
				1.2		225.2	0.3	286.8
				0.9				285.2
				1.8				285.2
				1.2		225.7	0.4	285.5
				1.8				285.4
				1.3		226.2	1.3	285.2
				1.1				285.1
–	0.0	–	0.0	1.9				286.2
–	0.0	1324.4	0.3	1.4		226.6	0.2	286.4
–	0.0	–	0.0	1.3				285.5
–	0.0	1325.0	0.4	1.3				284.9

Ga_2O_3 and As_2O_3 coverages were less than $1x10^{-10}$ moles cm^{-2} on this sample; the only evidence for oxidation was the small peak at 1326.0 eV in the surface-sensitive As 2p region (Figure 5.1d).

The presence of elemental As^0 was also of concern, because of its importance in various proposed GaAs surface passivation schemes. Excess elemental As has been observed to exhibit an XPS peak at 41.8(±0.3) eV in the As 3d region;[13] thus, the small chemical shift difference between As^0 and lattice As_{GaAs} precluded obtaining a distinct peak for As^0 using the available XPS instrumentation. However, the coverage of elemental As^0 can be determined from the As^0 contribution to the intensity of the higher binding energy peak of the As_{GaAs} doublet.[12,13] After etch A, the As_{GaAs} spin-orbit doublet was observed to have a 3:2 area ratio, as expected for a surface with no detectable, excess elemental As (Figure 5.1a).[12,13]

2. XPS Spectra of the Br_2-CH_3OH/KOH, 1:1:100 H_2SO_4:H_2O_2:H_2O, Etched GaAs Surface

Etch B has been shown previously by spectroscopic ellipsometry[11] and by XPS[12,13] to yield a surface with substantial excess elemental As^0. This was clearly reflected in the XPS data of Figure 5.1b by the additional intensity at 41.8 eV in the As 3d region and by the enhanced intensity of the As 2p peak at 1323.8 eV. Spectral fitting[12,13] in the As 3d region was used to obtain a quantitative estimate of the As^0 coverage, which had a value of $5.1x10^{-9}$ moles cm^{-2} for the sample of Figure 5.1b; analysis of the As 2p region yielded an elemental As^0 coverage of $4.2x10^{-9}$ (Table 5.II). As displayed in Figure 5.1b, negligible amounts of As_2O_3 (or Ga_2O_3) were routinely observed when etch B was used, and the sample was handled in an anaerobic environment.

3. XPS Spectra of Peroxide Etched GaAs Surfaces

GaAs surfaces exposed to etch C showed decreased absolute As_{GaAs} and Ga_{GaAs} peak intensities relative to those observed from GaAs samples exposed to Etch A. Additionally, a broad peak at 20.6 eV in the Ga 3d region indicated the presence of a

mixture of Ga_2O_3 and Ga_2O_5, and the peaks centered at 45.7 eV in the As 3d region and at 1326.9 eV in the As 2p region indicated the presence of a mixture of As_2O_3 and As_2O_5 (Figures 5.1c,f, and Table 5.II). This surface was clearly oxidized, as indicated by previous spectroscopic ellipsometry[11] and XPS[13] data. Unlike the previous spectra discussed above, the XPS data of Figure 5.1c,f were obtained on a nonmonochromatic XPS instrument; thus, the lack of resolution in the As_{GaAs} 3d doublet region is not an inherent property of these samples, but reflects the resolution limits of the instrumentation.[13] The elemental As^0 coverage was not of concern for this etch, so the lack of high-resolution XPS data in the As 3d region did not preclude use of this sample for the $Na_2S{\cdot}9H_2O$ experiments described below. The obvious differences in surface stoichiometry provided by these three different GaAs etches were exploited in our XPS investigations of the S-based, surface passivation chemistry.

B. Exposure of GaAs to $Na_2S \cdot 9H_2O$(aq) Solutions

1. GaAs Surface Composition After Exposure to 1.0 M $Na_2S{\cdot}9H_2O$(aq) and a H_2O(l) Rinse

The solid lines in Figures 5.1a-f display the As 3d and As 2p XP spectra obtained after exposure of the etched GaAs surfaces to 1.0 **M** $Na_2S{\cdot}9H_2O$ (aq). A striking feature of these spectra is that the three Na_2S-treated GaAs samples had extremely similar surface compositions, despite the significant differences in initial surface stoichiometry for the three etching procedures. The 1.0 **M** $Na_2S{\cdot}9H_2O$(aq) exposure removed almost all of the As oxides and Ga oxides (Figures 5.1c,f; Table 5.II) and substantially reduced the levels of As^0 (Figures 5.1b,d; Table 5.II) that were introduced by the etching steps. The only significant difference between the three final surfaces was the oxide peak evident in the As 2p region of Figure 5.1f. This residual, low level, oxide peak was observed in the surface-sensitive As 2p region on this sample because unlike the XPS instrument used for Figures 4a,b,d,e, the XPS instrument used for experiment 5.1c,f did not have an anaerobic

interlock to a glove box, and therefore atmospheric exposure could not be completely eliminated for this specimen.

Independent XPS experiments verified that As^{III} oxides, Ga^{III} oxides, and As^0 were not removed by rinsing the GaAs surface with pure H_2O; thus, the similarity of the GaAs spectra in Figure 5.1a-f after Na_2S(aq) immersion and H_2O rinsing indicates that excess As^0, As oxides, and Ga oxides were all removed by the Na_2S(aq) $\cdot 9H_2O$(aq) solutions. This is consistent with prior studies of the behavior of GaAs surfaces immersed into 1.0 **M** KOH-0.8 **M** K_2Se-0.1 **M** K_2Se_2 solutions, and is expected given the bulk solubility behavior of As-oxides in basic aqueous solutions[14] and of elemental As in basic aqueous chalcogenide solutions.[15,13] These spectra are clearly consistent with observations in section A, that the 1.0 **M** $Na_2S \cdot 9H_2O$(aq)-induced increase in steady-state PL intensity was not sensitive to the GaAs etching procedure.

Figure 5.2 shows fits to the XPS spectra obtained after the various etching and 1.0 **M** $Na_2S \cdot 9H_2O$ (aq) immersion steps. An As-S species was detectable on all of the GaAs samples exposed to 1.0 **M** $Na_2S \cdot 9H_2O$(aq), as evidenced by the presence of peaks at 43.3(±0.2) eV in the As 3d region and at 1324.1(±0.3) eV in the As 2p region. Although the As-S peak was more clearly evident in the surface-sensitive As 2p spectral region (Figure 5.1d-f vs. Figure 5.1a-c), fitting of the As 3d lineshape confirmed the presence of the As-S phase (Figure 5.2b,d); this peak could not be satisfactorily fit using only the known As_{GaAs}, As^0, and As_2O_3 peak energies and linewidths. The calculated coverage of the As_xS_y phase from the As 2p region was about 2-4-fold higher than the coverage obtained from the As 3d region (Table 5.II), indicating inhomogeneity in the film and/or a deviation from the experimental photoelectron cross section from those obtained from Scofield[16] because of the different response of the detector at low kinetic energies. The effective thickness of the As_xS_y phase was also considerably higher than that calculated from the As 3d region. The As-S peak position was slightly lower in binding energy than the As 3d value of 43.9 eV, and much lower than the As 2p value of 1325.7 eV from an

Figure 5.2. Peak fits for selected As 3d and 2p XP spectra of Figure 5.1. The As 3d doublets were constrained to a ratio of 1.5:1 and a separation of 0.7 eV. Substrate As doublet peaks are indicated as the dashed lines in the fits, and elemental As^0 peaks are indicated as the solid lines. a) As 3d Spectrum of etched GaAs sample from Figure 5.1a, with peak fits as shown. b) As 3d Spectrum of 1.0 **M** $Na_2S{\bullet}9H_2O$(aq) exposed GaAs sample of Figure 5.1a, with peak fits as shown. c) As 3d Spectrum of etched GaAs sample from Figure 5.1b, with peak fits as shown. d) As 3d Spectrum of 1.0 **M** $Na_2S{\bullet}9H_2O$(aq) exposed GaAs sample of Figure 5.1b, with peak fits as shown. e) As 2p region for the sample of panel 5.2a). f) As 2p region for the sample of panel 5.2b). g) As 2p region for the sample of panel 5.2c). h) As 2p region for the sample of panel 5.2d).

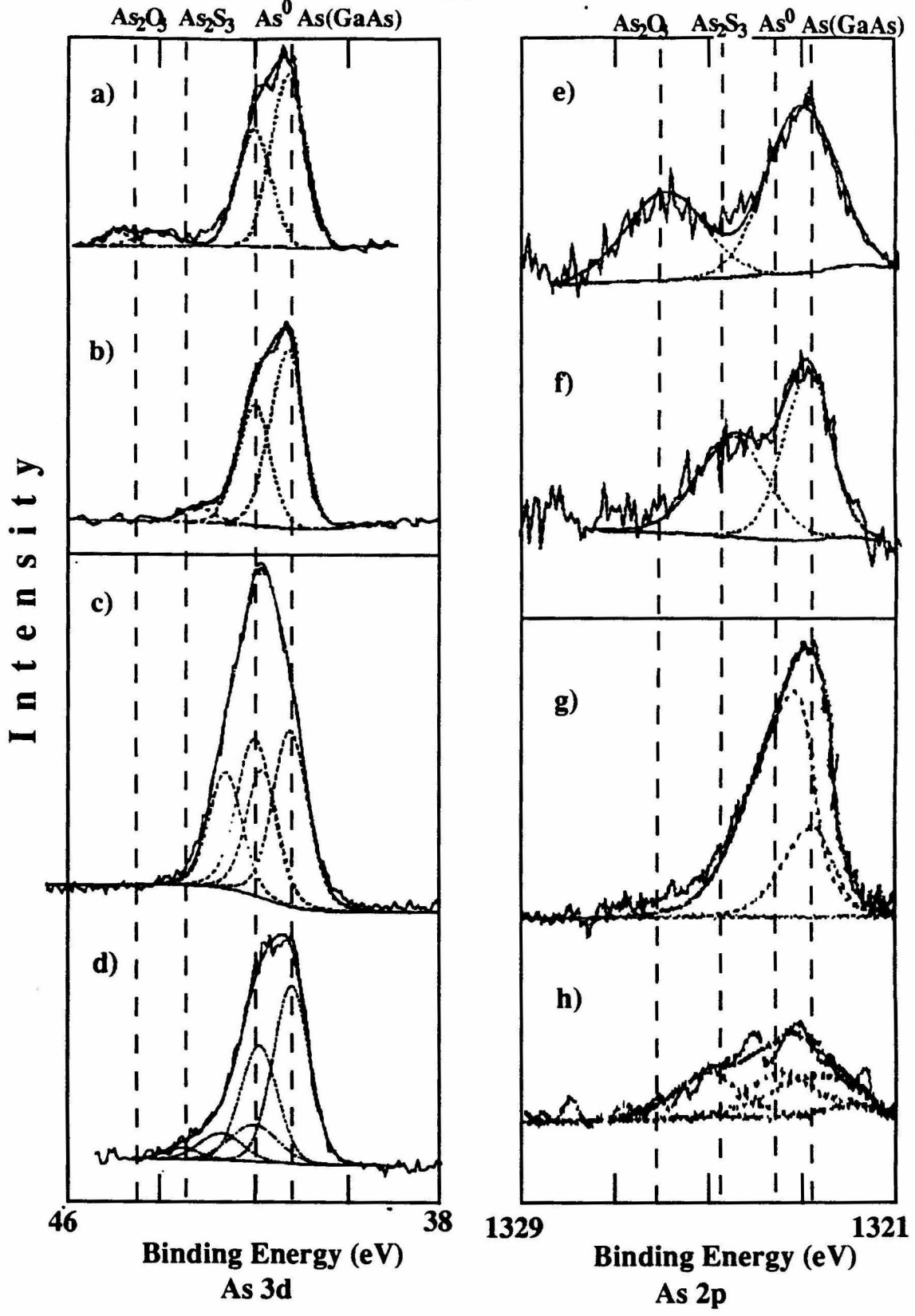
As2O3 As2S3 As0 As(GaAs)
a)
b)
c)
d)
Intensity
46
38
Binding Energy (eV)
As 3d
As2O3 As2S3 As0 As(GaAs)
e)
f)
g)
h)
1329
1321
Binding Energy (eV)
As 2p

authentic As_2S_3 sample on the same XPS instrument,[17] but is consistent with an As-S phase, most likely of As/S ratio somewhat higher than the value of 0.66 characteristic of As_2S_3.

The presence of sulfur on GaAs exposed to 1.0 M $Na_2S \cdot 9H_2O$(aq) was independently verified by collecting XPS data on an instrument equipped with a Mg anode. This allowed simultaneous investigation of the S 2s, Ga 3d, and As 3d regions by removing the interference between the S 2s line and the As Auger signal. The lower resolution of this instrument produced a broad S 2s peak, but the signal for a GaAs sample (exposed to either etch A or etch B) was centered at 226 eV, which is consistent with expectations for the S^{2-} oxidation state.[18] The sulfur coverages were fairly independent of the type of etch (Table 5.II), even though the coverage of As-S species did vary substantially for these same GaAs specimens. This change in the total S/As-S ratio was outside the error of the XPS instrumentation, and indicated that not all of the adsorbed sulfur participated in strong As-S bonding on the GaAs surface.

For all GaAs samples that had been treated with 1.0 M $Na_2S \cdot 9H_2O$(aq) and thoroughly rinsed with H_2O, the Ga 3d lineshape for the lattice Ga_{GaAs} peak was unperturbed relative to that from the near-stoichiometric surface of etch A. This is a qualitative indication that large amounts (> monolayer coverage) of a Ga-S species were not present after the Na_2S immersion and H_2O rinse. However, the chemical shift expected for Ga_2S_3 or related Ga sulfides is sufficiently close to that of lattice Ga_{GaAs} that no quantitative limits on the coverage of this species at submonolayer levels was possible with our XPS instrumentation.[19] Specifically, the low levels of Ga-S observed by Spindt et al.[2a] (using a synchrotron source) on NH_4S-treated GaAs samples would not have been readily observable, using our instrumentation.

2. GaAs Surface Composition After Exposure to 1.0 M $Na_2S \cdot 9H_2O$(aq): Depth Profiling with Controlled H_2O(l) Exposure

To investigate the depth profile of the overlayer obtained after exposure of GaAs to

1.0 **M** $Na_2S \cdot 9H_2O$(aq), a series of XP spectra were taken on a sample of low-doped GaAs that had been etched and then exposed to 1.0 **M** $Na_2S \cdot 9H_2O$(aq). The samples were profiled by exposure of the film to single droplets of water while the GaAs was spinning on a spin coater. This procedure was very similar to methods described previously for the wet chemical depth profiling of oxide films on Si and GaAs.[1,9]

For a GaAs sample that had been exposed to etch B and then to 1.0 **M** $Na_2S \cdot 9H_2O$(aq), XP spectra obtained after various stages of the rinse-spin profiling procedure are displayed in Figure 5.3. Examination of the film after immersion into 1.0 **M** $Na_2S \cdot 9H_2O$(aq) yielded negligible intensity from any peaks in the Ga 3d or As 3d region. At this stage, only S 2p signals characteristic of S^{2-} and partially oxidized sulfur (Figure 5.3f), and of Na 1s, C 1s, and O 1s were seen in the XPS data. When the films were completely rinsed to reveal the GaAs surface, small amounts of As^0, but no Ga or As oxides, were detected by XPS (Figure 5.3d). XP spectra obtained at intermediate depths were characteristic of the limiting spectra and showed the etching of As^0 by the $Na_2S \cdot 9H_2O$ film (Figure 5.3b,c), and the reduction of the amount of sulfur to levels that were not detectable above the As Auger background (Figure 5.3g,h). The final surface was As-deficient in the top layer, with respect to the lattice Ga_{GaAs} peak (Table 5.II). The extended rinsing used to obtain the spectrum of Figure 6d was also used for all of the samples of Figures 5.1-5.2. In some prior work, samples had not been rinsed with H_2O after immersion into $Na_2S \cdot 9H_2O$(aq) solutions;[2b] our data indicate that the Ga or As XP signals obtained from such specimens may not be characteristic of the general behavior of GaAs surfaces after contact with $Na_2S \cdot 9H_2O$(aq) solutions.

3. Surface Composition Changes After Exposure to $Na_2S \cdot 9H_2O$(aq); Variation in pH Changes

The effect of solution pH was investigated for the As^0-rich surface (etch B), because the pH may be an important factor in the removal of As^0 and in the related

Figure 5.3. As 2p and S 2p XP spectra for a sample of boron-compensated, low-doped, (100) n-GaAs. The sample was etched with etch B, treated with 1.0 **M** $Na_2S \cdot 9H_2O$ (aq) for 10 min., then gradually rinsed with H_2O. a) As 3d region after initial etch. b) As 3d region after sulfide treatment and one drop of H_2O. c) As 3d region after one more drop of H_2O. d) As 3d region after final, extensive rinse with H_2O. e) S 2p region of sample after initial etch; same experiment that yielded the As 3d region in panel a). f) S 2p region after Na_2S film was dried on the surface. g). S 2p region after one drop of H_2O; same experiment that yielded the As 3d region in panel b). h) S 2p region after 2 drops of H_2O; same experiment that yielded the As 3d region in panel c). No further changes in the S 2p region were observed with rinsing because the signal was already at its baseline value because of the presence of the As Auger line; therefore no S 2p region was collected for the extensively rinsed sample of panel d).

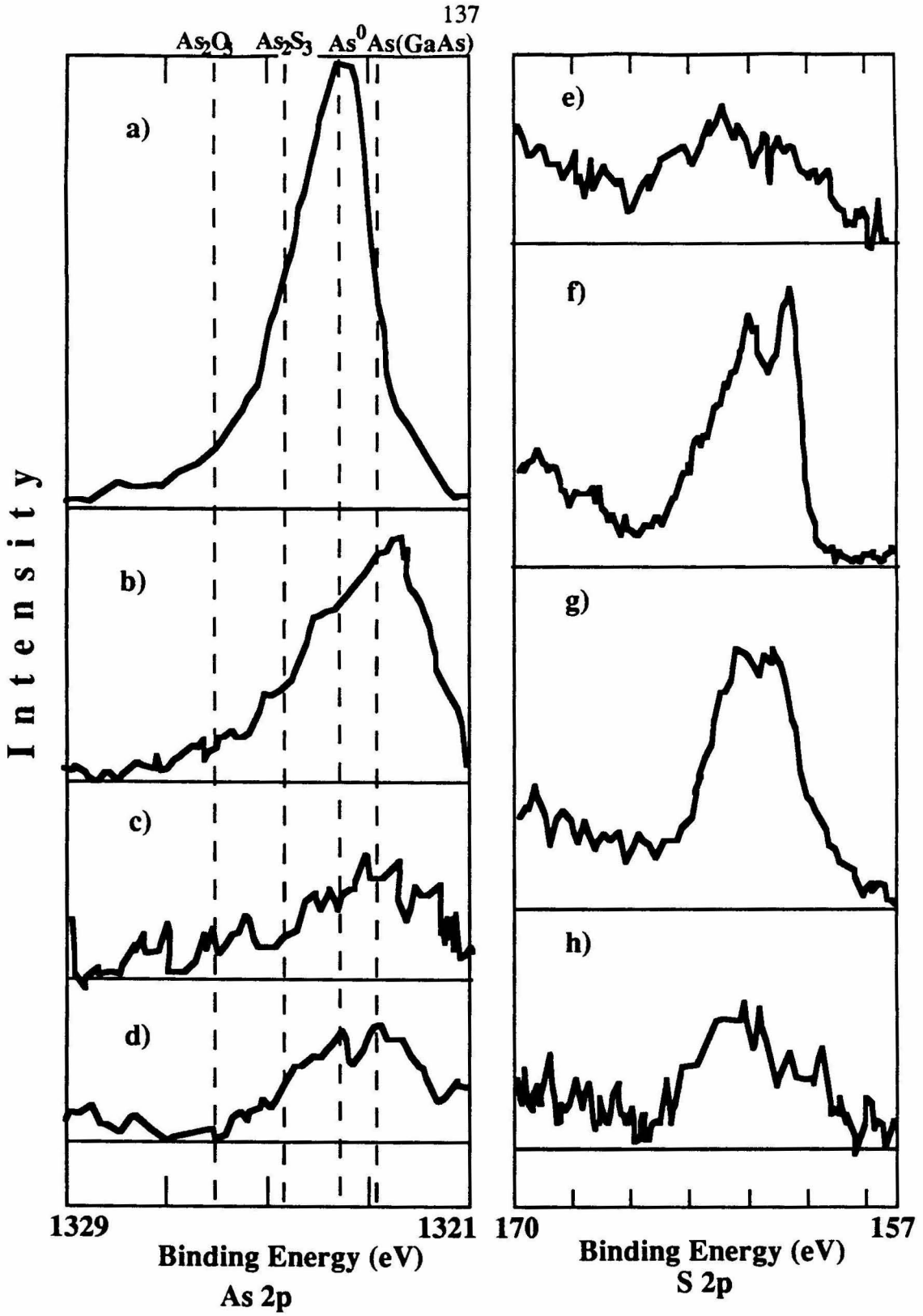
As2O3
As2S3
As0As(GaAs)
a)
b)
c)
d)
e)
f)
g)
h)
Intensity
1329
1321
Binding Energy (eV)
As 2p
170
157
Binding Energy (eV)
S 2p

improvement in PL intensity. The excess As^0 signal intensity produced by etch B was reduced substantially after immersion of the GaAs specimen into either 1.0 **M** $Na_2S•9H_2O$(aq) (pH=13) or 1.0 **M** $Na_2S•9H_2O$(aq) (aq) (pH=7) solutions (Table 5.II). Immersion into the pH=7 $Na_2S•9H_2O$(aq) solution resulted in slightly higher levels of sulfur remaining on the GaAs surface, but no other differences in surface composition were apparent in response to the variation of pH.

The effect of pH on an oxide-rich surface (etch C) was also investigated, since As_2S_3 is soluble in basic aqueous solutions, but is essentially insoluble in water,[20] and therefore a thicker layer of As_xS_y might be expected to result from the reaction of arsenic oxide with aqueous sulfide at a more neutral pH. However, a sample that had been etched with Etch C and then exposed to a solution of NaHS at pH 7 showed exactly the same behavior as the sample in Figure 5.1c,f.

C. Exposure of GaAs to Thiols and Other Nucleophiles

XP spectra were collected for a representative set of thiol reagents that were found to affect the GaAs steady-state photoluminescence intensity. Surfaces were investigated after etching to yield either a stoichiometric surface (etch A) or an As^0-rich surface (etch B). XPS peak energy and coverage information obtained from these experiments are summarized in Table 5.III.

The dashed line in Figure 5.4a displays the XP spectra of a GaAs sample that had been etched to obtain a near-stoichiometric surface (etch A). For comparison, the solid line in Figure 5.4a displays the spectrum of a nominally identical specimen that was etched in parallel but was exposed to a solution of 1.0 **M** 4-Cl-thiophenol in CCl_4 and rinsed with deaerated methanol before introduction into the XPS chamber. All etching and manipulations of these samples were done in a box containing flowing N_2(g), in order to minimize inadvertent oxide formation. The key feature of these As 3d spectra is that the surface As composition was essentially unchanged by exposure to the thiol solution. No signals ascribable to an As-S species were detected, despite the fact that exposure to this

Figure 5.4. As 3d and 2p XP spectra for bulk 10^{17} doped (100) n-GaAs samples, taken with monochromatic Al x-rays. The dashed lines are spectra for freshly etched samples, and solid lines are spectra obtained for a separate set of samples that had been etched and then immersed into 1.0 **M** 4-chlorothiophenol in CCl_4 for 30 min., followed by rinsing with methanol.. a) As 3d regions after etch A ,and after exposure to the thiol. b) As 3d regions after exposure to etch B, and after exposure to the thiol. c) As 2p regions corresponding to the sample of panel b).

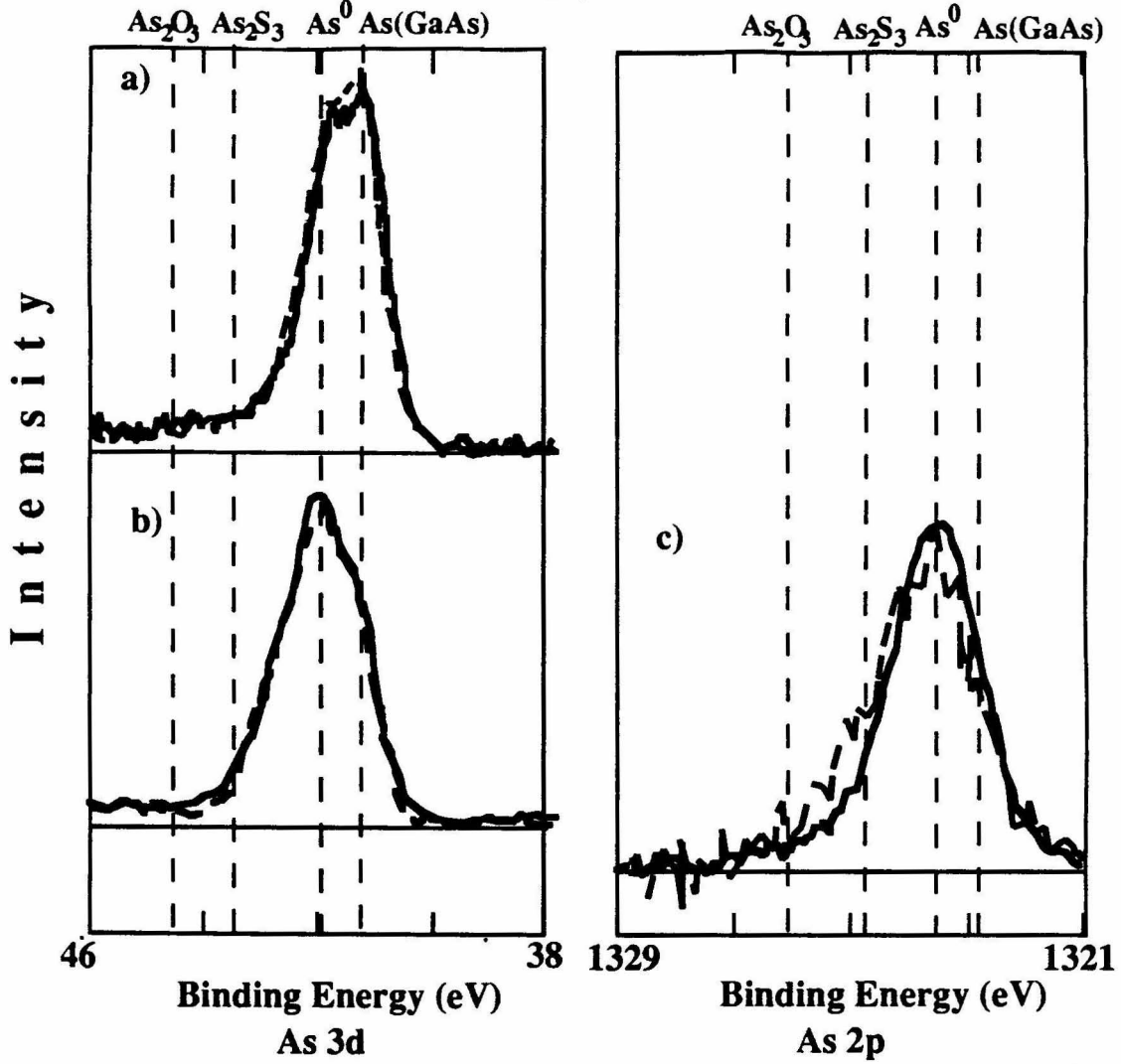
As2O3 As2S3 As0 As(GaAs)
a)
b)
Intensity
46
38
Binding Energy (eV)
As 3d
As2O3 As2S3 As0 As(GaAs)
c)
1329
1321
Binding Energy (eV)
As 2p

Table 5.III. XPS data of GaAs exposed to nonaqueous solutions of thiols and sodium methoxide. All coverages were calculated relative to the As 3d GaAs substrate peak. A value of 0.0 indicates that the level was less than 0.1 X 10^{-9} moles/cm^2. "--" indicates that the peaks were undetectable because of either sensitivity or resolution.

Sample	x-ray[a] source	Ga 3d			As 3d	
		Ga (GaAs) eV	Ga (Ga_2O_3) eV	Γ (Ga_2O_3) moles cm^2 X 10^9	As (GaAs) eV	As (As_2O_3) eV
Etch A[c]	Al	19.2	20.0	0.4	41.0	–
+ 1.0 M 4-Cl-C_6H_4-SH in CCl_4 (30 min)	Al	19.2	20.1	0.5	41.1	–
+ 1.0 M 4-Cl-C_6H_4-SH in CCl_4 (30 min)	Mg	20.0	20.9	0.2	42.0	–
+ 1.0 M 4-Cl-C_6H_4-SH + 1.0 M $NaOCH_3$ in methanol (30 min)	Al	18.8	19.8	0.6	40.7	44.4
	Mg				41.3	–
Etch B	Al	19.7	20.6	0.4	41.6	44.4
+ 1.0 M 4-Cl-C_6H_4-SH in CCl_4 (30 min)	Al	19.4	–	0.0	41.2	–
+ HS-CH_2CH_2-SH (liquid) (1 hr)	Al	19.0	20.2	0.2	40.8	–
Etch B	Al	19.6	–	0.0	41.4	44.2
+ 1 M $NaOCH_3$ in methanol (30 min)	Al	19.2	–	0.0	41.0	–

[a]Al=Data taken with monochromatic Al K_α x-rays (1486.6 eV) on a Surface Science Instruments Model 100.

Mg=Data taken with Mg K_α x-rays (1254 eV) on a VG Mark II.

[b]The Ga/As ratio is based on substrate peaks and does not include oxides.

[c]Etch A=1.0 M KOH (15s), 0.5% Br_2/Methanol (15 s), repeated 3 times and ending in KOH.

Etch B= Etch A + 30s 1:1:100 (H_2SO_4:30% H_2O_2:H_2O).

[d]The coverage of thiol based on the Cl 2p region is 0.9 X 10^{-9} moles/cm^2.

[e]The coverage of thiol based on the Cl 2p region is 1.7 X 10^{-9} moles/cm^2.

Table 5.III. continued.

As 3d					As 2p				
Γ (As_2O_3) moles/cm² X 10^9	As (As^O) eV	Γ (As^O) moles/cm² X 10^9	As (As_xS_y) eV	Γ (As_xS_y) moles/cm² X 10^9	As (GaAs) eV	As (As_2O_3) eV	Γ (As_2O_3) moles/cm² X 10^9	As (As^O) eV	Γ (As^O) moles/cm² X 10^9
0.0	41.7	0.8	–	0.0					
0.0	41.8	0.8	–	0.0					
0.0	–	0.0	–	0.0					
0.4	–	0.0	–	0.0					
0.0	–	0.0	–	0.0					
0.4	42.3	2.7			1323.3	1325.6	0.7	1324.1	3.7
0.0	42.0	4.9	–	0.0	1323.0	1325.2	0.3	1323.9	3.4
0.0	41.6	3.0	–	0.0					
0.6	42.1	3.6	–	0.0	1323.3	1325.9	0.6	1324.1	2.5
0.0	41.8	1.9	–	0.0	1322.8	–	0.0	1323.8	2.6

Table 5.III. continued.

As 2p		Ga/As	S 2s		C 1s
As (As_xS_y) eV	Γ (As_xS_y) moles cm^2 X 10^9	3d region[b]	eV	Γ (S) moles cm^2 X 10^9	eV
		1.7			285.3
		1.1		d	285.2
		1.0	227.6	0.4	285.1
		1.1			285.6
		–	227.0	0.4	286.6
	–	1.5			284.7
	–	1.6		e	285.1
		0.8			285.5
	–	1.9			284.9
	–	1.9			285.3

thiol yielded a significant increase in the both the steady-state PL intensity and in the time-resolved PL lifetime (Chapter 4) of GaAs epilayer samples. The thiol was clearly adsorbed onto the GaAs surface, because the Cl 2p intensity was significantly above background levels.

To further investigate the potential reactivity of surface As^0, another set of GaAs samples was exposed to the As^0-rich etch (etch B) and then to 1.0 **M** 4-Cl-thiophenol in CCl_4. The As XPS data for these samples, displayed in Figure 5.4b,c, showed that excess As^0 introduced by the etching process was not removed by immersion into the thiol solution. Also, no As-sulfide peaks were detectable on this surface. This can be seen more clearly from the spectral fits to the As 2p region that are displayed in Figure 5.5. Although there was a peak at higher binding energy, this peak was also present in the etched sample (Figure 5.5a) and is most likely due to an As suboxide. Any As-S signal was certainly minor compared to the levels detected after exposure to 1.0 **M** $Na_2S{\cdot}9H_2O$(aq), as shown in Figures 5.2f,h. This lack of a detectable As-S phase was found to be representative of all the thiols investigated by XPS (1,2-dithiolethane and 4-Cl-thiophenol) on As^0-rich GaAs surfaces (Table 5.III).

To insure that the Cl signals in the wide scan using the Al x-ray source instrument were indicative of the persistent adsorption of the 4-Cl-thiophenol, XPS data were also collected with the Mg x-ray source. For GaAs samples exposed to either the stoichiometric or As^0-rich etches (etch A or B) and then exposed to 1.0 **M** 4-Cl-thiophenol in CCl_4, a Cl:S elemental ratio of (1.1±0.2), and a lack of Ga-Cl or As-Cl peaks, was observed (Table 5.III). This implies that the Cl intensity obtained on the high-resolution, Al x-ray photoelectron spectrometer was a reliable indication of the adsorbed 4-Cl-thiophenol coverage, and that the lack of As-S formation in these samples was not due to a lack of reactivity of these surfaces with the thiol.

An additional set of experiments was done to determine if there was any photochemical formation of an As-S phase under laser irradiation, since some time

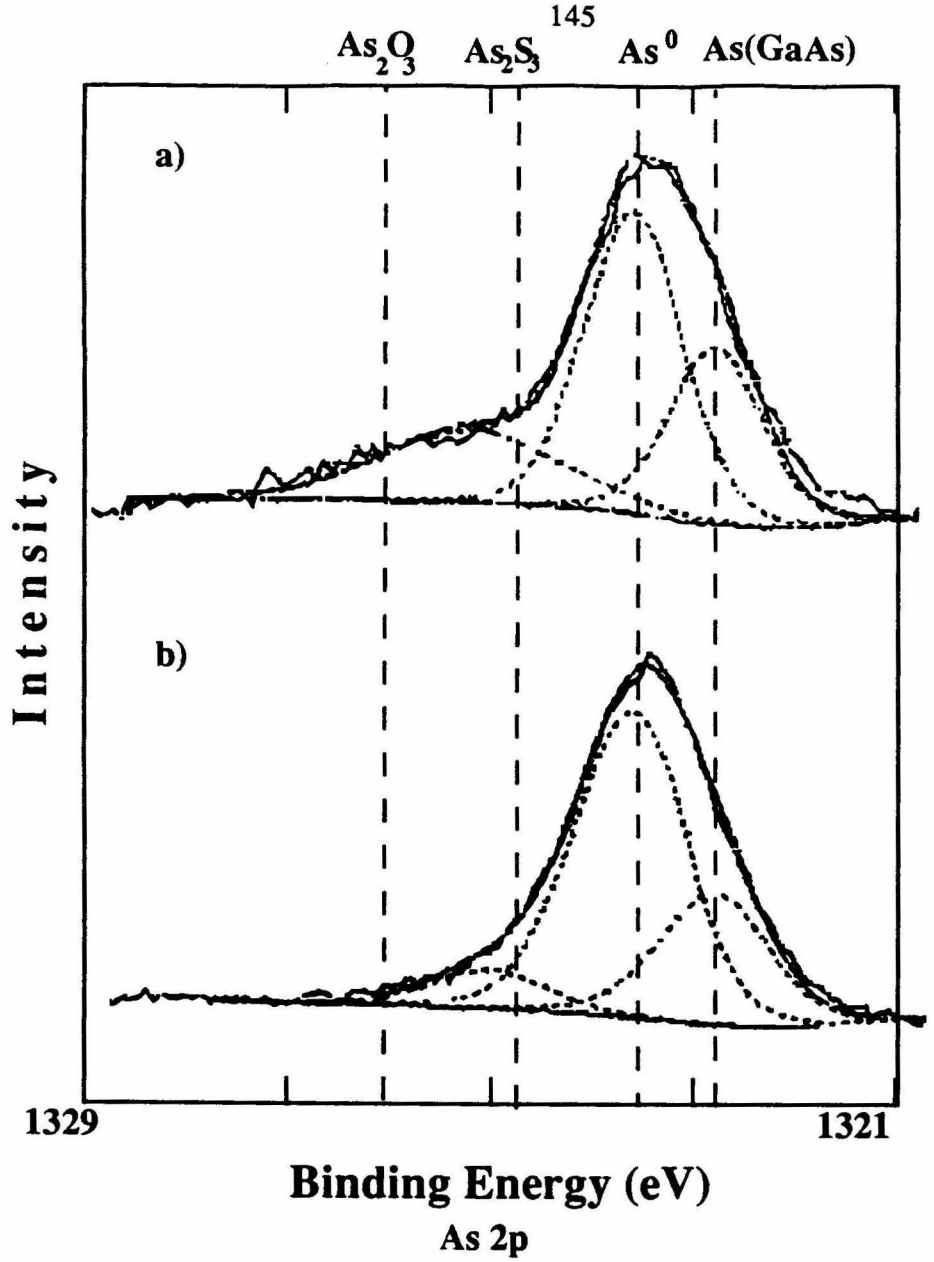

Figure 5.5. Peak fits for the As 2p XP spectra of Figure 5.4c. a) Spectrum and fits after etch B. b) Spectrum and fits after etching and exposure to the thiol solution.

dependence of steady-state PL intensity was occasionally observed. A sample of the 1.0 μm thick GaAs epilayer was etched to remove the top AlGaAs layer, exposed to etch A in a glove box containing flowing N_2(g), sealed in a glass cell, and subjected to XPS analysis. XPS data collected on this sample revealed a spectrum identical to that displayed in Figure 5.4a.. The sample was then returned to the glove box, soaked in a 1.0 M 4-Cl-thiophenol solution as described above, sealed again in a glass cell and irradiated for 20 minutes. XPS obtained after this process showed no change in the GaAs surface composition except for the detection of the anticipated small amount of Cl from the adsorbed thiol.

XP spectra were also collected for GaAs surfaces that had been exposed to two other organic reagents. For a sample of GaAs that had been etched to yield an As^0-rich surface (etch B) and then exposed to 3-methylthiophene (liquid), XPS data showed no change in the surface As or Ga regions and no detectable sulfur in the S 2p region. 3-methylthiophene did not produce significant increases in the steady-state PL intensity of GaAs surfaces; the XPS data imply that this is simply due to an extremely weak, or readily reversible, interaction between the thiophene and the GaAs surface.

It was also of interest to examine the surface composition of a GaAs sample that had been exposed to sodium methoxide, because this reagent yielded a large increase in the steady-state PL intensity without a concomitant increase in the high-level injection PL decay time. Figure 5.6 depicts the XP spectrum that was obtained for a GaAs surface that had been treated with etch B, and also displays the XP spectrum for a similar sample that had been exposed to 1.0 M $NaOCH_3$ in CH_3OH. Although the elemental As^0 coverage was reduced slightly by exposure to 1.0 M $NaOCH_3$, most of the As^0 ($2x10^{-9}$ moles cm^{-2}) remained on the GaAs surface. The lack of gross stoichiometry changes, or the appearance of new chemical species after OCH_3^- exposure, implies that the resulting small changes in surface stoichiometry effected by this reagent were not detectable with the sensitivity levels of conventional XPS analysis.

Figure 5.6. a) As 3d and b) As 2p XP spectra for bulk 10^{17} doped (100) n-GaAs taken with monochromatic Al x-rays. The dashed lines are the spectra obtained after exposure to etch B, while the solid lines represent the XPS data obtained after immersion of the GaAs into 1.0 **M** sodium methoxide for 30 min., followed by extensive rinsing with methanol.

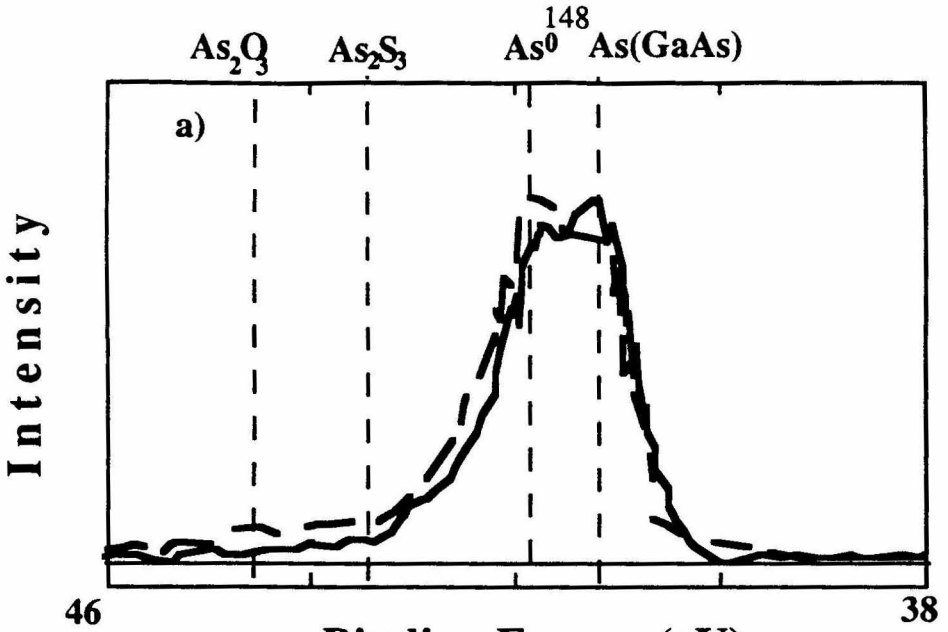
As2O3
As2S3
As0
As(GaAs)
a)
Intensity
46
38
Binding Energy (eV)
As 3d

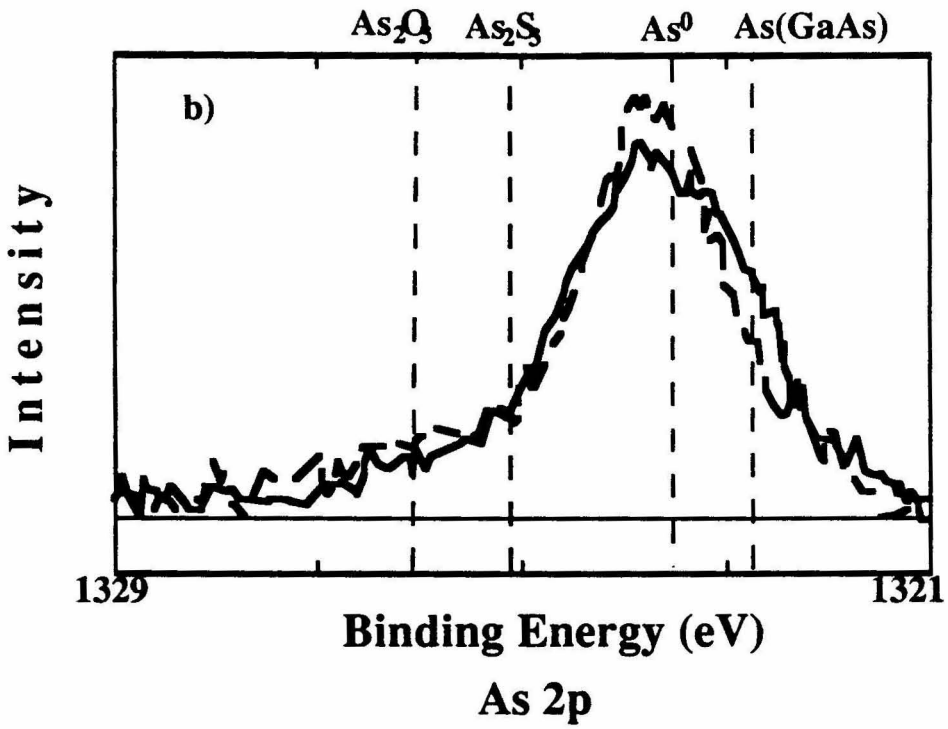
As2O3
As2S3
As0
As(GaAs)
b)
Intensity
1329
1321
Binding Energy (eV)
As 2p

IV. Discussion

A key result of the XPS studies reported herein is that in certain cases, substantial As^0 remained on the GaAs surface even when the surface recombination velocity was significantly lower than that of the etched, air-exposed GaAs surface. Although the basic 1.0 M $Na_2S \cdot 9H_2O$(aq) solutions were found to be effective in removing excess As^0, exposure to thiols in nonaqueous solvents did not substantially reduce the As^0 content of the GaAs surface. 4-Cl-thiophenol did, however, yield substantial reductions in both the low-level and high-level surface recombination velocity. Furthermore, no As_2S_3 signal was evident after exposure of GaAs surfaces to the nonaqueous thiol solutions, indicating that the formation of an epitaxial overlayer of As_2S_3 from excess As^0 is not the key chemical process responsible for lowering surface recombination in these systems.

Another significant observation is that only submonolayer (about one half to three quarters of a monolayer) levels of As-sulfides were observed in this work after exposure either to $Na_2S \cdot 9H_2O$(aq) solutions or to NaHS(aq) solutions. These low As_xS_y signals are in qualitative accord with the results of Tiedje, et al.,[3] but the As_xS_y peak intensities and calculated As_xS_y coverages are substantially lower than those reported in the work of Sandroff and co-workers.[6] Sandroff and co-workers observed a slightly higher binding energy As_xS_y phase after treatment with Na_2S than after treatment with NH_4S.[6] One possible explanation for the difference in the As 2p XP spectra is that in the Sandroff study the Na_2S films were rinsed with CS_2 so that the surface was visible by XPS. NaOH, which is a component of a dried Na_2S film, reacts with CS_2 to form $NaCS_3$.[21] This compound could further react with any arsenic sulfide that was present on the surface to form an arsenic polysulfide. In our study and the study by Tiedje, et. al,[3] water was used to rinse the film before XPS investigation. Also, our study has shown that the large amount of oxide present in some prior studies[2b,5,6] is a result of handling procedures and is not inherent in the chemistry of the surface.

The magnitude of the steady-state PL intensity change discussed in Chapter 4 is in accord with prior observations on epilayer-type GaAs samples. Taken together with XPS measurements described above, this set of observations indicates that the PL changes resulting from immersed and dried GaAs surfaces do not correlate with the As_2S_3 coverages determined on thoroughly rinsed GaAs samples exposed to thiols and aqueous sulfides. This conclusion was verified in this work for GaAs samples that were handled under a variety of conditions, including aerobic vs. anaerobic etching and sulfide treatment, exposure to partially oxidized or totally reduced sulfide solutions, and exposure to Na_2S(aq) following establishment of a variety of different GaAs surface stoichiometries.

The similarity of the final GaAs surface stoichiometry after exposure to aqueous sulfides, despite the substantial differences in the three initial GaAs surface compositions induced by the various etching procedures, is also of interest with respect to the surface passivation effect. This behavior can be readily understood by reference to the solubility properties of Ga oxides, As oxides, and elemental As, and by reference to prior experimental investigations of GaAs surface reactivity after contact with basic aqueous chalcogenide solutions.[12,22] Specifically, after immersion into a 1.0 **M** KOH-0.80 **M** K_2Se(aq)-0.1 **M** K_2Se_2(aq) solution, a remarkably clean, near-stoichiometric, GaAs surface was produced regardless of the initial GaAs etching procedure.[12] Although the prior work dealt specifically with reactions of GaAs in contact with KOH-K_2Se(aq) solutions, the observations of GaAs/NaOH-Na_2S(aq) surface chemistry reported herein (Table 5.II, Figure 5.1) are fully consistent with these earlier XPS observations.

This surface chemistry of oxidized As also naturally provides a mechanism for the formation of the As_2S_3 that has been observed in this work and in prior studies of the GaAs/Na_2S(aq) chemistry.[2b,3-6] Oxidized As (i.e., As^{III}) and oxidized Ga (Ga^{III}) readily react with aqueous sulfide solutions to yield As_2S_3 and Ga_2S_3;[23a] thus, oxidized GaAs surfaces are expected to produce As_2S_3 and Ga_2S_3 without the concomitant formation of covalent bonds to the substrate or passivation of surface states. Deposition of the product

of a precipitation reaction has been observed previously on GaAs surfaces that have been exposed to basic solutions of Co^{II} or Co^{III} complexes; this procedure resulted in deposition of multilayer coverages of a $Co(OH)_2$ surface species that persisted on the GaAs surface even after thorough rinsing with H_2O.[22] However, unlike $Co(OH)_2$, As_2S_3 is partially soluble in aqueous, basic solutions (because of the formation of soluble thio and oxy anions),[23b] so the observed As_2S_3 coverages on an air-exposed GaAs sample that has been exposed to 1.0 **M** Na_2S(aq) and rinsed with H_2O are not expected to reflect accurately either the initial As_2S_3 levels or the coverage of sulfur that is covalently bound to the surface.

One interesting aspect of the $Na_2S{\cdot}9H_2O$(aq)-GaAs chemistry evident from Table 5.II is that even heavily oxidized surfaces show little As_xS_y when exposed to sulfide in a pH 7 solution. This result is a bit surprising in light of the solubility behavior of As_2S_3 discussed above. A GaAs surface that had been etched to have a large amount of oxide initially would presumably react with the sulfide solution and precipitate an As-S phase on the surface, similar to the behavior of Co^{II} and Co^{III} ammine complexes at a pH > 8.[22] The fact that the oxidized GaAs surface exposed to sulfide in pH 7 solution did not show evidence of the formation of any more As_xS_y than a sample exposed to a basic solution indicates two possible chemistries. The first is that the equilibrium constant of the product formed from reaction of arsenic oxides and aqueous sulfides with the solution is of sufficient magnitude to dissolve all but a small amount of an As_xS_y phase, even at a lower pH. The second is that the local pH at the surface is sufficiently basic to dissolve off the reaction product. The differentiation between these two mechanisms would require further studies in carefully buffered solutions, and also at even lower solution pH. This rather complex surface chemistry may well account for the differences in As-S coverages reported in various studies.[3,6]

Furthermore, on GaAs surfaces without substantial As^{III} or As^0 present initially, and in fully reduced sulfide solutions, formation of monolayer levels of As_2S_3 from GaAs

must result in the formation of reduced products, which would presumably be elemental Ga and/or $H_2(g)$. No XPS signals from elemental Ga were observed after $Na_2S(aq)$ immersion and H_2O rinsing, implying coverages of $Ga^0 < 1x10^{-10}$ mol/cm^2. Additionally, estimates of the thermodynamics of the reaction ($2GaAs + 6S_2^- + 12\ H_2O = As_2S_3 + Ga_2S_3 + 12\ OH^- + 6H_2$) from the appropriate half-cell potentials[42] indicate that it is unlikely to be exoergic. These arguments, combined with the observation that the PL intensity was independent of the initial etching solution (Chapter 4), and with the fact that As_2S_3 formation was not observed from the thiol exposure in nonaqueous solvents, lend support to the notion that bulk As_2S_3 formation is not directly related to passivation of the key chemical trapping species at the GaAs surface.

Similar arguments can be applied to the formation of Ga_2S_3 from oxidized Ga. Spindt et al.[2a] have suggested that bulk thermodynamics based on heats of formation indicate that Ga_2S_3 should be formed preferentially with respect to As_2S_3, and suggest that this species plays a key role in the GaAs/Na_2S interface passivation chemistry. The above analysis for As_2S_3 formation suggests that an alternative mechanism for Ga_2S_3 formation is the reaction of inadvertently oxidized Ga with the aqueous sulfide solutions. This implies that unless rigorously anaerobic conditions are maintained throughout the experiment, the detection of Ga_2S_3 on the GaAs surface may not indicate formation of a covalent bond between the Ga_2S_3-type layer and the GaAs itself, and may not correlate with the bonding to the important electrical trap sites. This is consistent with the rather high levels of oxide evident in some earlier XPS work on Na_2S-treated surfaces,[2b] and suggests that observation of Ga_2S_3 may be unrelated to the chemistry of the important surface trap levels.

It should be noted, with regard to whether Ga or As sulfide would be the most thermodynamically favorable, that kinetics can frequently dominate in surface reactions. Of course, when heated to high temperatures, equilibrium may be established and the thermodynamically predicted species of Ga_2S_3 should then be observed for the

GaAs/$Na_2S \cdot 9H_2O$ interface; however, bond-strength arguments must be used with caution to predict surface compositions obtained in the kinetically limited situations commonly encountered when semiconductor surfaces are immersed in aqueous solutions at room temperature.

With respect to the energetics of the GaAs surface, ultraviolet photoelectron spectroscopy (UPS) of Na_2S-treated GaAs surfaces has been used to show that the surface Fermi level is still pinned at a value of 0.7-0.9 eV below the bottom of the conduction band edge.[2b] The XPS spectrum obtained in the present work after immersion of GaAs into 1.0 M Na_2S(aq) solutions did not display any signals from the Ga or As substrate lines (Table III), and therefore suggests that independent support for the UPS measurements is needed from another type of experiment. A nonhomogeneous surface coating procedure could yield XPS signals from the uncovered and untreated portion of the GaAs substrate, and this scenario would explain the XPS and UPS spectra reported in previous work on unrinsed samples.[2b] The high coverage of oxidized As in the UPS sample reported earlier, combined with the observations above that Ga oxides and As oxides are readily dissolved by basic Na_2S(aq) solutions, strongly suggests that the areas contributing to the observed XPS and UPS signals were not exposed to the Na_2S treatment. This is consistent with the extensive literature indicating that oxidized GaAs surfaces have their surface Fermi levels pinned 0.7-0.9 eV positive of the conduction band edge.[24] The rf conductivity data of Yablonovitch et al.[25] indicates that the surface Fermi level position on Na_2S-coated surfaces depends on the injection level and that it can be unpinned under high-level injection conditions. Although the data of Yablonovitch et al.[25] are not consistent with a strongly pinned surface Fermi level at 0.7-0.9 eV below the conduction band edge, their observations are consistent with the increased PL decay times observed in this work for the Na_2S and 4-Cl-thiophenol treatments of epilayer-type GaAs samples and with the analysis of the XPS and UPS data presented above.

In general, it can be seen that the chemistry of GaAs with sulfides is complex and varied. The chemical probes indicate that the important surface recombination site is "soft" and electron deficient in nature, but the sulfide binding constant must be relatively weak because rinsing with solvent substantially diminishes the steady-state GaAs PL intensity. This fact presents a severe impediment to obtaining useful correlations between the surface chemistry determined with vacuum spectroscopic methods and the reactivity of the actual electrical recombination sites on $Na_2S \cdot 9H_2O$(aq)-coated GaAs interfaces. The nonaqueous thiol solutions are better suited to formulate these correlations, but no changes in gross surface stoichiometry have been observed for thiol reagents that yield large improvements in the steady-state PL intensity. Further spectroscopic-based advances in our understanding of the chemistry of the recombination sites will require methods that directly probe the bonding of a limited number of surface sites in the presence of higher coverages of precipitates and other spectator surface species.

V. Conclusions

The XPS studies described in this chapter indicate that while aqueous Na_2S treatments and exposure to thiols exhibit similar changes in steady-state PL yield (Chapter 4), these two classes of compounds do not interact with the GaAs surface in the same way. The aqueous Na_2S treatments acted as an etch for oxides and elemental arsenic, and yielded a small residual As_xS_y signal on the GaAs surface. However, exposure of GaAs surfaces to thiols did not yield detectable residual As_xS_y signals, indicating that the As_xS_y phase was not necessary for an increase in the GaAs PL signal. XPS data on GaAs samples exposed to thiols also showed that an enhancement in the PL signal could not be correlated with the amount of elemental arsenic initially present on the surface.

The lack of a clear correlation with surface stoichiometry and changes in surface recombination velocity is probably because the trap density is sufficiently low that gross changes in surface stoichiometry may not accompany (or yield information regarding) the reactivity of the important surface recombination centers. However, these studies have

served to indicate that the presence of As^0 does not always result in an interface with high surface recombination velocities, and that the formation of an As_xS_y phase is most likely due to a byproduct of reaction of arsenic oxides with aqueous sulfides and is not an essential part of the GaAs surface passivation process.

The XPS data presented in this chapter, taken together with the PL results described in Chapter 4, have shown that variation in the nature of the passivating reagent from a complex mixture of aqueous sulfides to nonaqueous, organic species has yielded valuable information on the chemical nature of the important surface recombination sites and the GaAs surface chemistry relevant to the observed decrease in surface recombination velocity.

References

1. P. J. Grunthaner, R. P. Vasquez, and F. J. Grunthaner, *J. Vac. Sci. Technol.* **17**, 1045 (1980).

2. a) C. J. Spindt, D. Liu, K. Miyano, P.L. Meissner, T.I. Chaing, T. Kendelewicz, I. Lindau, and W. E. Spicer, *Appl. Phys. Lett.* **55**, 861 (1989). b) C. J. Spindt, R. S. Besser, R. Cao, K. Miyano, C. R. Helms, and W. E. Spicer, *J. Vac. Sci. Technol. A* **7**, 2466 (1989).

3. T. Tiedje, P. C. Wongk, A. R. Mitchell, W. Eberhardt, Z. Fu, and D. Sondericker, *Solid State Comm.* **70**, 355 (1989).

4. a) B. A. Cowans, Z. Dardas, and W. N. Delgass, *Appl. Phys. Lett.* **54**, 365 (1989). b) M. S. Carpenter, M. R. Melloch, B. A. Cowans, Z. Dardas, and W. N. Delgass, *J. Vac. Sci. Technol. B* **7**, 845 (1989).

5. H. Hirayama, Y. Matsumato, H. Oigawa, and Y. Nannichi, *Appl. Phys. Lett.* **54**, 2565 (1989).

6. C. J. Sandroff, M. S. Hegde, L. A. Farrow, C. C.Chang, and J. P. Harbison, *Appl. Phys. Lett.* **54**, 362 (1989).

7. a) K. M. Geib, J. Shin, and C. W. Wilmsen, *J. Vac. Sci. Technol. B* **8**, 838 (1990). b) J. Shin, K. M. Geib, C. W. Wilmsen, and Z. Lilliental-Weber, *J. Vac. Sci. Technol. A* **8**, 1894 (1990).

8. R. P. Vasquez, B. F. Lewis, and F. J. Grunthaner, *J. Vac. Sci. Technol. B* **1**, 791 (1983).

9. J. A. Wurzbach and F. J. Grunthaner, *J. Electrochem. Soc.* **130**, 691 (1983).

10. The specta for etch C were taken with a VG nonmonchromatic Al K_α x-ray source on a modified VG HB50, ESCA III system.

11. H. J. Stocker and D. E. Aspnes, *Appl. Phys. Lett.* **42**, 85 (1983).

12. B. J. Tufts, L. G. Casagrande, N. S. Lewis, and F. J. Grunthaner, *Appl. Phys. Lett.* **57**, 2262 (1990).

13. R. P. Vasquez, B. F. Lewis, and F. J. Grunthaner, *J. Vac. Sci. Technol. B* **1**, 791 (1983).

14. M. Pourbaix, *Atlas of Electrochemical Equilibria in Aqueous Solutions* (Pergamon, New York, 1966).

15. A. Heller, in *Photoeffects at Semiconductor-Eletrolyte Interfaces*, edited by A. Nozik, ACS Symposium Series 146 (ACS, Washington DC, 1981), pp. 57-77.

16. J. H. Scofield, *J. Electron. Spectrosc. Relat. Phenom.* **8**, 129 (1976).

17. The sample was oxidized and the lowest binding energy peak was taken to be As_2S_3. This value matches well with that found in M. K. Bahl, R. O. Woodall, R. L. Watson, and K. J. Irgolic, *J. Chem. Phys.* **64**, 1210 (1976).

18. C. D. Wagner, W. M. Riggs, L. E. Davis, J. F. Moulder, and G. E. Muilenberg, *Handbook of X-ray Photoelectron Spectroscopy* (Perkin Elmer, Eden Prairie, MN, 1979).

19. C.P. Srivastanva, D. F. Van de Vondel, and G. P. Van Der Kelen, *Inorg. Chim. Acta* **23**, L29 (1977).

20. a) A. M. Comey, *A Dictionary of Chemical Solubilities* (MacMillan, London, 1896), p. 30. b) *Solubilities of Inorganic and Metal-organic Compounds, Vol. I, 4th Ed.*, W. F. Linke, Ed. (American Chemical Society, Washington D. C., 1958), p. 242.

21. J. C. Bailor, H. J. Emeleus, R. Nyholu, and A. F. Trotman-Dickenson, *Comprehensive Inorganic Chemistry Vol. I* (Pergamon, Oxford, 1973), p. 1238.

22. B. J. Tufts, I. L. Abrahams, C. E. Caley, S. R. Lunt, G. M. Miskelly, M. J. Sailor, P. G. Santangelo, N. S. Lewis, A. L. Roe, and K. O. Hodgson, *J. Am. Chem. Soc.* **112**, 5123 (1990).

23. a) J. C. Bailor, H. J. Emeleus, R. Nyholu, and A. F. Trotman-Dickenson, *Comprehensive Inorganic Chemistry Vol. II* (Pergamon, Oxford, 1973), p. 919. b) F. A. Cotton and G. Wilkinson, *Advanced Inorganic Chemistry, 4th Ed.*, (Wiley, New York, 1980), p. 458.

24. W. E. Spicer, Z. Liliental-Weber, E. Weber, N. Newman, T. Kendelewicz, R. Cao, C. McCants, P. Mahowald, K. Miyano, and I. Lindau, *J. Vac Sci. Technol. B* **6**, 1245 (1988).

25. E. Yablonovitch, B. J.Skromme, R. Bhat, J. P. Harbinson, and T. J. Gmitter, *Appl. Phys. Lett.* **54**, 555 (1989).

Chapter 6. Reaction of the Basal Plane of Various Metal Dichalcogenides with Organometallic Reagents

I. Introduction

Chapters 2-5 have been concerned exclusively with the chemistry of GaAs or similar III-V surfaces in relation to the observed surface electronic properties. The experiments described in this chapter apply the same types of techniques to study the reactivity of the basal plane of a series of metal dichalcogenide compounds in order to relate reactivity to the electronic properties of the metal-dichalcogenide surface.

The transition-metal dichalcogenide semiconductors have a layered crystal structure with the chalcogenide atoms on the surface.[1] The metal-chalcogenide bonds are generally rather strong, but the bonds between layers are rather weak, so that these compounds are mostly air-stable, but also have a strong tendency to form intercalation complexes.[2]

Even though all the different types of materials discussed in this chapter have a similar bulk structure, the details of the crystal symmetry, and metal and chalcogenide orbital contributions to the makeup of the conduction band, result in marked differences in reactivity. The group VIB metal dichalcogenides (e.g., MoS_2, WSe_2) have a trigonal crystal lattice and a conduction band that is primarily metal d in character, with small amount of chalcogenide p character.[1,3] The amount of mixing of the metal d and chalcogenide p orbitals increases in the order S < Se <Te, since the energy difference between the d and p orbitals becomes smaller as the atomic number increases.

Two other metal-dichalcogenide layered compounds were studied in order to compare the surface reactivity with the group VIB metal dichalcogenides. $ZrSe_2$ is very similar in structure to the group VIB materials, but the Zr-Se bond is more ionic, and so the bond strength is not as great as WSe_2 or $MoSe_2$.[4] SnS_2 has an octahedral crystal symmetry and a conduction band composed primarily of chalcogenide 2p orbitals.

Like the III-V semiconductors discussed in Chapter 2, metal dichalcogenides have been used in semiconductor/liquid junction solar cells, because the band gap of many of the

group VIB compounds are at an energy that is optimum for the efficient collection of the solar spectrum.[5] However, while oxidation and corrosion reactions similar to GaAs do not usually occur, these cells are not without losses that are due to surface recombination processes.

Canfield and Parkinson found that in the case of $MoSe_2$ or WSe_2, step sites of exposed transition metals were responsible for poor current-voltage characteristics because they provided a trap site for recombination.[6] By reacting the crystals with bis(1,2-diphenyl-phosphino)ethane or t-butylpyridine prior to use in the photoelectrochemical cells, improved current voltage (I-V) curves were obtained, presumably because the ligating reactants reduced the cross section of the traps on the step edges. Razzini, et al. used EDTA to affect trap sites on these same materials.[7]

Similar behavior was found by Folmer, et al., in the case of PdPS after reaction with ferrocyanide.[8] Treatment of the surface with ferrocyanide resulted in a stable cell with improved I-V properties. The proposed mechanism was that ferrocyanide bonded to the edge sites and mediated the charge transfer from the semiconductor into the electrolyte, so that the charge transfer was competive with photocorrosion at these sites.

This chapter discusses work done to explore the reactivity of metal chalcogenide surfaces as a function of the Lewis acidity of the reactant, as a function of the electronic structure of the surface. The emphasis for this chapter is not on reaction with defect sites or step edges, but on reaction with chalcogenide atoms on the basal plane of the metal-chalcogenide surface. Even though materials such as MoS_2 and $MoSe_2$ are rather inert, there is some precedent for this type of reaction. Jaegermann, et al., found that when Cu was depositied on SnS_2, a CuSnS compound was formed.[9] Lynch and coworkers have experimented with increasing the reactivity of MoS_2 by creating reactive sites through bombardment with Ne^+.[10] Under these conditons, MoS_2 reacts with Mn[10a] and Fe[10b] deposited on the surface. Our approach has been to try to react the surface with strong Lewis acids targeted at the chalcogenides.

II. Experimental

All metal chaclcogenides used in this work were single crystal, basal plane material. MoS_2 was naturally occurring material. WSe_2 and $MoSe_2$ were grown by L. Schnemeyer of AT&T Bell Laboratorites. SnS_2 and $ZrSe_2$ were grown by B. A. Parkinson of Dupont Central Research and Development. All crystals were cleaved prior to chemical exposure by peeling with tape.

$W(CO)_3(CH_3CH_2CH_2CN)_3$ was synthesized by refluxing $W(CO)_6$ in butylnitrile[11] $(C_5H_5)Fe(CO)_2((CH_3)_2CHCH_2)BF_4$[12a], and $(C_5H_5)Fe(CO)_2$(dibenzothiophene)[12b] were also synthesized following literature procedures.[12] $[(C_5H_5)Fe(CO)_2]_2$, K_2PtCl_4 (Strem), $AgCF_3SO_3$ (Aldrich), and $HgCl_2$ (Strem)were used as received. Butylnitrile, which had been dearated prior to use, was used as the solvent for samples treated with $W(CO)_3(CH_3CH_2CH_2CN)_3$. Nitromethane, which was dried over CaH and dearated prior to use, was used for $(C_5H_5)Fe(CO)_2$-$((CH_3)_2CHCH_2)BF_4$ exposures. The samples were treated by placing the substrate in 2-5 ml. of ~0.01 **M** metal complex solution in a glass vial. All treatments were done in a drybox and treatment time varied from 1-72 hours depending on the substrate. The samples were throughly rinsed with the appropriate solvent before mounting on XPS sample stubs.

The XPS instrumentation and data workup procedures have been described in detail in Chapters 3 and 5. The cross sections and escape depths used for the complexes described here are reported in Table 6.I. In order to avoid possible interfrence from the stainless steel sample stub, XPS experiments on surfaces exposed to Fe complexes were performed on Al foil-coated sample stubs fitted with brass screws. The samples were transported to the XPS instruments in sealed vials under N_2, then quickly transfered to the entry lock through air.

III. Results

A. Reaction of MoS_2 with K_2PtCl_4, $AgCF_3SO_3$, and $HgCl_2$

A summary of the metal chalcogenide samples, the treatment times, and XPS

Table 6.I. Cross sections (σ), escape depth (λ) and atomic density (n) used for calculation of coverages and mole ratios on MX_2 substrates. Values are for an Al K_α x-ray source.

Element Region	σ	λ (Å)	n (atom/cm^3) (x10^{-22})
MoS_2 (Mo $3d_{5/2}$):	5.62 (S 2s=1.43)	20	1.81
$MoSe_2$ (Mo $3d_{5/2}$):	5.77[a] (Se 3d=1.46[a])	20[a]	1.41
WSe_2 (W 4f):	10.27[a] (Se 3d=1.46[a])	23[a]	1.32
$ZrSe_2$ (Zr 3d)	4.17 (Se 3d=1.82)	28	0.94
SnS_2 (Sn 3d)	14.8 (S 2p = 1.67)	19	1.48
K_2PtCl_4 (Pt $4f_{7/2}$)	8.65	46	0.49
$AgCF_3SO_3$ (Ag 3d)	10.66	26	0.94
$HgCl_2$ (Hg $4f_{7/2}$)	10.57	44	1.21
$W(CO)_3(C_3H_7CN)_3$ (W 4f)	9.8	33	0.45
$Fe(C_5H_5)(CO)_2(C_4H_8)BF_4$ (Fe $2p_{3/2}$)	10.82 (10.54[a])	26	0.3

[a]Values for a Mg K_α x-ray source.

results is given in Table 6.II. XPS of MoS_2 exposed to K_2PtCl_4 showed a large amount of Pt, some Cl and no K. While the Cl/Pt ratio (2.1) and the binding energy of the Pt [13] (Table 5.II) are consistent with the values expected for K_2PtCl_4, the large amount of Pt (~5 monolayers calculated coverage) indicates that the K_2PtCl_4 is associating with itself as well as with the surface.

$HgCl_2$ apparently dissociated, because the Cl/Hg ratio is quite high (4.0) and the surface coverage of Hg was calculated to be greater than a monolayer. The $AgCF_3SO_3$, however, apparently did adsorb in monolayer coverages and there was also signal detected from the fluorines on the triflate. No change in the metal or chalcogenide regions of the

Table 6.II. XPS data for various metal dichalcogenides (designated "MX_2") exposed to several metal complexes (metal designated "Y"). Data were taken on a VG HP580 or VG Mark II system. All ratios are normalized using appropriate cross sections.

Substrate (treatment time)	M (eV)	X (eV)	$\frac{M}{X}$	Y (eV)	$\frac{Y}{M}$	Γ x10^9 $\frac{moles}{cm^2}$
K_2PtCl_4 + MoS_2[a]	Mo 3d 230.2 (Δ=3.2)	S 2s 228.2	0.7	Pt 4f 74.3 (Δ=3.6)	3.5	4.7
$HgCl_4$ + MoS_2[a]	Mo 3d 230.1 (Δ=3.1)	S 2s 227.3	0.6	Hg 4f 101.6(Δ=4.0)	0.5	2.0
$AgCF_3SO_3$ + MoS_2[a]		S 2p 163.1		Ag 3d 368.9(Δ=4.0)		0.7[b]
$W(CO)_3(C_3H_7CN)_3$ on SnS_2[a]	Sn $3d_{5/2}$ 487.0	S 2p 162.1	0.5	W 4f 36.4(Δ=2.0)	0.1	0.7
on $ZrSe_2$[a]	Zr 2p 180.9 (Δ=2.4) 182.1 (Δ=2.4)	Se 3d 53.4 55.3	0.4	35.6 (Δ=2.1)	0.05	0.2
$Fe(C_5H_5)(CO)_2(C_4H_8)^+$ on MoS_2 (20 hrs)[a]	Mo 3d 229.7 (Δ=3.4)	S 2s 227.2	1.0	711.4 (Δ=13.4)	0.4	0.8
on MoS_2 (3 days)[c]	Mo 3d 229.6 (Δ=3.2)	S 2s 226.9	1.0	712.6 (Δ=13.2)	0.4	0.9
on $MoSe_2$[c]	Mo 3d 229.2 (Δ=3.2)	Se 3d 54.9	0.3	711.6 (Δ=13.4)	0.1	0.5
on WSe_2[c]	W 3d 32.8 (Δ=2.1)	Se 3d 55.1	0.2	712.0 (Δ=13.3)	0.4	1.1
$Fe(C_5H_5)(CO)_2$ (dibenzothiophene)BF_4 on In foil[a]				711.6 (Δ=13.1)		
$Fe(C_5H_5)(CO)_2(C_4H_8)BF_4$ on In foil[a]				710.7 (Δ=12.8)		

[a]Al K_α x-ray source.

[b]Calculated with respect to the S 2p peak.

[c] Mg K_α x-ray source.

XPS was observed after exposure of any of the suraces to any of the above metal complexes.

B. Reaction of $MoSe_2$, MoS_2, WSe_2, and SnS_2 with $[Fe(C_5H_5)(CO)_2(C_4H_8)]BF_4$

$MoSe_2$, MoS_2, WSe_2, and SnS_2 were all exposed to $Fe(C_5H_5)(CO)_2(C_4H_8)^+$ in nitromethane. The amount of time needed before Fe was detectable by XPS was a function of the type of chalcogenide. MoS_2 exhibited very slow kinetics. As can be seen from Figure 6.1, the amount of Fe adsorbed on the MoS_2 surface gradually increases as the exposure time increases, with ~1-2 monolayers adsorbing after 3 days. An equivalent amount of Fe as in Figure 6.1a was adsorbed by both $MoSe_2$ and WSe_2 after overnight exposure to $Fe(C_5H_5)(CO)_2(C_4H_8)^+$. The interference of the Sn 3p lines prevented definitive identification of Fe on the SnS_2 surface. No changes were observed by XPS in the metal or chalcogenide regions on any of the samples after reaction with $Fe(C_5H_5)(CO)_2(C_4H_8)^+$.

The $[Fe(C_5H_5)(CO)_2]_2$ dimer also showed some reactivity with all metal chalcogenide surfaces discussed above, though further work has revealed that this complex forms clusters on the surface.[14] In order to determine if the Fe complex was intercalating, rather than bonding to the surface, a sample of $MoSe_2$ was placed in contact with ferrocene for a period of 18 hours. No Fe was detected on this surface by XPS .

C. Reaction of SnS_2, MoS_2, $MoSe_2$, and $ZrSe_2$ with $W(CO)_3(C_3H_7CN)$

SnS_2, MoS_2, $MoSe_2$, and $ZrSe_2$ were all exposed to $W(CO)_3(C_3H_7CN)_3$ in butylnitrile. The SnS_2 and $ZrSe_2$ reacted readily with the W complex after 2 hours or less (Table 6.II). Exposure of SnS_2 to $W(CO)_6$ for the same time period did not result in any detectable W above background levels. The $MoSe_2$, however, did not react after 3 hours, and MoS_2 did not show any XPS signals attributable to W, even after an exposure time of more than 3 days. No change in the metal or chalcogenide regions of the XPS was observed after reaction with any of the above substrates. The $ZrSe_2$ did show a small

Figure 6.1. Fe 2p XPS region for MoS_2 exposed to 0.01 **M** $Fe(C_5H_5)(CO)_2(C_4H_8)BF_4$ in nitromethane for several different times-a) 3 days exposure time, b) 20 hours, c) 14 hours, d) background spectra. Data were obtained on a VG HP580 system using nonmonochromatic Al K_α x-rays.

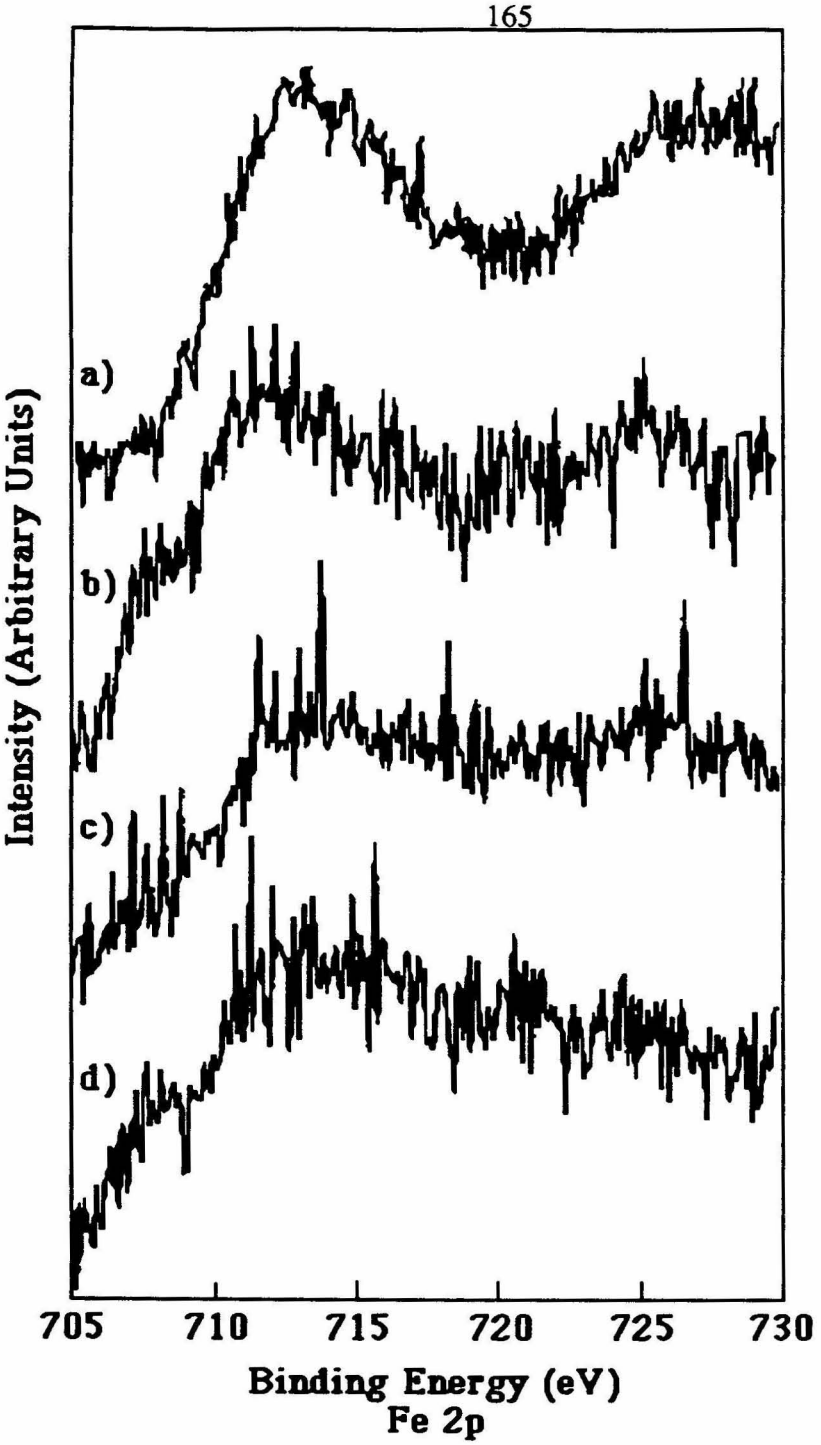
a)
b)
c)
d)
Intensity (Arbitrary Units)
705
710
715
720
725
730
Binding Energy (eV)
Fe 2p

shifted component (Table 6.II), even on a freshly peeled sample, but these peaks account for only about 10% of the fitted peak area. The SnS_2 substrate was also studied, using high-resolution XPS (SSI), and no contribution from a component with a shift in binding energy was observed on a W exposed surface.

IV. Discussion

The reactivity trends exhibited by the group VIB metal chalcogenides with $Fe(C_5H_5)(CO)_2(C_4H_8)^+$ and $W(CO)_3(C_3H_7CN)_3$ can be understood by the amount of chalcogenide orbital mixing into the conduction band. The selenide complexes would be expected to have more chalcogenide character, and therefore more chalcogenide electron density available for bonding interactions. This is borne out by the fact that $MoSe_2$ and WSe_2 reacted with $Fe(C_5H_5)(CO)_2(C_4H_8)^+$ on a much shorter time scale than did MoS_2.

The conduction band of SnS_2 is primarily S 3p in character, and so it is not surprising that this substrate readily reacts with $W(CO)_3(C_3H_7CN)_3$. $ZrSe_2$ also reacted readily with the W complex as the Zr-Se bond is rather weak compared to other metal chalcogenide materials. The group VIB substrates are unreactive towards $W(CO)_3(C_3H_7CN)_3$. Apparently, the Lewis acidity of the W complex is not quite as high as that of the Fe complex.

An interesting side note to the reactivity of these surfaces is the apparent behavior of $ZrSe_2$ exposed to Te complexes. A sample of $ZrSe_2$ was exposed to $W(CO)_3(C_3H_7CN)_3$ in a glove box that was contaminated with $(CH_3)_2Te$. The resulting XPS showed a significant amount of Te had been adsorbed and that there was a large amount of the oxidized Zr component. While this experiment was only preliminary, and needs independint conformation under more controlled conditions, the results from the inadvertent Te exposure seem to indicate that the Zr component is much more vulnerable to attack than the Se, and further study of the reactivity of the metal component of metal chalcogenides is in progress in our laboratory.

The interaction of metal complexes with metal chalcogenide surfaces also provides a possible route towards probing the electron denstiy imaged by STM. There is some controversy as to whether STM images of MoS_2 and other metal chalcogenides are maps of the metal or sulfide electron density.[15] By binding complexes to the surface, the density imaged by the microscope should change and contributions of the different components may be separable. Preliminary studies of SnS_2 exposed to $W(CO)_3(C_3H_7CN)_3$, however, showed that these types of experiments are hindered by etching of the substrates by the STM tip. Such etching behavior has been observed for a variety of substrates,[16] and has been observed by us on $MoSe_2$ and SnS_2 surfaces. Perhaps if a well-behaved reactant is found for MoS_2, then this surface would be sufficiently stable under STM conditions that the nature of the metal complex/ surface interaction could be studied.

IV. Conclusions

There is a marked difference in reactivity between different types of metal dichalcogenide substrates. If the metal is a group VIB metal, the surface is rather unreactive, with the selenide-containing materials exhibiting faster kinetics than the sulfides in the case of exposure to $[Fe(C_5H_5)(CO)_2(C_4H_8)]BF_4$. The only complexes studied here that reacted with MoS_2 in close to monolayer coverages were $AgCF_3SO_3$ and $[Fe(C_5H_5)(CO)_2(C_4H_8)]BF_4$, though the latter complex shows a tendency to form clusters. Other types of metal chalcogenides, i. e. SnS_2 and $ZrTe_2$, were much more reactive. The study of the reactivity of the surface of metal chalcogenides not only provides fundamental insight into the chemistry of this class of materials, but also will provide for ways of attaching various electron donating and accepting species to the surface in order to study electron transfer properties at the interface.

References

1. E. Doni and R. Girlanda, in *Electonic Structure and Eletronic Transitions in Layered Materials*, V. Grasso, Ed. (Reidel, Dordrecht, 1986), pp. 1-164.

2 S. L. Sulb, L. R.Faulkner, G. D. Stucky, and R. J. Blattner, *Anal. Chem.* **51**, 1060 (1979).

3 D. E. Haycock, D. S. Urch, and G. Wiech, *Faraday Trans. 2* **75**, 1692 (1979).

4. H. Isomaki, and H. Von Boehm, Phs. Scr. **24**, 465 (1981).

5. B. Scrotsati, in *Semiconductor Electrodes*, H. O. Finklea, Ed. (Elsevier, Amsterdam, 1988), pp. 457-508.

6. D. Canfield and B A. Parkinson, *J. Am. Chem. Soc.* **103**, 1279 (1981).

7. G. Razzini, L. P. Bicelli, G. Pini, and B. Scrosati, *J. Electrochem. Soc.* **128**, 2134 (1981).

8. J. C. W. Folmer, J. A. Turner, and B. A. Parkinson, *Inorg. Chem.* **24**, 4028 (1985).

9. W. Jaegermann, F. S. Ohuchi, and B. A. Parkinson, *Ber. Bunsenges. Phys. Chem.***93**, 29 (1989).

10 a) J. R. Lince, T. B. Stewart, P. D. Fleischauer, J. A. Yarmaff, and A.Taleb-Ibrahimi, *J. Vac. Sci. Technol. A* **7**, 2469 (1989). b) J. R. Lince, T. B. Stewart, P. D. Fleischauer, J. A. Yarmaff, and A.Taleb-Ibrahimi, *Surf. Sci.* **223**, 65 (1989).

11. G. J. Kubas, *Inorg. Chem.* **22**, 692 (1983).

12. a) M. Rosenblum, W. P. Giering, and S.-B., Samuels, *Inorg. Synth.* **26**, 163 (1986). b) J. D. Goodrich, P. N. Nickias, and J. P. Selegue, *Inorg. Chem.* **26**, 3424 (1987).

13. C. D. Wagner, W. M. Riggs, L. E. Davis, J. F. Moulder, and G. E. Muilenberg, *Handbook of X-ray Photoelectron Spectroscopy* (Perkin Elmer, Eden Prairie, MN, 1979).

14. Angle resolved XPS studies showed that an inhomogeneous layer was formed - S. Nguyen, personal communication.

15. G. W. Stupian , and M. S. Leung, Appl. Phys. Lett. **51**, 1560 (1987).

16. B. Parkinson, J. Am. Chem. Soc.**112**, 7498 (1990).